ENGINEERING A WHOLE-CELL ZINC BIOSENSOR

A Dissertation
Presented to
The Academic Faculty

By

Daniel M. Watstein

In Partial Fulfillment
Of the Requirements for the Degree
Doctor of Philosophy in the
School of Chemical & Biomolecular Engineering

Georgia Institute of Technology

December 2017

ENGINEERING A WHOLE-CELL ZINC BIOSENSOR

Approved by:

Dr. Mark P. Styczynski, Advisor
School of Chemical & Biomolecular Engineering
Georgia Institute of Technology

Dr. Brian Hammer
School of Biological Sciences
Georgia Institute of Technology

Dr. Julie A. Champion
School of Chemical & Biomolecular Engineering
Georgia Institute of Technology

Dr. Harold Kim
School of Physics
Georgia Institute of Technology

Dr. Rachel Chen
School of Chemical & Biomolecular Engineering
Georgia Institute of Technology

Date Approved: August 17th, 2017

ACKNOWLEDGEMENTS

I would like to thank my parents, who have guided me and supported me throughout my academic endeavors and without whom I would not be here on multiple levels.

I would like to thank my advisor, Dr. Mark Styczynski for putting up with me for the six years of my graduate education and for making me a more critical person and a better scientist.

I would like to thank my lab and my graduate committee for their assistance along the way, suggestions, and guidance.

I would like to thank my colleagues, who provided me with guidance, commiseration, and libation.

I would like to thank Monica for assistance with the grueling work in Switzerland, Ethiopia, Mexico, and most importantly Los Angeles.

I would like to thank Jeff and Christine for supporting me through bizarre and disturbing trials.

TABLE OF CONTENTS

LIST OF TABLES

LIST OF FIGURES

LIST OF SYMBOLS AND ABBREVIATIONS

ASSURED	Affordable, sensitive, specific, user friendly, rapid and robust, delivered
ATC	Anhydrotetracycline
CCD	Charge-coupled device
CFE	Cell-free extract
CFU	Colony forming units
GFP	Green fluorescent protein
HI NHS	Heat-inactivated NHS
IPTG	Isopentenyl ß-D-1-thiogalactopyranoside
NHS	Normal human serum
PCR	Polymerase chain reaction
RBS	Ribosomal binding site
RFP	Red fluorescent protein

SUMMARY

Malnutrition is a significant healthcare concern across the globe. Though normally evocative of images of starvation or hunger, malnutrition also encompasses deficiencies of critical micronutrients such as zinc. Studies have implicated zinc malnutrition as a contributing factor to numerous developmental disorders and to diarrheal disease, one of the leading causes of death among children. However, current analytical techniques are inappropriate for measuring population-level deficiency in locations where these measurements are most needed. An effective test must be inexpensive to produce, require little training to administer and interpret, and be usable at point of care, eschewing sample transportation and expensive laboratory techniques. As obligate consumers of zinc, bacteria possess diverse cellular machinery to sense and regulate intracellular zinc concentrations in response to changes in their environment through allosteric transcriptional regulation of a variety of mechanisms of zinc influx, efflux, or sequestration. Bacteria are also relatively simple and inexpensive to produce at scale. This work describes efforts to leverage existing cellular mechanisms to sense and respond to zinc, to tie that response to heterologous pathways to produce human-readable pigmented metabolic outputs, to tune the machinery to respond to medically relevant levels in serum rather than levels originally useful to the bacterium, and to grow the resulting biosensor in human serum to demonstrate proof-of-principle of a whole cell zinc biosensor as the basis of inexpensive, colorimetric zinc assay, deployable directly at point of care with no additional analytic equipment.

CHAPTER 1. INTRODUCTION

In this dissertation, I develop a whole-cell zinc biosensor as the basis of an assay for use in low-resource environments. The cost of current analytical techniques precludes their sustained widespread use for zinc status monitoring. Additionally, current approaches to whole-cell biosensors are not well adapted to deployment in the developing world. The World Health Organization has coined the acronym ASSURED to describe the characteristics of an ideal diagnostic test. Such a test would be: Affordable by those who need it, Sensitive, Specific, User-friendly (requiring minimal training), Rapid and Robust (does not require refrigerated storage), Equipment-free, and Delivered to those who need it[1]. I describe my contributions to tailor the design and implementation of synthetic, whole-cell biosensors to form the basis of an ASSURED zinc diagnostic test.

1.1 Zinc Deficiency and Supplementation

Zinc deficiency is most prevalent in developing nations, affecting an estimated 17% of the world's population[2]. Of those affected, the most profound effects of zinc deficiency are seen in pregnant women and children under the age of five[3]. Deficient zinc status in pregnant women has been implicated in low birth weight, preterm delivery, and congenital abnormalities[4]. In 2004, low birth weight and prematurity were responsible for 31% of neonatal deaths, which was 11% of all child mortality[5]. In those that survive, low birth weight and premature birth directly increase the risk of stunting or wasting (height-for-age at less than two standard deviations from the mean or weight-for-height at less than three standard deviations from the mean, respectively), both of which directly increase the risk of child mortality[6]. After birth, continued zinc deficiency contributes to

stunting and increased incidence of diarrheal disease and pneumonia. Diarrheal disease is of particular importance, both because it is directly responsible for 16% of global child mortality[5] and because it is implicated in zinc malabsorption[7]. In 2011, 116,000 under-5 deaths (1.7% of 2011 child mortality) were attributable to zinc deficiency[6].

Estimates of zinc deficiency prevalence are based on an average dietary analysis, indicative of a major obstacle in developing a solution: reliable data on the zinc status of the world's population is currently unavailable. Currently, the primary biomarker used to assess zinc status is serum or plasma zinc concentration, which is typically maintained at approximately 12 to 15 μM in healthy adults[8]. A review of zinc depletion and repletion studies in otherwise healthy adults concluded that serum zinc responds fairly rapidly (3-5 weeks) to zinc-depleted diets and recovers to basal levels within a week of resumption of normal zinc intake[8], indicating serum zinc concentration is an adequate indicator for zinc status and response to changes in dietary intake.

Two potential strategies for addressing micronutrient deficiencies are biofortification and direct micronutrient supplementation. Biofortification is the selective breeding or genetic engineering of food crops to produce or accumulate more micronutrients. There have been a handful of successful efforts to engineer micronutrient accumulation phenotypes into food crops,[9,10] and analysis of micronutrient biofortification has shown its general efficacy for providing provitamin A[11]. However, biofortification cannot alone meet requirements for treating acute severe zinc deficiency and for supplementation in pregnant and lactating women[11]. In an attempt to address the problem, studies have examined the effectiveness of direct zinc supplementation, mostly focusing on pregnant women and children under the age of 5. While the results have not always been

conclusive, broader meta-analyses of studies have evidenced the general efficacy of zinc supplementation. One such analysis found that zinc supplementation causes a statistically significant reduction in the incidence of diarrhea by 20%, of acute lower respiratory tract infections by 15%, and an overall reduction in mortality of 18% in children older than 12 months[12]. A similar study found statistically significant reductions of diarrhea of 13% and pneumonia morbidity of 19% but failed to find a statistically significant decrease in all-cause mortality[13]. Multiple studies found small but significant increases in linear growth over the course of supplementation in young children[12,14,15]. The results for pregnant women were less conclusive, but supplementation has been found to reduce the incidence of preterm births by a statistically significant 14%. Troublingly, one trial of powdered micronutrient supplements comparing iron powders and combined iron and zinc powders to no-supplement controls found an increase of diarrhea and acute respiratory morbidities in children and failed to detect a statistically significant change in serum levels[14], highlighting the need to thoroughly evaluate the efficacy of specific supplementation strategies.

Though valuable information can be extracted from meta-analyses of many small scale studies, complete pictures of population zinc status remain elusive. One of the most prohibitive obstacles to achieving this is simply cost. Traditional lab testing requires constant refrigeration from the time the sample is taken to the time it is prepared for testing. Current state of the art testing involves flame atomic absorption spectroscopy[14] or mass spectrometry, requiring established laboratories and skilled technicians. The cost and logistics associated with testing an arbitrary percentage of a population for zinc status with traditional methods are generally prohibitive. This is especially true in the

developing world and in the wake of significant natural disasters, where access to electricity may be limited or nonexistent.

One potential solution is the widespread supplementation of zinc similar to current efforts in India to reduce anemia with the Weekly Iron and Folic Acid supplementation program[16]. As part of a broader assessment of undernutrition intervention strategies, a recent review estimated the cost of zinc supplementation in early childhood with 90% population coverage in countries representing 90% of the global deficiency burden would be $1.182 billion/year (2010 international dollars)[17]. This non-negligible cost associated with large-scale supplementation combined with the risk of potential side effects associated with particular strategies supports a more focused and informed approach; this in turn highlights the need for improved tests to aid in the design, implementation, and monitoring of such programs. Whole-cell biosensors have the potential to meet the economic and logistical constraints of population-level testing with an inexpensive and preservable bacterial chassis. Here, I apply synthetic biology to design a whole-cell biosensor for such testing.

1.2 Synthetic Biology and Whole-Cell Biosensors

Synthetic biology is a broad field involving the design of new biological components or redesign of existing systems such as reaction networks, genetic circuits, or whole cells[18]. Though synthetic biologists may have fundamentally different goals—pure biology, metabolic engineering, biocomputing, etc.—they all view the underlying biology of their chosen systems as a tool to achieve novel functionality or to solve specific problems.

An important concept in synthetic biology is the genetic circuit, a collection of genetic elements designed to produce some desired output by modulating transcription, translation, protein interactions, or other regulatory phenomena. Early work saw the construction of simple artificial circuits like genetic toggle switches[19] or basic digital logic gates, opening up the possibility for biological computation along the lines of traditional digital processors. To that end, a variety of logic gates have been successfully demonstrated *in vivo*[20]. Serious hurdles still exist to realizing the goal of whole-cell biocomputing, such as the intrinsic noisiness of most biological systems and the limited number of available and appropriate regulatory elements, but efforts to solve both of those problems are ongoing.

Genetic circuits lay the foundations for the concept of the whole-cell biosensor. These 'devices' are entire organisms with the ability to produce some measurable signal to provide information about a system of interest. One of the most significant advantages of whole-cell sensors is that they are self-replicating, drastically simplifying production, reducing cost, and permitting easy scale up. In contrast to traditional analytical techniques, biosensors need not require expensive equipment if designed appropriately. They are also able to provide information on the bioavailability of analytes rather than overall concentration, a property largely responsible for their widespread appeal in environmental monitoring, where they can be used to more directly assess the risk of pollutants to ecosystems[21,22].

Though they likely did not consider themselves to be synthetic biologists, early geneticists pioneered some of the most fundamental techniques involved in genetic reporting and the manipulation of genetic systems. Early genetic work exploring

expression of proteins of unknown function and regulation used reporter gene fusions with unknown operons to investigate their response to different chemicals or growth conditions. The concept of whole-cell biosensors was also pioneered before the deliberate design of genetic reporting circuits. A sensor made from *Photobacterium phosphoreum*[23], a bioluminescent marine organism, was used commercially to assess nonspecific toxicity in samples. Bioluminescence levels were compared to a control, using a reduction in signal as a rough indicator of sample toxicity. Other generic stress sensors were constructed through the translational coupling of reporters to known biological stress response systems both to investigate basic biology and to aid in developing other generic toxicity assays.

Though there is undoubtedly utility in nonspecific sensors (e.g., the generic stress response sensors described above), one significant promise of biosensors is the detection of specific analytes of interest by exploiting the exquisite sensing mechanisms microorganisms have evolved to adapt to different environments. Isolating these regulatory elements and coupling them to reporters in their native organism or in a well-characterized chassis like *E. coli* is a common approach which has seen a wide variety of uses from monitoring environmental pollutants[21,24,25] to enabling high throughput screening for drug design[26,27]. Increasing understanding of regulatory mechanisms has allowed both rational design[26,28] and combinatoric[29,30] generation of new functionality. Indeed, some families of sensor-regulators have modular domains[29,31,32], potentially allowing the generation of multiple orthogonal artificial regulatory systems.

Upon sensing and processing a signal, the biosensor must produce some detectable output. There are a number of available reporting systems currently in use, each with

their own sets of advantages and disadvantages. A common, general use reporter is the fluorescent protein, which offers simple detection of sensor output with widely available fluorimeters. Many different types of fluorescent proteins have been engineered for application in diverse conditions. Other reporter systems increasingly used for biosensor applications are luciferases, enzymes which catalyze light-producing reactions. These offer high quantum yield, allowing excellent sensitivity with appropriate detectors. The miniaturization of charge coupled device (CCD) detectors has encouraged the use bioluminescence-based reporters, improving their prospects of incorporation into portable whole-cell detection devices.

A more indirect approach to reporting uses a protein's enzymatic activity to convert a substrate to something easily detectible, such as a fluorescent or pigmented product. These were some of the earliest reporters used, and include *E. coli*-derived chloramphenicol acetyltransferase and β-galactosidase[23]. Enzymatic assays are still commonly used but require the addition of reagents to produce a signal which must still be measured with equipment like fluorimeters or spectrophotometers to produce quantitative measurements. A related approach is the use of enzymes that produce pigments as secondary metabolites. These do not require the addition of substrates, but the rate of pigment production is tied to the cell's metabolism, sometimes making it difficult to directly correlate inferred enzymatic activity with expression levels. Many examples of biosensors reporting with pigment production are available[33,34], but quantification often presents a challenge, requiring quantitative extraction or limiting the biosensors to more qualitative applications such as blue/white screening or other binary tests.

1.3 Zn^{2+}-Responsive elements

The construction of biosensors relies on the ability to control the transcription of circuit elements and the expression of reporter genes in response to the signal of interest. My efforts were primarily concerned with the determination of zinc concentration. Fortunately, much work has been done to elucidate the metalloregulatory responses of many organisms, including *E. coli*. Zinc is an important component of biological chemistry, with over 300 metalloenzymes in *E. coli* known to form complexes with zinc as structural or catalytic elements[35]. Unsurprisingly, *E. coli* possesses an impressive array of proteins dedicated to sensing, importing, and exporting zinc and other metal ions. These systems allow the bacterium to survive in environments with a wide range of zinc concentrations.

E. coli typically maintains intracellular zinc concentrations around 200 μM[36] in laboratory conditions. Nevertheless, the bacterium can grow in media with zinc concentrations ranging from ~30 nM[37] to ~1 mM[38], depending on the other components of the growth media. It accomplishes this through a combination of constitutive and inducible ion-transport systems including but not limited to *zntA*, *zupT*, *zitB*, *znuABC*, and *zinT*. The gene *zntA* encodes a zinc- and cadmium- specific p-type ATPase positively regulated by the transcriptional activator ZntR in response to increased zinc stress[31]. The gene *zupT* encodes a constitutive[36], non-specific metal transporter capable of importing zinc ions[39]. ZitB is a cation efflux diffusion facilitator, dependent on the proton gradient. The *znuABC* operon codes for three proteins in a zinc import system: ZnuA is a periplasmic zinc binding protein, ZnuB is an integral membrane protein, and ZnuC is an ATPase. The expression of the *znu* gene cluster is controlled by Zur, a transcriptional

repressor which binds DNA in high zinc environments. ZinT, also negatively regulated by Zur, is a high-affinity periplasmic zinc binding protein involved in either direct transport across the inner membrane or the delivery of zinc for binding to membrane proteins.

The response of *E. coli* to both zinc starvation and poisoning has been investigated through transcriptomics[35,37,38] and proteomics[39,40], demonstrating many differentially regulated genes. Unfortunately, differing culture conditions (batch vs. chemostat), methods of zinc depletion (rigorous media preparation vs. chelation), and analytical techniques make it difficult to isolate the effects of zinc alone, with much of the differential regulation not consistent across studies. A great deal is still unknown about zinc regulation in *E. coli*, but both ZntR and Zur are two well-characterized zinc-responsive transcription factors. Knowledge of the operator sequence for Zur in the *znu* operon led to the discovery that *zinT* is also regulated by Zur[37]. The promoter P_{zntA} has been used in biosensors for cadmium, mercury, and zinc in wastewater[22,25,41], but no application has gone beyond the direct fusion of bioluminescent or fluorescent proteins to promoters. These studies did not go further than cloning a fluorescent protein under control of P_{zntA} and measuring zinc, cadmium, and lead response in LB[41], or using genomic ZntR and P_{zntA} to assess response two 13 environmental candidates with bioluminescence[22]. The most in-depth use case investigated was the use of P_{zntA} controlling expression of luciferase genes to monitor wastewater for the presence of cadmium, mercury, and copper in which a fluidics device was constructed and successfully tested to mix wastewater and nutrients for online monitoring of a wastewater stream[25], demonstrating that this promoter can be implemented usefully in whole-cell

biosensors, but no complex tuning was performed. Cells were still used primarily to alert of the presence of some (nonspecific) contaminate. Investigation into modification of any of these systems to change promoter response to zinc by altering transcription factor gene dosage, decoy site abundance, and other zinc regulatory machinery has heretofore been absent.

1.4 Pigments

Much of the recent work on whole-cell biosensors has concerned platforms for high sensitivity bioluminescence detection for field or online applications[42]. Increasing portability and minimizing assay time, while undoubtedly critical for most applications, do nothing to enhance the prospect of minimal cost assays if the improvements come with the requirement of integrated CCD detectors, microfluidics, or other expensive alternatives. To develop the most economical solution for a zinc status assay, reporting mechanisms should be developed that require no specialized detectors; reporter systems based on the production of multiple pigments represent a promising strategy in this regard. Such approaches offer the advantage of creating discrete changes in coloration detectable with the naked eye while avoiding the subjectivity of visual quantification of the amount of a single pigment. This work will utilize two families of pigments: those from the violacein pathway, and those from the carotenoid pathway.

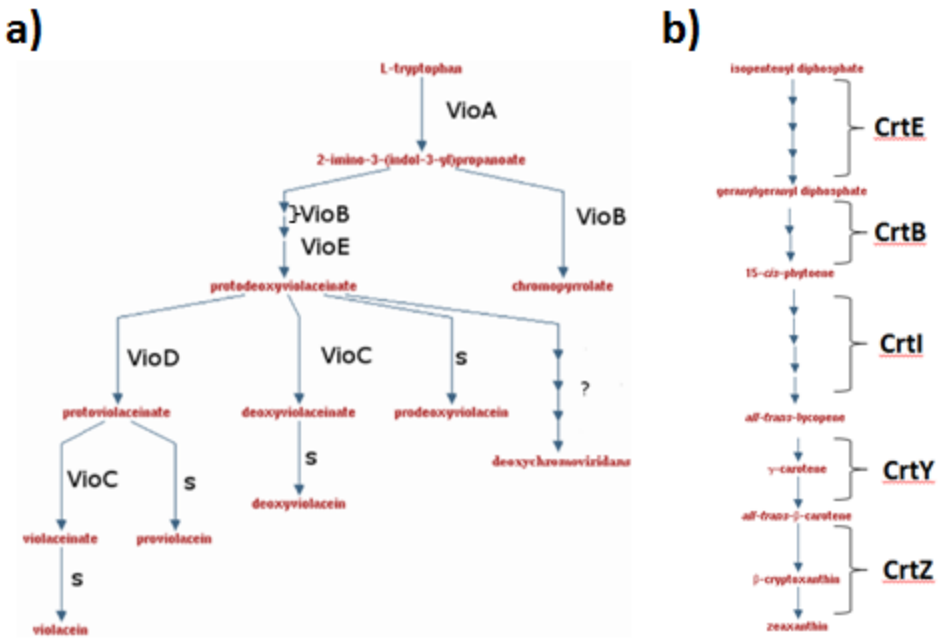

Figure 1: Simplified map of the *vio* (a) and *crt* (b) biosynthesis pathways beginning with the last metabolite native to *E. coli*. Reactions are labeled with enzyme if known or 's' if spontaneous.

Violacein is a pigmented secondary metabolite produced by a number of bacteria. Natural production of the pigment is thought to protect bacteria from predation by organisms to which violacein is toxic. Its selective antibiotic activity may also reduce competition in the environment[43]. The pigment is of scientific interest primarily due to its antibiotic and antitumor[44] activity and because its biosynthetic pathway produces intermediates similar to other medically important compounds such as rebeccamycin and staurosporine[45]. The pigment is produced through a series of enzymatic, autooxidation, and autodecarboxylation reactions directed by the five genes in the *vio* operon. The biosynthetic pathway involved has been almost completely mapped, revealing a unique biosynthetic mechanism, a 1,2-indole shift, found in no other known pathway to date.

Though its mechanism of antibiotic activity is unknown, violacein can be stably overexpressed in *E. coli*[46], albeit only with especially stable expression plasmids for toxic heterologous protein production. Critically, the pathway has multiple colored intermediate side products[43], allowing several reporters to be produced by controlling the expression of just a handful of *vio* genes. A simplified map of the *vio* biosynthetic pathway is presented in Figure 1a.

The carotenoid (Figure 1b) pathway is another source of pigments including the pink-red lycopene, the orange β-carotene, and the yellow zeaxanthin. The pathway is present in numerous plants and bacteria, where it serves a number of purposes. The production of carotenoids has been extensively studied, both for useful properties of the carotenoids themselves and the value of many other industrial or medically important isoprenoids (compounds based on multiple isoprene units) such as the antimalarial drug artemisinin and provitamin A, which is a group of carotenoids including β-carotene. In order to make biological production of these compounds feasible, both the carotenoid biosynthesis pathway and upstream precursor pathways in *S. cerevisiae* and *E. coli* have been the focus of metabolic engineering efforts to increase production rates and maximum titer[47-50], the results of which could prove useful in reducing assay time in pigment-based biosensors.

To date, the use of pigments as reporters in whole-cell biosensors has been limited. Some successful attempts have correlated degree of pigmentation with qualitative analyte concentration by examining degree of coloration of the culture[34]; however, the majority of the focus in biosensor research has been on producing rapid, quantitative output. By employing multiple color outputs, we can implement pigment-based whole-cell sensors

to provide semi-quantitative reporting of defined analyte concentration ranges without the use of additional equipment.

1.5 Overview

The promise of biosensors presents a unique opportunity to bring the power of synthetic biology to bear on significant global humanitarian problems. Though accurate, current testing methods are not capable of meeting the economic and logistical constraints of population-level micronutrient status testing. Efforts to combat zinc deficiency have been hampered by insufficient information on the extent of the problem and the uncertainty about the most effective methods of treating zinc deficiency in the developing world or in the wake of emergency humanitarian crises. Pigment-based bacterial biosensors offer the potential for an inexpensive zinc status assay that, when combined with other established low-resource sample preparations such as centrifuges based on egg beaters[51], centrifuges based on children's toys[52], or paper-based[53] separation technologies, would require no laboratory equipment, electricity, or sample transport and minimal training to administer. This technology could facilitate consistent monitoring of zinc status, aiding not only in the identification of population-level deficiencies, but ultimately in the development of supplementation strategies; these capabilities would in turn allow more targeted interventions by identifying explicitly deficient subpopulations, eliminating a portion of the significant cost and logistical challenge of whole-population micronutrient supplementation.

CHAPTER 2. USING METABOLISM TO AUGMENT BIOSENSOR TUNING

Portions of this chapter are reproduced from my publication "Precise metabolic engineering of carotenoid biosynthesis in Escherichia coli towards a low-cost biosensor"[54] in *Metabolic Engineering* with permission from the publisher.

2.1 Introduction

Metabolic engineering has played a key role in advancing a number of critical biotechnological research areas and applications, but there remain numerous areas where control of metabolism has not been leveraged to solve critical problems, such as enabling biosensors for applications like blood micronutrient measurement at a population scale. The biofuels[55-57], pharmaceutical[58,59], and specialty and commodity chemicals[60,61] applications of metabolic engineering are well-known. Moreover, the techniques of metabolic engineering have been used to engineer plants and foodstocks to help battle problems such as nutrient and micronutrient deficiency, with one of the most prominent examples being the development of Golden Rice[9,10]. We sought to investigate using metabolic engineering in a novel application—to tune the output of a pigment-based biosensor independent of the transcriptionally based sensor-actuators.

This work has potential broader applications to any biosensor using pigments as a reporting mechanism, but here we investigated altering metabolism and adjusting metabolic precursor availability as a means of enabling or improving the function of the carotenoid pathway as a reporting mechanism for the zinc biosensor. Previous

technologies for sensing zinc produced fluorescence or luminescence proportional to zinc concentrations[41,62]; while such assays give the potential for quantitative results, they require specialized equipment to detect and quantify these readouts that limit application in low-resource areas. Instead, we designed our assay to use pigment production as a readout, removing the need for quantification. Pigment production is performed by heterologous genes expressed in *E. coli* under the control of zinc-responsive transcription factor/promoter systems. We further sought to make the color outputs as discrete as possible, transitioning sharply from one color to another so as to remove potential ambiguity from the reading.

The pigments used for this biosensor were the red and orange carotenoids lycopene and β-carotene and the purple pigment violacein, each of which have previously been the targets of metabolic engineering efforts whose results and insights have contributed to the engineering efforts described here. There has been extensive work on the engineered overproduction of lycopene and other isoprenoids[63-65], as they have significant industrial value as chemicals, and isoprenoids are a precursor to yet other extremely valuable chemicals, including taxol[50]. Violacein has also been the subject of significant metabolic engineering efforts[66-68], both due to the novelty and complexity of the pathway that produces it, and for its potential value as an antimicrobial or antitumor drug. In these cases, the chief goal of the metabolic engineering efforts to date has been high titer production with the downstream goal of purification. For our application, though, tightly controlled expression rather than high titer was the primary goal of our metabolic engineering efforts.

An effective bacterial-based, pigment-producing diagnostic for our application required (1) sufficient pigment to be visible to the naked eye (2) in a reasonable amount of time (3) with sufficient control over production of all pigments to enable discrete color states. The first two of these criteria directly relate to traditional metabolic engineering efforts, though with a greater emphasis on productivity to meet a minimum (visible) titer rather than maximizing titer. Meeting the third criterion was the most challenging for the final engineering implementation of the sensor, and is the focus of this chapter. We chose to use two pigments (lycopene and β-carotene) from the linear carotenoid pathway with the expectation that it would facilitate the creation of discrete color states: each molecule of red lycopene could be stoichiometrically converted into orange β-carotene upon induction of the appropriate enzyme by the presence of sufficient zinc, leaving no residual red color in the orange state. This advantage is also a potential challenge, though, if that zinc-inducible promoter has substantial baseline uninduced transcription of that enzyme, which could prevent accumulation of lycopene. However, our application constrains selection of promoters: the promoter must be zinc-inducible, and there are few well-characterized zinc-inducible promoters.

Here, we present a proof-of-principle, metabolically engineered bacterial biosensor with pigment outputs that require no equipment for measurement and interpretation, for potential use in micronutrient (zinc) blood testing. We present the initial results from a straightforward implementation of the desired biosensor, which indicated the need for metabolic engineering in order to achieve the desired discrete color states. We explore multiple avenues to achieve the desired outcome, and we assess which are necessary and sufficient for this specific application. The trends identified in

optimizing the construction of the sensor are likely generalizable to similar pigment-based micronutrient sensors or whenever promoter selection is constrained. As metabolic engineering finds more diverse applications, it is likely that techniques to not just optimize production but tightly control it will be increasingly necessary.

2.2 Materials and methods

2.2.1 Materials

T4 DNA ligase, T5 exonuclease, Taq ligase, Phusion polymerase, Q5 polymerase, and restriction endonucleases were purchased from New England Biolabs (Ipswich, MA, USA). QIAprep Spin Miniprep Kits, QIAquick Gel Extraction Kits,and QIAquick PCR Purification Kits were purchased from QIAGEN (Valencia, CA, USA). Lycopene (98%) was purchased from Cayman Chemical (Ann Arbor, MI, USA). β carotene (97%) was purchased from TCI America (Portland, OR, USA). SC-Ura amino acid supplement was purchased from Sunrise Science (San Diego, CA, USA).

2.2.2 Carotenoid extraction

1 mL of bacterial culture was pelleted at 16,000 rcf for 7 minutes. Cell pellets were resuspended in 50 µl of water from a MilliQ water handling system (EMD Millipore). Carotenoids were extracted with 1 mL of acetone at 55 C for 20 minutes with continuous shaking in a Grant Thermoshaker at 1400 rpm. Cellular debris was pelleted at 16,000 rcf and the supernatant was removed for analysis. All carotenoid extraction was carried out in low light conditions.

2.2.3 HPLC analysis

All HPLC analysis was conducted on a Shimadzu LC-20AD Liquid Chromatograph using a Shimadzu C18 4.6 mm x 50 mm column with a 5 µm particle size and a SPD-20A UV-Vis detector. The instrument was run with a flow rate of 0.6 mL/min and a solvent ratio of 90:10 acetonitrile:THF. Retention times and intensities were compared to analytical standards spiked into control extractions from DH10B cells and calibration curves to convert peak areas to analyte concentrations were constructed.

2.2.4 Cell Culture

For eGFP library expression, freshly transformed DH10B colonies were inoculated in triplicate into 5 mL LB media and were grown for 24 hours. 125 µL of each culture was aliquotted into 96-well plates and measured on a Biotek Synergy H4 plate reader for OD600 and fluorescence at 488 nm excitation and 509 nm emission. Samples were also analyzed on a BD Accuri C6 flow cytometer.

For zinc carotenoid experiments, each strain was inoculated from freshly transformed colonies in triplicate into LB and minimal media at the following concentrations of supplemented $ZnSO_4$: 0, 50, 500, 1000 µM (LB) and 0, 5, 50, 500 µM (Minimal).

To allow zinc titration, a modified minimal media based on M9 but lacking inorganic phosphate was developed containing the following: 2.5 g/L beta-glycerophosphate pentahydrate, 1.64 g/L KCl, 4.5 g/L NaCl, 1 g/L NH_4Cl, 3.9 g/L MES, 2 mM $MgSO_4$, 0.1 mM $CaCl_2$, 0.01% thiamine, 0.6% glycerol, and 1.92 g/L SC-Ura amino acid supplement. pH was adjusted to 7.4. The following antibiotics were used as needed for selection: carbenicillin (100 µg/mL), chloramphenicol (34 µg/mL), kanamycin (30 µg/mL).

Gradient agar plates were made by allowing supplemented media to gel on inclined petri dishes, forming wedges. The plates were then laid flat and filled in with unsupplemented media. LB gradient plates were made with three sections: supplemented 10 μM TPEN, LB alone, and LB with 250 μM $ZnSO_4$. Minimal gradient plates were made with two sections: plain minimal medium and 250 μM $ZnSO_4$. TPEN was used to simulate zinc deprivation in rich media.

2.2.5 Cloning and construct assembly

Most construct assembly was carried out via restriction endonuclease digestion of components and subsequent ligation and transformation following the BioBricks idempotent standard assembly. Constructs in pCC1FOS were first assembled as above in BioBrick-compliant vectors. These were then digested with NotI and ligated into pCC1FOS.

The initial attempted multi-state pigment-producing construct was assembled via Gibson assembly[69]. This method was also used to add ssrA tags to eGFP and CrtY and to remove illegal restriction sites for BioBrick standard assembly from coding sequences for *eGFP*, *zur*, and *tetR*.Plasmids and regulatory sequences

2.2.6 Plasmids and regulatory sequences

A list of all vectors used is provided in Table 1, along with their expected copy number. ZntR, Zur, and P_{znuC} were amplified from DH10B genomic DNA. pJBEI-6409 was obtained from Addgene (Cambridge, MA, USA) and is referred to here as pJBEI-MEV. P_{zntA} sequence was synthesized by Genewiz (South Plainfield, NJ, USA). eGFP was

provided by Julie Champion, and pCC1FOS was provided by Brian Hammer. All other parts, including ribosomal binding sites, promoters, and pigment biosynthesis genes, were obtained from the Registry of Standard Biological Parts and were sequence-confirmed before use.

Table 1: Vectors and source plasmids used in this work.

Vector or plasmid name	Putative copy number	Origin of replication
pJBEI-MEV	Medium	p15A
pSB1C3	High	PUC colE1
pSB1AK3	High	PUC colE1
pSB3C5	Low	p15A Mutated
pSB6A1	Medium	pBR322 colE1
pCC1FOS	Approximately single	F

2.2.7 Strain naming convention

Fluorescence library members were named by concatenating the name or Parts Registry part number of the promoter, the last two digits of the Parts Registry part number for the ribosomal binding site, and then potentially three letters indicating whether a strong (LAA) or weak (DAS) ssrA protein degradation tag was added (AANDENYALAA or

AANDENYADAS). Carotenoid test parts were named by concatenating the Parts Registry part number of the RBS in front of *crtY*, an indicator of whether there was a degradation tag on *crtY* (LAA, DAS, or nothing), and the last three characters of the name of vector the construct was cloned into (1C3, 3C5, 6A1, or FOS). The presence of +J indicates the carotenoid construct was co-transformed with pJBEI-MEV.

2.3 Results and Discussion

To move towards the goal of population-scale monitoring of blood micronutrient status (specifically zinc), a low-cost, portable, equipment-free approach is necessary. The overall workflow of the final envisioned biosensor is illustrated in Figure 2A: sensor cells would be lyophilized or otherwise preserved for long term storage. A blood sample would be separated in the field via a low-cost, equipment-free approach such as the egg beater centrifuge[51] or paper centrifuge[52]. The resulting plasma would then be added to the preserved cells (potentially with additional, zinc-free defined medium), and the cells would produce different pigments in response to the levels of zinc in the physiologically relevant range of 8-15 μM[8] corresponding to normal, borderline, and low levels of zinc.

To implement the desired functionality, we designed a circuit using heterologous pigment production pathways driven by zinc-responsive transcription factor/promoter pairs present in *E. coli* (Figure 2B). The first heterologous pigment production pathway was the purple violacein biosynthesis pathway, which uses the *vioABCDE* operon (originally derived from *Chromobacterium violaceum*) to produce violacein from endogenous tryptophan. The second pigment production pathway was carotenoid biosynthesis, which uses the *crtE*, *crtB*, and *crtI* genes to produce red lycopene starting from endogenous

FPP, and uses *crtY* to produce orange β-carotene from lycopene; these genes were originally derived from *Pantoea ananatis*. Expression of these pigment production pathways was driven by two endogenous *E. coli* zinc-responsive promoter/transcription factor pairs, P_{znuC}/Zur and P_{zntA}/ZntR, which control expression of zinc importer and exporter genes, respectively. (Zur is a zinc-activated transcriptional repressor and ZntR is a zinc-activated transcriptional activator.) Previous work[38] suggested that Zur is able to fully repress expression from P_{znuC} at approximately 10 μM zinc, while induction of transcription from P_{zntA} should begin at least by 100 μM zinc (preliminary results suggested induction by 10 μM) with full induction not until approximately 1.1 mM[31].

These pieces were then combined together such that the circuit would provide discrete color states of purple, red, and orange depending on the zinc concentration of the sample. P_{znuC} was used to drive expression of *vioABCDE* and P_{zntA} was used to drive expression of *crtY*; *zntR* and *zur* were expressed from the same plasmid using their genomic promoters, while *crtEBI* was expressed from a mutated pλ-based, extremely weak promoter (avoiding toxic expression; discussed in Chapter 4). At low zinc concentrations (below 10 μM), transcription from P_{zntA} would be low and transcription from P_{znuC} would be induced, resulting in violacein biosynthesis (which is so dark as to visibly overwhelm minor lycopene production). At borderline levels of zinc (approximately 10 μM), Zur would become activated and repress expression from P_{znuC}. This would repress expression of the violacein biosynthesis operon, but expression of *crtY* to produce β-carotene would not be sufficiently induced, resulting in the production of only the red

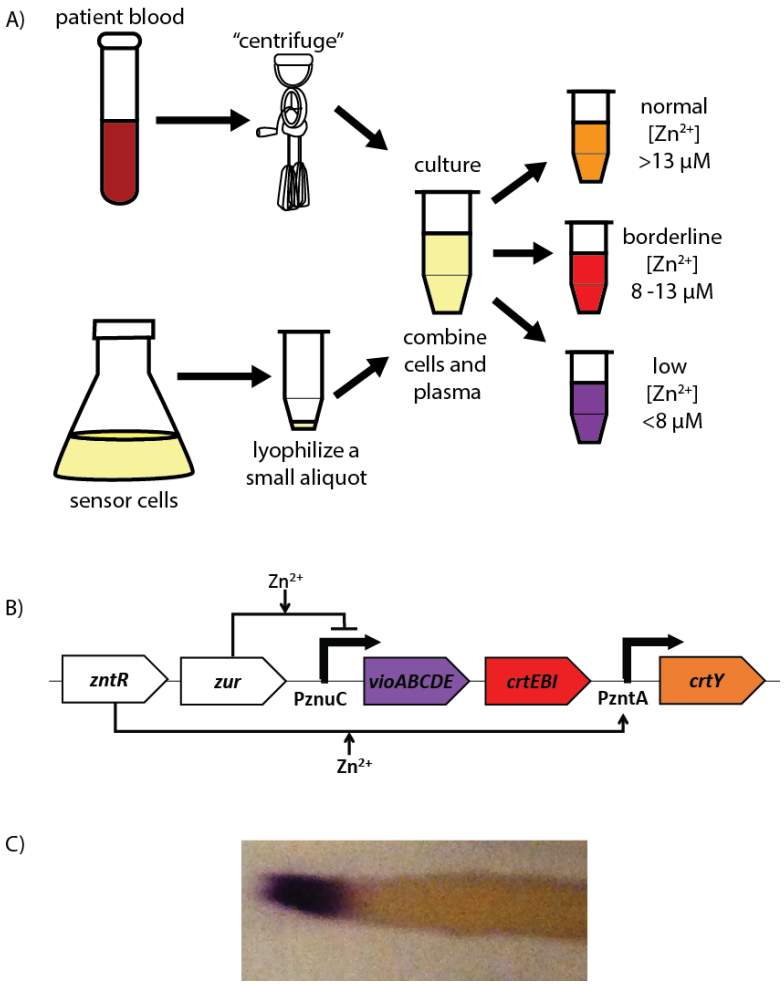

Figure 2: An initial synthetic biology-based zinc biosensor for application to equipment-free blood tests. a) A schematic of the workflow envisioned for the eventual final implementation of the diagnostic biosensor. Cells from general culture (bottom) are lyophilized for long-term storage. A blood sample (top) is centrifuged using minimal equipment on-site technique such as an egg beater[70] or paper centrifuge[52] to separate plasma, which is then added to the stored cells. These cells then produce pigment (right) based on the level of zinc in the plasma sample. Physiological concentrations of zinc are included for reference. b) Schematic of the circuit design intended for implementation of the initial biosensor. Transcriptional regulators ZntR and Zur are expressed on the same plasmid as the construct with violacein synthesis driven by the zinc-repressible P_{znuC} promoter, lycopene synthesis driven by a weak promoter, and the gene catalyzing the transformation of lycopene to β-carotene driven by the zinc-inducible P_{zntA} promoter. The bolded zinc annotation for P_{zntA} indicates that activation by zinc happens at higher concentrations than for P_{znuC}. c) Streak from a zinc gradient plate demonstrating direct transition from purple to orange without an intervening lycopene-dominated, red state. (Image contrast was adjusted to reduce the background from the agar plate; the original image is included in Figure 26)

pigment lycopene. At normal levels of zinc (over 10 μM), violacein production would still be repressed, but ZntR would then be activated and *crtY* expression would increase, facilitating the transformation of lycopene to β-carotene and yielding only orange pigment.

2.3.1 Initial circuit restricted to two distinct color states

We implemented the circuit design and expressed it on a high copy number plasmid in *E. coli*. The entire construct was sequence confirmed. The behavior of the implemented construct is shown in Figure 2c, as a streak on a zinc gradient plate. There is a clear, fairly sharp transition between two color states, purple (low zinc) and orange (high zinc), but no observable red (intermediate zinc) state. This behavior provides a number of key insights. First, the fact that *crtEBI* is very weakly and constitutively expressed is not a problem, as the dark color produced by violacein overwhelms any potential background signal of carotenoid production. Next, the repression of violacein production at higher zinc concentrations is sufficient to allow for the carotenoid production to be visible without any interference from leakiness of the P_{znuC} promoter. Finally, the basal uninduced expression of *crtY* from P_{zntA} at low and intermediate zinc levels is too great to allow precise control over the pathway, as lycopene is converted to β-carotene even at zinc levels where crtY should not be strongly induced.

2.3.2 Absence of a lycopene-only state is due to overlap in expression regimes

To investigate the cause of the absence of a lycopene-only state, we implemented a fluorescence-based construct to assess the induction and repression of P_{zntA} and P_{znuC}, respectively. Figure 3a shows the structure of this construct: RFP expression is driven by

the zinc-inducible P_{zntA} promoter, while GFP expression is driven by the zinc-repressible P_{znuC} promoter, with the transcription factors for each promoter (ZntR and Zur, respectively) constitutively expressed from the same high-copy plasmid. Figure 3b shows the quantitative results of GFP and RFP expression from the promoters. It is thus clear that while P_{zntA} and P_{znuC} can be significantly induced and repressed, respectively, there is some overlap in their expression regimes, whether due to their response curves to zinc or due to baseline leaky expression. It is worth noting that most of the repression from P_{znuC} occurs over the low concentrations of zinc, yet there is clearly (Figure 2c) a regime where violacein is not visible. Since violacein is much easier to detect visually than the carotenoids, this suggests that even though there is measurable fluorescence (and thus measurable leakiness) for this test construct, the production of violacein corresponding to that level of fluorescence would not be visually detectable. Combined with knowledge that the maximum repression of P_{znuC} has been shown to happen at the bottom end of the P_{zntA} induction range, this supports the idea that the reason why no lycopene-only state is detectable is that *crtY* expression is too great at low zinc levels, rather than *vioABCDE* expression being too great at higher zinc levels. Expression of mRFP from P_{znuC} and P_{zntA} on parallel regulated constructs suggests that visibly there is likely to be a significant region of non-overlap between the repression of P_{znuC} and the induction of P_{zntA} (Figure 27)

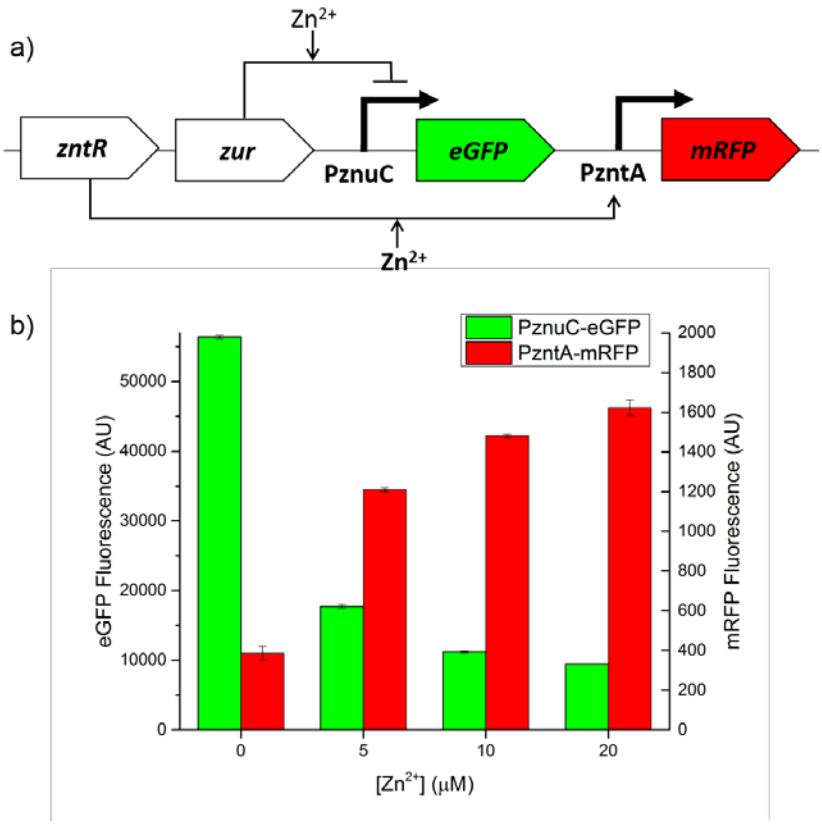

Figure 3: Fluorescence reporter construct shows overlap in P_{znuC} and P_{zntA} expression. a) Schematic of the reporter construct used to simultaneously measure expression from P_{znuC} and P_{zntA} promoters. The transcription factors regulating expression from each promoter were included on the plasmid. The bolded zinc annotation for P_{zntA} indicates that activation by zinc happens at higher concentrations than for P_{znuC}. b) Expression from each promoter in arbitrary units specific to each fluorescent protein (RFP is right axis, GFP is left axis). There is significant induction of expression from P_{zntA} even at low levels of added zinc and significant repression of expression from P_{znuC}, suggesting that the baseline expression of *crtY* may be the cause of a lycopene-only state being difficult to capture. Error bars represent standard error of the mean.

2.3.3 Fluorescence reporter library for characterisation of post-transcriptional control

In order to gain sufficient control over the lycopene to β-carotene reaction step to generate a three-color-state sensor, we then sought to adjust post-transcriptional

regulatory elements. Specifically, modification of ribosomal binding sites and tagging of proteins for degradation were identified as the simplest approaches to decrease the level of CrtY at low levels of zinc. To do this most efficiently, we characterized the impact of multiple regulatory elements within our specific host strain using an eGFP reporter. We also sought to characterize the strength of multiple potentially constitutive promoters (which could drive expression of the zinc-responsive transcription factors) and the strength of our zinc-responsive promoters (without coexpressed regulators). This characterization was intended to facilitate more rational and focused selection of regulatory elements for the final sensor construct rather than performing combinatorial syntheses that would be challenging based on product toxicities; the results of the characterization are presented in Figure 4.

Taken together, manipulating promoters and post-transcriptional regulatory sequences yielded over five orders of magnitude of variation of fluorescence (Figure 4a). Each level alone (transcriptional and post-transcriptional) offered at least three orders of magnitude dynamic range, with low-fluorescence measurements being confounded by limits of detectability even at high plate reader gain settings.

Measurements of promoter strength across multiple sets of post-transcriptional regulatory sequences provided information for later selection of promoters (i.e., for *zntR* and *zur*) and provided an estimate of the strength of the P_{znuC} and P_{zntA} promoters. Unsurprisingly, the P_{λ}-based promoters (R0040 and R0011) were the strongest. Known weaker promoters (J23117 and J23116) performed roughly as expected, though the difference between these two promoters was greater than previously reported. We used the expression levels of these promoters to characterize some of the transcriptional behavior of the two inducible

promoters. Since these constructs had no supplementary regulator expression (i.e. Zur or ZntR) in order to be consistent with the rest of the library, the expression from P_{znuC} is indicative of essentially unrepressed transcription, while expression from P_{zntA} is indicative of essentially uninduced transcription. We found that baseline expression from P_{zntA} was stronger than at least one known weak constitutive promoter, J23117. This suggests that the underlying reason for the lycopene state being difficult to stabilize may be that the baseline transcription from P_{zntA} is sufficiently high to result in significant production of CrtY.

Changing ribosomal binding sites (RBSs) also enabled many orders of magnitude of reduction for overall gene expression. Figure 4b demonstrates the impact of using four different ribosomal binding sites taken from the Registry of Standard Biological Parts: B0031-B0034. The patterns of RBS strength as measured here were qualitatively consistent with previously measured values, with a few exceptions. First, we found B0031 was slightly stronger than B0032 rather than vice versa; this was consistent across all promoter strengths. Second, we found that expression from B0034 was usually not much stronger than from B0031, whereas previous reports have shown an order of magnitude difference between these two RBS options. Flow cytometry for library members with strong promoters (Figure 4c) showed that the reason for the unexpected low levels of fluorescence from B0034 is a bimodal population of low-expressing and high-expressing cells. This population split was ultimately due to mutation of promoters in library members with the B0034 RBS due to physiological stress from the high levels of protein expression: while measurements of all library members were done from fresh transformants from sequence-verified DNA, plasmid sequencing for B0034 library

transformants exhibiting these bimodal populations returned multiple competing signals indicating that the dual operator sites in R0040 and R0011 had combined to heavily mutate the promoter.

Figure 4d shows that LAA and DAS protein degradation tags can significantly curtail the net expression of a gene and that the LAA tag can do so by three orders of magnitude. We tagged the C-terminus of eGFP with one of two ssrA tags, the strong AANDENYALAA tag or the weaker AANDENYADAS tag. These tags induce sspB-mediated binding to the ClpX and ClpA proteases, which increases a protein's degradation rate[71]. The magnitude of the effect of the LAA tag is as much as or greater than the impact of using the lowest-efficiency ribosomal binding site. Of note is the interaction between expression level and the efficiency of repression via tagging for protein degradation. The LAA tag effectively reduces protein levels even for highly-expressed proteins, whereas the DAS tag is most effective for lowly-expressed proteins (giving a reduction of up to 10-fold; for example, B0033 RBS or weak promoters) compared to highly-expressed proteins (with reductions typically closer to 2-fold; for example, B0031 RBS with a strong promoter). This suggests that overall gene dosage may play a role in the effectiveness of post-transcriptional regulation in some cases, though the mechanism by which this would occur is unclear.

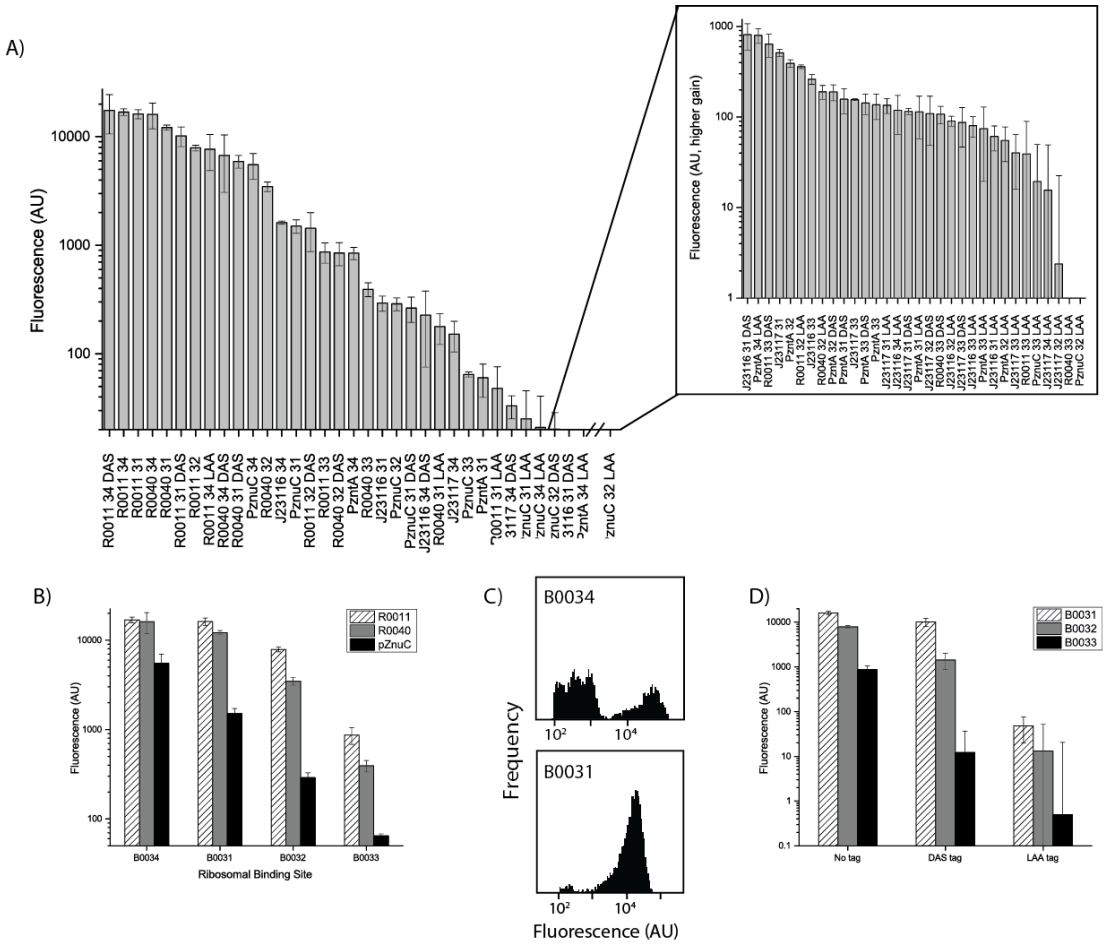

Figure 4: A library of regulatory elements provides five orders of magnitude of control over expression. a) Fluorescence measurements of the library of regulatory element combinations. Inset illustrates fluorescence levels at a higher gain setting for library members with insufficient fluorescence to be measured accurately at the same gain setting as in the main plot. Construct names are the promoter name (R0011 & R0040 known strong promoters, J23116 &J23117 known weak promoters, and the P_{znuC} and P_{zntA} promoters), followed by an indicator of the ribosomal binding site part number (31-34), and then the degradation signal added to the protein sequence (no signal, weak DAS signal, or strong LAA signal). Error bars represent the standard error of the mean. b) Changing ribosomal binding sites for strong or weak promoters provides orders of magnitude reduction in expression. Error bars represent the standard error of the mean. c) Flow cytometry plots showing increasingly mixed populations for higher-strength (B0034) ribosomal binding sites (top) as opposed to weaker ribosomal binding sites (bottom), indicating that the bulk fluorescence measured for B0034 RBS under the strong promoters used here is an underestimate of the actual per-cell fluorescence for B0034 under unaltered promoters. Sequencing of plasmid DNA from cultures with bimodal populations yielded mixed traces, indicating mutation of the plasmids to reduce…

Figure 4 continued: …fluorescence production. d) Degradation tags can also yield orders of magnitude reduction of protein levels; the strong LAA tag typically provides two or more orders of magnitude of decrease in fluorescence, while the weaker DAS tag is more variable in its reduction of fluorescence. Error bars represent standard error of the mean; only positive error is indicated due to the logarithmic scale of the plot because the lowest values are near the detection limits of the instrument and would include zero in the opposite direction.

2.3.4 Post-transcriptional control of carotenoid production

Using this library of regulatory element combinations and the insights gleaned from them, we then assembled thirteen targeted carotenoid-expressing constructs to identify those that could produce two distinct states: one dominated by lycopene and one dominated by β-carotene, which was not observed in our initial attempts. The test constructs consisted of (Figure 5a) *crtY* being driven by the P_{zntA} promoter and *zntR* driven by a weak constitutive promoter. *crtEBI* was cloned in without an explicit promoter (for reasons of severe growth restriction which are discussed and explored in Chapter 4) so as to yield very low transcription, consistent with previous work where *crtEBI* had an inducible promoter that was never induced since its expression was detrimental to cell growth[64]. Regulatory elements of *crtY* were varied to control conversion of lycopene to β-carotene.

To manipulate levels of CrtY, we selected variants from the fluorescence characterization presented in Figure 4, as well as additional methods for manipulation of expression levels. We varied the RBS of *crtY* and added the strong (LAA) degradation tag to *crtY*. We did not explore further the strong B0034 RBS since preliminary pilot experiments indicated we would need such substantial reduction in expression to allow a lycopene-dominated state that RBS variation would likely be necessary. We also added another

level of control over the amount of gene expression via variation of vectors, employing high, medium, low, and essentially-single copy vectors. This would titrate not only the total amount of CrtY in the cell from leaky or mildly-induced expression, but also the expression of *crtEBI*, which also may cause toxicity and could prevent greater accumulation of carotenoids.

Changing only the RBS of *crtY* was insufficient to yield a distinct lycopene state. Replacing the original B0034 RBS with the B0033 RBS yielded no visible lycopene in an uninduced state (and essentially no measurable lycopene), but a substantial amount of β-carotene (Figure 5b), despite the B0033 RBS being two to three orders of magnitude weaker than the B0034 RBS used in the original construct. (Again, this supports the earlier assessment that the reason why no lycopene-only state could be detected was due to too much *crtY* expression at low zinc rather than too much *vioABCDE* expression at high zinc.) Even combining a lower-strength (B0032) RBS with a strong (LAA) degradation tag, which should yield four or more orders of magnitude less CrtY, was not sufficient to allow lycopene to persist in an uninduced state (Figure 5c).

When the vector was varied, substantial amounts of lycopene were produced (Figure 5d). Medium and low copy number plasmids yielded substantial lycopene at low zinc that is repressed at high zinc, and a fosmid yielded such substantial production of lycopene that CrtY could not be induced enough to consume it (yielding a single state in the pathway dominated only by lycopene instead of by β-carotene). The most promising combinations appear to be the medium- and low-copy plasmid with a degradation tag and a moderate RBS, yielding a lycopene-dominated state and a β-carotene dominated state, though with

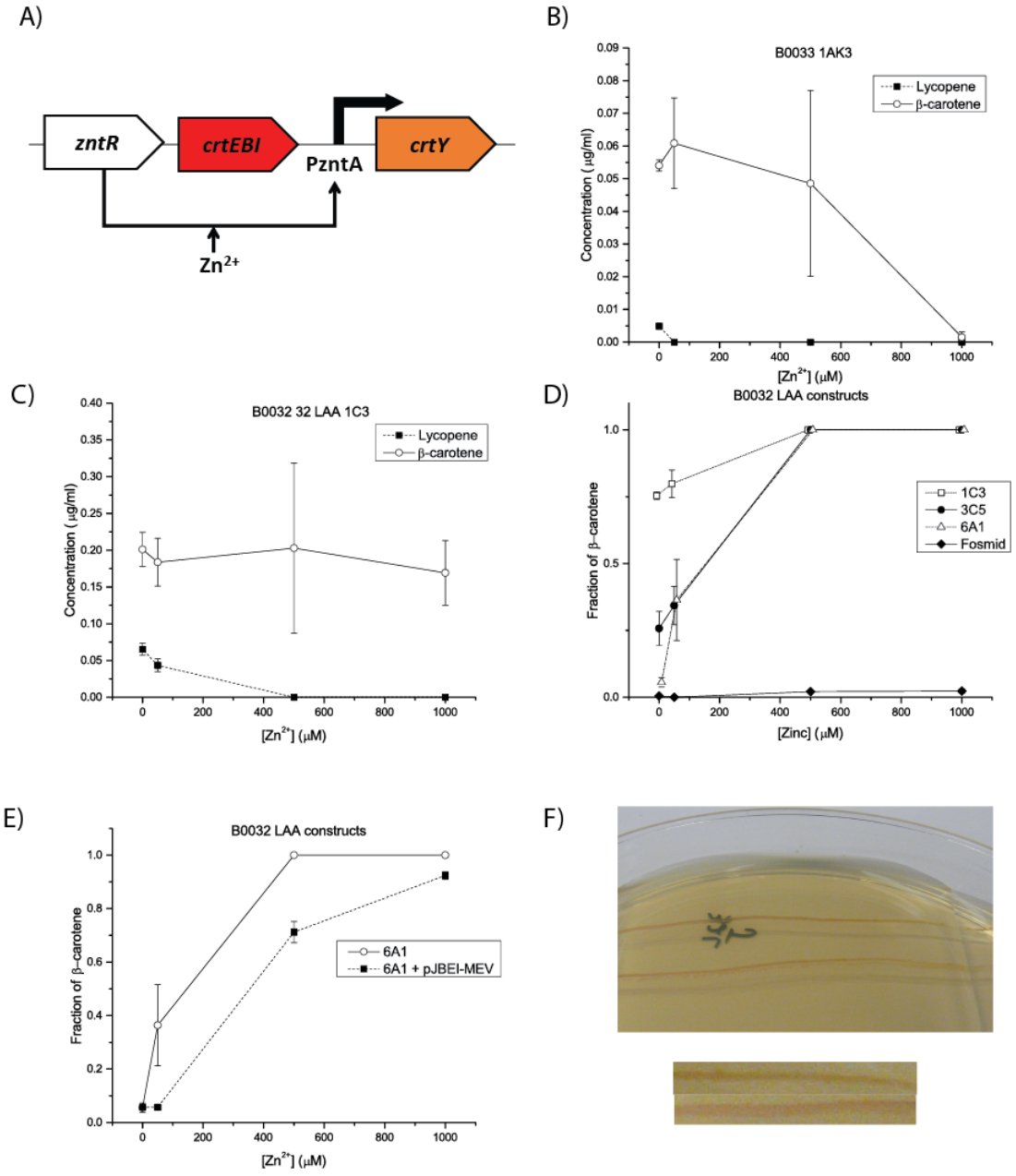

Figure 5: Varying regulatory sequences and vector enables a lycopene-dominated state and allows manipulation of the concentration at which it disappears. All error bars represent the standard error of the mean. All measurements were taken at 0, 50, 500, or 1000 µM zinc, though an offset has been applied in panel D for visualization purposes. a) A simplified version of the construct used to test only carotenoid production for a selection of constructs with varied regulatory sequences and vectors. Ribosomal binding sites and degradation tags are omitted for simplicity. b) Changing only to a very weak ribosomal binding site is insufficient to produce a lycopene-only state, and generally insufficient to produce any lycopene at all. This suggests that multiple levels of control must be used. c) Using a…

Figure 5 continued: …moderate ribosomal binding site and a strong degradation tag (LAA) enables the detectable production of lycopene but still does not enable a lycopene-dominated state. d) Changing the vector carrying the construct from panel C enables the presence of a lycopene-only state. For the lowest-copy plasmid (the fosmid), so little CrtY is accumulated even at full zinc induction that only a lycopene-dominated state can be observed. The medium-copy 6A1 vector offers two distinct states. e) Co-transforming with a plasmid containing the mevalonate pathway (pJBEI-MEV) to supplement production of lycopene alters the transition point between the lycopene and β-carotene states. At 50 µM Zn^{2+}, the pJBEI-MEV-supplemented cells have still produced orders of magnitude more lycopene than β-carotene, while the non-supplemented strain is already transitioning to a β-carotene state. Of note is that the lycopene production at no supplemented zinc is three times higher in the supplemented strain, as expected. f) Streak of pJBEI-MEV-supplemented strain from panel E on zinc gradient plates showing a fairly distinct transition between states. The cells change from red to orange going left to right. Below the plates are two parts of the same image cropped next to each other to highlight the color differences.

less switch-like behavior than expected. Similar behaviors were observed in minimal medium cultures (Figure 6). Worth noting is that in many constructs, the lycopene and/or β-carotene levels decrease at the 1 mM zinc condition. In previous literature, the full induction level of P_{zntA} was found to be at 1.1 mM zinc, and *E. coli* has been shown to be capable of normal growth in an excess of 1 mM extracellular zinc. We suspect that the additional metabolic stress of the cells from substantial transcription, translation, and pigment synthesis, combined with the toxicity of carotenoid operon genes and potential interference with zinc homeostasis due to overexpression of native regulators, increases the sensitivity of the engineered cells to zinc. Fortunately, this level of zinc is nowhere near that which would be relevant to the ultimate application of this biosensor in a blood micronutrient diagnostic[8].

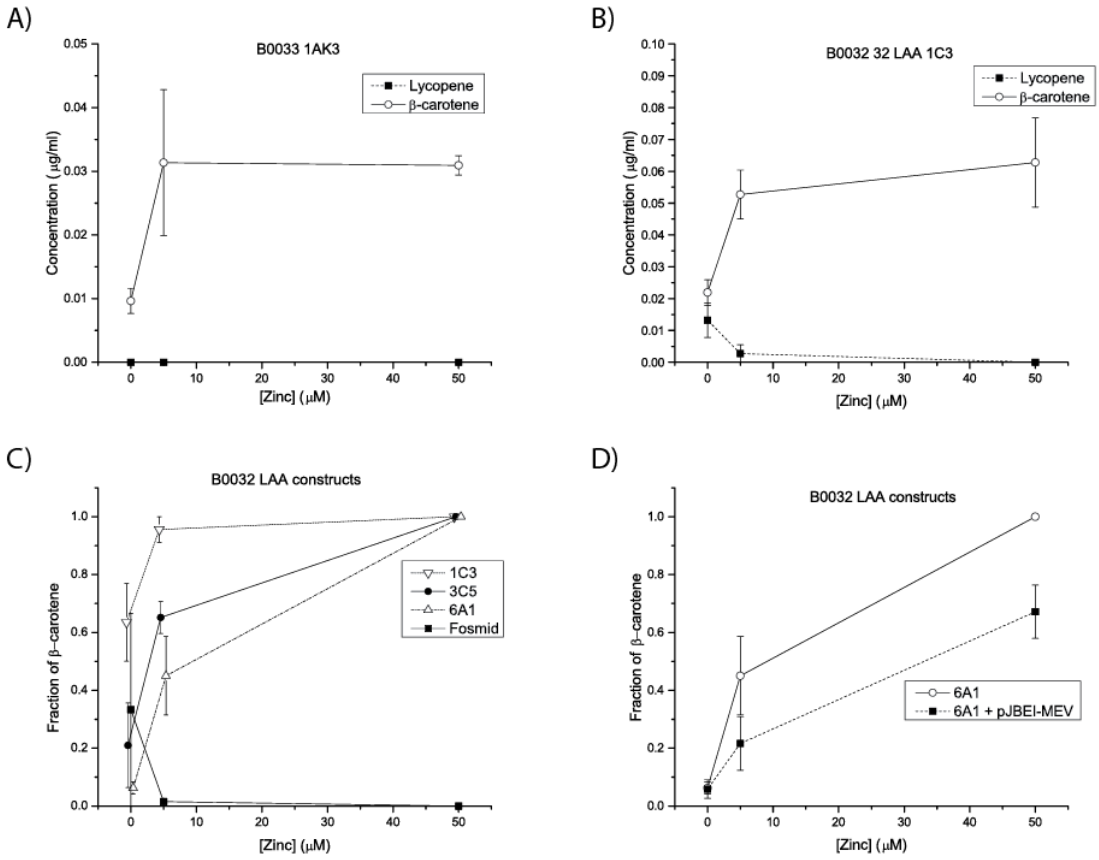

Figure 6: M9 cultures show similar behavior to LB cultures. Panels A through D in this figure correspond to panels B through E in Figure 5, showing that the behavior of the cells in minimal and rich medium (which includes an expected baseline level of zinc) is extremely similar. Error bars all represent the standard error of the mean. Measurements were all taken at 0, 5 and 50 μM Zn^{2+}, though in panel C an offset has been applied for visualization purposes. A) Changing only to a very weak ribosomal binding site is insufficient to produce a lycopene-only state, and generally insufficient to produce any lycopene at all. This suggests that multiple levels of control must be used. B) Using a moderate ribosomal binding site and a strong degradation tag (LAA) enables the detectable production of lycopene but still does not enable a lycopene-dominated state. C) Changing the vector carrying the construct from panel C enables the presence of a lycopene-only state. For the lowest-copy plasmid (the fosmid), so little CrtY is accumulated even at full zinc induction that only a lycopene-dominated state can be observed. The medium-copy 6A1 vector offers two distinct states. D) Co-transforming with a plasmid containing the mevalonate pathway (pJBEI-MEV) to supplement production of lycopene alters the transition point between the lycopene and β-carotene states. At 50 μM Zn2+, the pJBEI-MEV-supplemented cells still have still produced much more lycopene than β-carotene, while the non-supplemented strain is already transitioning to a…

Figure 6 continued: … ß-carotene state. Of note is that the lycopene production at no supplemented zinc is three times higher in the supplemented strain, as expected.

2.3.5 Enhancing lycopene production affects sensor response

Another alternative to manipulate the apparent response of P_{zntA}-driven expression is to stimulate the overall production of lycopene in the cells. The root cause of a β-carotene-only state is that there is sufficient CrtY to enzymatically act on all of the lycopene that is present. To this point, we had primarily explored just approaches designed to decrease the levels of CrtY. Instead, we could increase the production of lycopene such that there is insufficient CrtY to act on all of the lycopene in the cell. Lycopene production, or more generally the production of carotenoids and isoprenoids, has long been a target for metabolic engineering studies, with significant advances made in terms of overproducing background strains and identification of multiple independent ways to increase carotenoid titers. One well-known approach is the introduction of a mevalonate pathway to supplement the production of precursors for the carotenoid and isoprenoid pathways[64].

By co-transforming engineered carotenoid constructs with a plasmid containing the mevalonate pathway (pJBEI-MEV), we substantially affected the response of the carotenoid-producing sensor (Figure 5e). A moderate RBS combined with a strong degradation tag and a low-copy plasmid initially yielded a system offering a crossover in production from lycopene to β-carotene. At approximately 50 μM of zinc, the levels of lycopene and β-carotene were of the same order of magnitude. However, by supplementing with pJBEI-MEV, production of lycopene was increased threefold, and at 50 μM lycopene levels remained much higher than β-carotene levels. This effectively

changed the "switching point" between lycopene and β-carotene states in the supplemented cells. This behavior was observed both in rich medium and in minimal medium. While in this case it moved the switching point perhaps to a level beyond physiological relevance, application of this approach with other constructs allows for another level of manipulation to engineer the precise response desired.

2.3.6 Engineered distinct red and orange system states

Figure 5f demonstrates that a transition between red and orange states is now possible after substantial pathway engineering. In order for both states to be possible for the same cells, multiple components needed to be precisely controlled in combination. With a moderate RBS, a strong degradation tag, and the medium-copy plasmid, levels of CrtY were limited at low zinc levels (preventing reaction of lycopene) but were adequately inducible to allow a switch to β-carotene at higher zinc levels. Selection of a different plasmid in this configuration would have different results: for example, on the fosmid, CrtY levels are limited so much that the β-carotene state can never be reached (though for other configurations, for example without LAA tags, the fosmid did allow for accumulation of CrtY and production of β-carotene). Supplementation of lycopene production via the mevalonate pathway enabled further tuning of the zinc levels at which that transition occurred. Taken together, these strategies enabled the ultimate within-pathway state-switching goal of the biosensor.

2.4 Discussion

In this chapter, we present the design and engineering of a biosensor capable of responding to extracellular levels of a micronutrient, zinc, with potential application to

blood test diagnostics. Specifically, the biosensor was designed to produce pigment, rather than fluorescence or related readouts, to facilitate equipment-free usage since the color of the readout can be assessed with the naked eye. Our initial efforts yielded only a two-state sensor, despite the design of the construct to have three distinct regimes of pigment production. (A two-color sensor would still be useful, though having a third state provides increased zinc status resolution and thus more information for determining when and where to perform nutritional interventions.) This prompted the need for metabolic engineering of the construct, as baseline levels of the last gene in one pigment production pathway prevented the accumulation of an intermediate intended to represent a distinct readout state in the device.

These efforts present advances in a number of different directions within the purview of developing metabolically engineered pigment-based biosensors. We integrated two different heterologous pigment production pathways, and were able to shut one off completely so as to enable the visibility of the other. Our use of natural zinc-responsive promoters and transcription factors provided one system (Zur/P_{znuC}) that was appropriate for our application, but another system (ZntR/P_{zntA}), with a wide dynamic range and excessively high baseline expression when in an uninduced state, required significant engineering to be usable in the sensor. Engineering efforts were limited to components besides the promoter and regulator themselves, as mutating those would likely have been prone to loss of zinc specificity [72] (particularly true given the mechanism of action of ZntR). Without promoter engineering as a viable possibility, we focused on post-transcriptional regulation to harness a very small portion of the dynamic range of the system and to sufficiently suppress expression to allow multiple color states within a

single pathway. The system started with no switching capability whatsoever, but we were able to engineer in switching capability as well as demonstrate our ability to change the level at where the switch occurs. This is particularly relevant since our application limits us to the small fraction of ZntR's dynamic range that is physiologically relevant.

We achieved our goals via a directed, rational approach to synthesizing pigment-producing constructs, driven by knowledge gained from initial fluorescence characterization of regulatory elements. We did this due to the difficulty in high-throughput screening for our desired phenotype: screening a library of transformants for a single color at a single zinc concentration does not provide sufficient information, decreasing the potential throughput substantially. Gradient plates as a secondary screen are too qualitative and spatially complex, though a replica plating approach on multiple zinc concentrations could have been a viable strategy. Ultimately, though, our rational approach also provided deeper insight into the requirements for getting the correct level of regulation to allow multiple color states in one pathway, which may not have emerged from a library screen.

To sufficiently control the production of our most downstream enzyme in the carotenoid production pathway, CrtY, multiple levels of regulation were necessary. Combining the use of weaker ribosomal binding sites with protein degradation tags and changing the vector allowed for the establishment of inducible color change and tuning of the zinc concentration at which the color change occurred. While we observed that the lower copy vectors were more effective at allowing a lycopene-dominated state, this phenomenon cannot be solely attributed to copy number since vector-specific differences in readthrough transcription affect the level of transcription of (promoterless) *crtEBI* and

thus the balance of lycopene and *crtY*. Nonetheless, our data, along with intuition, suggest that copy number likely plays a role in this process; even if not, the fact that selection of vector has such a substantial effect on the metabolic phenotype of the cells is still an important observation.

We used fluorescence measurements on a library of regulatory combinations as the basis for rational exploration of the design space for production of carotenoids. It is possible that the reduction in fluorescence caused by the addition of degradation tags was not just due to increased degradation, but caused also by decreased fluorescence per molecule due to the tag changing the protein conformation. While this was not something controlled for and tempers the interpretations of tag effectiveness from the fluorescence data, the carotenoid production results are consistent with our interpretation of the fluorescence data on the importance of degradation tags for tuning the behavior of the cells.

We also note that while the use of native, rather than orthogonal, sensing (zinc-responsive) elements is not commonplace, it did not prevent successful metabolic engineering of the strain. While this aspect of our approach may have led to more non-linear impacts of the various regulatory changes we implemented due to impacts on host cell behavior or impacts of host cell genomic expression, this disadvantage was outweighed by the many tools available for genetic manipulation in *E. coli* and the fact that the regulators we used are well-characterized zinc-responsive elements, one of which was already known to respond within a physiologically relevant concentration range.

It is worth noting that these experiments were carried out at a single temperature that is not necessarily the same as the physiological temperature of the organisms used as

sources for the heterologous pigment biosynethesis pathways. Since it is known that enzymatic activities of some of the components we have employed are temperature-dependent (i.e., enzymes in the violacein pathway[66]), it is possible that some characteristics of our sensor's behavior may also change as a function of incubation temperature. Exploring the temperature dependence of the switching point of our construct is an important next step, as the results will have design implications for the ultimate implementation of a blood testing device incorporating our sensor.

The desire for tightly controlled but inducible transcription is not unique to our application. For example, there has been recent work developing dynamically controlled metabolic engineering, where the genes for target production remain uninduced during growth phase to avoid toxicity, or where genes crucial for growth are turned off at a specific time to redirect carbon flux towards the production of desired products[73-76]. While one way to achieve this would be through small molecule induction after sufficient growth, as might be done for protein expression, there have also been efforts to have automated induction upon sufficient accumulation of cells, for example via response to phosphate limitation or quorum-sensing molecules[77-81]. These latter cases are the most likely to experience issues similar to the challenges in our biosensor: where the promoter selection is driven by the specific needs of the application and is relatively inflexible, meaning that control of expression must be exerted through other means.

2.5 Conclusion

The sensitivity of metabolic pathways to low levels of enzymatic expression – a key aspect of what one could call "precision metabolic engineering" – is not something that

has been widely explored in the literature. Nonetheless, it is an extremely important aspect to harnessing metabolism for biosensor applications while minimizing the transcriptional and metabolic burden on cells (and thus using the same pathway to produce multiple different visible outputs). At the outset, we naïvely implemented the pigment-based sensor without addressing the underlying metabolic pathway engineering problem. It soon became clear that at least some degree of pathway engineering would be critical to make a functional reporter that could express two different carotenoids. While we initially used pathway engineering to allow a lycopene-only intermediate state to persist, we also found that tuning the carotenoid pathway could strongly affect sensor response. Adjusting both upstream and downstream pathway expression controlled the zinc concentration at which pigment production switched, allowing more control over what concentrations would map to ‘intermediate zinc’ and ‘high zinc’ outputs.

Overall, the most difficult aspect of the engineering task was compensating for leaky expression of enzymes downstream of the first pigment indicator. This suggests that (when possible) the selection of regulatable promoters with the lowest levels of leakiness may outweigh other important factors (e.g., whether it is inducible or repressible, or the expected response threshold) when designing future pigment-based sensors. However, for natural promoters this will often not be possible, necessitating the precision engineering efforts that we have described. Ultimately, multiple levels of control were necessary to achieve the desired metabolite production given the limitations in inducible regulation and intermediate or product toxicity; we expect that such extensive control will typically be necessary in regulating the response of sensors using metabolite reporters. Perhaps the most interesting lesson for future strain design was that controlling the levels of

precursors for the heterologous biosynthetic pathways can affect the switch point of the circuit. This provides a powerful, modular, orthogonal approach to basic pathway engineering of heterologous pigment production pathways, and could be considered an earlier option in strain design if (as in the mevalonate pathway) there are well-established methods to adjust precursor availability to optimize pigment switching around input levels of interest from arbitrary sensors.

The approaches identified and lessons learned could also be generalizable to other "precision" applications where extremely selective production of specific molecules is critical, including the design of multifunctional (potentially portable) microbial cell factories that can produce different products in response to different environmental conditions. A key result of this work is that significant, combinatorial regulation was necessary in order to limit the immediate production of β-carotene in our construct; while it was unsurprising that pigments from two different heterologous pathways could be combined via a switch for a visible output, the level of control necessary to prevent the reaction of all lycopene to β-carotene was unexpected. While the level of control necessary would ultimately be dependent upon enzyme turnover number rate, knowledge that such levels would need to be so precisely regulated for pathway control will likely play a key role in other precision metabolic engineering applications in the future.

CHAPTER 3. IMPLEMENTATION OF A THREE COLOR ZINC SENSOR

3.1 Introduction

The previous chapter detailed our initial efforts to tune the output of P_{zntA} such that the two colored molecules from the carotenoid pathway would be available to us as output states for our sensor. This was done using standard techniques like altering RBS efficiency, controlling overall gene dosage with plasmids of differing copy number, and altering protein half-life through use of ssrA degradation tags, as well as the novel approach (at least from a synthetic biology perspective) of tuning sensor output independent of the sensory components by altering the availability of the native metabolic precursors to the carotenoid pathway, IPP and DMAPP. While we demonstrated the ability to tune performance of the carotenoid pathway to alter the behavior of pigment production in response to zinc, that work did not go so far as to successfully tune the response over a physiologically relevant concentration of zinc for a human serum zinc assay. Additionally, while we showed the proof-of-concept three color strain which led us to a detailed investigation of transcriptional, translational, post-translational, and metabolic strategies to control when different carotenoids are produced, we did not discuss any tuning of P_{znuC} and the other pigment used as a reporter, violacein.

In this chapter, we expand upon the work presented in Chapter 2 by varying expression of both regulators, ZntR and Zur, with the goal of enabling the transition between pigmented states between lycopene and ß-carotene within a reasonable concentration

range of zinc that would be present in human serum. We also present the tuning of P_{znuC} and violacein expression by altering the ability of Zur to bind P_{znuC} by introducing decoy operator sites for Zur, as well as the creation of an inverter for P_{zntA} by using it to control the expression of Zur, thus allowing increases in transcription from P_{zntA} in response to increases in zinc to map to a decrease in transcription from P_{znuC}. Finally, we investigate growth of *E. coli* and sensor response in cultures with varying amounts of normal human serum (NHS) and serum preprocessed by heat shock and/or removal of zinc with a chelating resin to simulate zinc deficiency.

3.2 Results and discussion

3.2.1 Dynamic range of promoter regulator pairs

In initial efforts, we identified that the expression levels of the zinc-responsive regulators ZntR and Zur can have a major impact on the dynamic range of the reporters that they regulate (data not shown). Since a requisite step in our efforts is the precise engineering of metabolic state to enable production of (hopefully) only one pigment at a time[82], a high degree of dynamic range would enable a transition between repressed or uninduced levels of a pigment that are not visually detectable and induced levels that are obvious to the naked eye in a reasonable amount of time. We thus first sought to characterize the dynamic ranges of the two regulator/promoter systems at varying expression levels of the regulators.

To identify regulator expression levels that maximize the range of transcription rates available over a physiologically relevant concentration range of zinc, a series of fluorescent reporter plasmids was constructed consisting of transcriptionally insulated

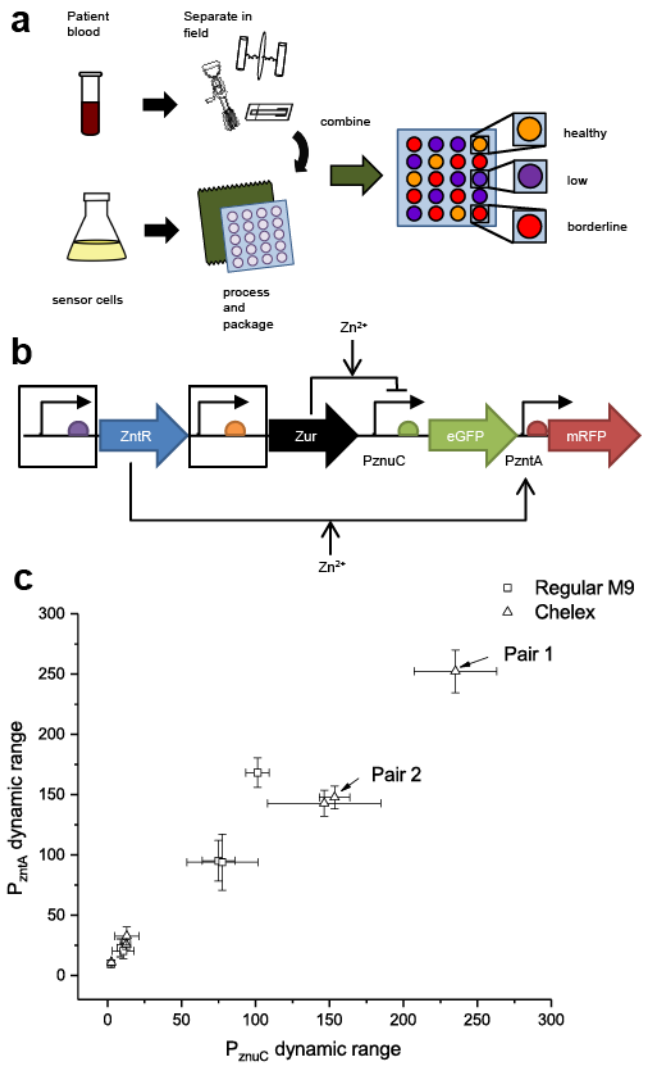

Figure 7: (a) Schematic of envisioned test implementation. Patient blood is collected in the field, separated using field-friendly approaches, and combined with packaged sensor cells. The cells grow and produce pigment indicative of subject micronutrient status. (b) Schematic of regulator test construct. The promoters and ribosomal binding sites (boxed) for zinc-responsive regulators ZntR and Zur were varied to determine optimal expression for improved dynamic range over physiologically relevant zinc concentrations. (c) Fluorescent reporter output demonstrating sensor dynamic range from 0 to 20 µM Zn^{2+} with different expression levels for ZntR and Zur. Regulator pairs one and two (arrows) were used in subsequent two and three color pigment biosensors. Error bars indicate standard deviation.

P_{zntA} and P_{znuC} controlling expression of mRFP and eGFP. The regulators ZntR and Zur were constitutively expressed with different combinations of promoters and ribosomal binding sites (Figure 7b). These plasmids were transformed into *E. coli* and grown in minimal media with and without treatment by Chelex 100, a zinc-selective chelating resin, each with and without 20 µM supplemented $ZnSO_4$. Fluorescent output of both reporters was measured and compared to determine promoter performance over this range of zinc. The dynamic ranges of both promoter/regulator systems are plotted against each other in Figure 7c. The two highest dynamic range regulator pairs (referred to hereafter as Pair 1 and Pair 2) were selected for subsequent experiments with two- and three-pigment output sensors.

These efforts yielded some straightforward results as well as others that were not quite as expected. Unsurprisingly, most of the best performance was observed in the resin-treated media; both regulator systems already exhibit some degree of response (induction or repression) starting at low micromolar levels of zinc or below, so the trace levels of zinc present in untreated medium would cause the unsupplemented medium to yield lower dynamic ranges. Interestingly, the highest dynamic ranges do not correspond in rank simply to the highest expected expression of regulators estimated by combining the relative translation rate predicted by RBS Calculator[83] and the previously-characterized relative transcriptional output of constitutive promoters (Table 2, Table 3). For example, in normal media for P_{zntA}, lower dynamic range over 20 µM was observed in 3-4 3-4 than in 2-4 7-1, even though the promoter controlling ZntR is exceptionally weak. A possible explanation for this behavior is that the two regulators have different affinities for zinc and are both competing for zinc from the same pool[36,84]. Overexpression of these zinc-

binding proteins likely affects the natural partitioning of zinc ions throughout the proteome. As a result, a change in expression of Zur could, for example, alter the availability of zinc for ZntR and thus change P_{zntA} transcriptional output for a given

Table 2: Rank order list of top six fluorescent reporter dynamic ranges of 0-20 µM zinc for P_{zntA} (left) and P_{znuC} (right).

P_{zntA} dynamic range	Rank order for ZntR	Zur apparent expression	ZntR apparent expression	P_{znuC} Dynamic range	Rank order for Zur	Zur apparent expression	ZntR apparent expression
252.3088	7-4 7-1c	480364	429402.1	235.0797	7-4 7-1c	480364	429402.1
168.3276	7-4 7-1	480364	429402.1	153.4526	3-4 3-4 c	334146.1	55663.23
147.7143	3-4 3-4c	334146.1	55663.23	146.4823	2-4 7-1c	480364	2650.63
142.8567	2-4 7-1c	480364	2650.63	101.292	7-4 7-1	480364	429402.1
95.211	2-4 7-1	480364	2650.63	77.5182	2-4 7-1	480364	2650.63
93.86331	3-4 3-4	334146.1	55663.23	74.88951	3-4 3-4	334146.1	55663.23

Table 3: Output from the RBS Calculator and relative transcriptional strength of promoters in Table 2.

ID	RBS Calculator prediction	Promoter	relative transcriptional output
31zur	2965.21	112	1
32zur	5074.87	113	21
33zur	353.89	117	162
34zur	15911.72		
34zntr	2650.63		

concentration of zinc.

The behavior between media with and without treatment by Chelex between regulator pairs is also noteworthy. For Zur/P_{znuC}, the three arrangements exhibiting maximum dynamic range were all in Chelex-treated media, and the next three were the same constructs in untreated media. The relative rank order of 3-4 3-4 and 2-4 7-1 is reversed in untreated vs treated media, however the results in both cases are close enough that the differences are not significant. For P_{zntA}/ZntR, the top two performers were 7-4 7-1 in each media type. It is interesting to note that nearly all of the top P_{zntA}/ZntR candidates seem to correspond more with expected Zur expression than expected ZntR expression. This is consistent with increased levels of Zur outcompeting ZntR for zinc at low zinc concentrations, suppressing output from P_{zntA}

3.2.2 Two-color and three-color pigment sensors

Using regulator levels from Pair 1 and Pair 2 from above, a library of pigment-based reporters was constructed with varying ribosomal binding strength and an LAA protein degradation tag[71] on *crtY*, the gene that converts lycopene to β-carotene. (When plasmids are described here, they are identified by regulator pair and RBS on *crtY*, with an 'L' denoting the presence of a degradation tag on *crtY* – for example, Pair 1 33 or Pair 2 33L.) The lycopene operon from *Pantoea ananatis*, *crtEBI*, was constitutively expressed from a weak promoter. The library was grown at 0, 10, 20, and 100 μM zinc in minimal media for twenty four hours and carotenoids were extracted for HPLC analysis.

Figure 8a shows four representative library members demonstrating a variety of behavior over the tested zinc concentrations. First, at the two extrema, sensors were produced that

were unable to appreciably respond to changes in zinc. In one case, the only accessible state at all tested zinc concentrations was β-carotene. This is a challenge in using two consecutive pigments in a metabolic pathway as reporters: tight control of downstream enzymes is necessary to maintain a color output of an intermediate metabolite, problems we previously found could be addressed by adjusting precursor availability[54]. This indicates that even with superior dynamic range from Regulator Pair 1, leaky transcription from P_{zntA} is still sufficient to prevent access to a lycopene-only state with a weak ribosomal binding site alone. At the other extreme, adding a degradation tag to *crtY* in concert with a weak ribosomal binding site is sufficient to prevent access to the β-carotene state. In between, stronger ribosomal binding sites coupled with a LAA degradation tag shift the switch point from between 0 and 10 μM Zn^{2+} (32L) to between 20 and 100 μM Zn^{2+} (34L), demonstrating that with these regulator pairs, precursor supplementation is not strictly necessary to switch states in the carotenoid pathway at these zinc levels. Nevertheless, altering precursor availability remains a viable option for tuning a biosensor based on pigmented metabolites.

Based on a significant difference in fluorescent reporter output, it seemed likely that switching between regulator pairs one and two would also allow fine tuning of pigment control over the concentration range tested; however, two different pigment reporter constructs (32L and 34L) exhibited little to no change based on the regulator pair with which they were coupled (Figure 8b). In the case of 34L, no significant differences between the two regulator pairs were observed in lycopene and β-carotene measurements at any concentration range, including 10 and 20 μM Zn^{2+} at which there were intermediate amounts of both pigments. The 32L construct had significant differences in

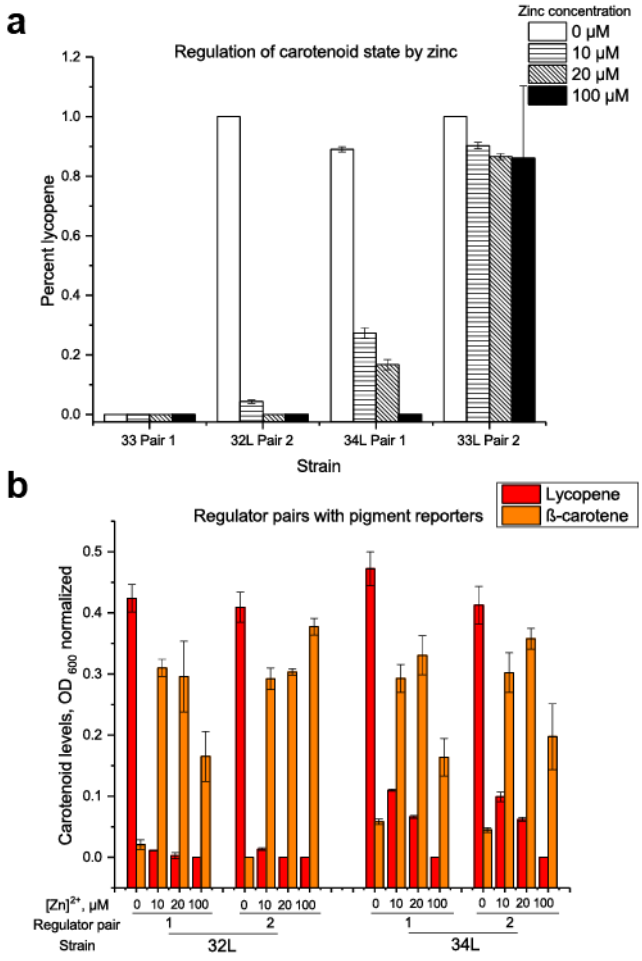

Figure 8: (a) Representative output of two-color biosensors showing two extreme cases in which sensor output does not switch (left, right) and two intermediate cases demonstrating a shift in concentration of zinc at which sensor switches from lycopene to β-carotene (middle). (b) Carotenoid output comparing regulator pairs. While a substantial difference between regulator pairs was observed with fluorescent reporters (Figure 7c), two different pigment reporters (32L and 34L) show different lycopene production behavior in response to zinc but little difference in carotenoid production as a function of regulator pair. Error bars indicate standard deviation.

behavior of the two regulator pairs only at 100 µM, and only in the total amount of β-carotene produced as no lycopene was detected in either strain. This suggests that the response of the carotenoid pigment reporter is relatively robust to regulator expression

levels. This was somewhat surprising, as we had previously observed that similar reporter constructs with genomic regulators alone or with genomic regulator operons co-expressed on the reporter plasmid were unable to switch state between lycopene and β-carotene.

With the carotenoid reporter functioning over the desired concentration range, the second zinc-responsive promoter, P_{znuC}, was added to the sensor to control expression of the *vio* operon that produces the pigment violacein. This resulted in a strain that produced three distinct color states over a 20 μM Zn^{2+} concentration range (Figure 9a). At 0 and 0.1 μM Zn^{2+}, P_{znuC} was derepressed and higher quantities of violacein were produced. At 0.5 and 1 μM Zn^{2+}, the sensor output was dominated by lycopene production. An intermediate state in which both lycopene and β-carotene were present in appreciable quantities was observed at 5 and 10 μM zinc, but by 20 μM zinc, the sensor output was dominated by β-carotene. The strategy in using these pigments was to tune violacein production to visually overpower lycopene in low zinc states such that the cells would appear purple even though lycopene was still present. In this construct, violacein production was not high enough at low zinc concentrations to produce a cell pellet in which only violacein was visibly detectable (Figure 9b); however, there remained a clear difference in pellet coloration between the high violacein states at low zinc and all other conditions.

Additionally, though measured levels of both lycopene and β-carotene were intermediate at 5 and 10 μM zinc, there was little observable difference between the cell pellets at these conditions and those at 20 μM, at which essentially only β-carotene was detected in

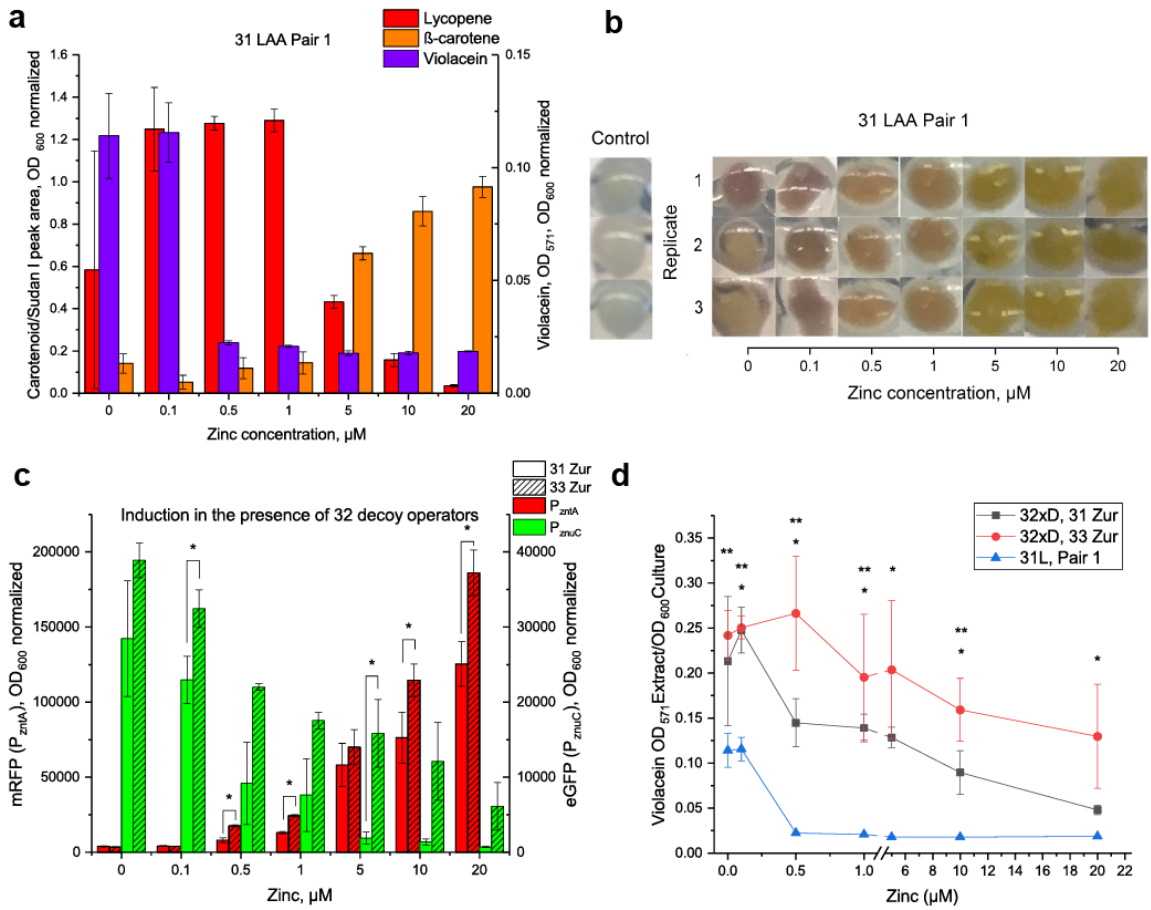

Figure 9: (a) Demonstration of a three-color sensor. At very low zinc, the cells produce substantial violacein and lycopene. At increasing concentrations of zinc, violacein production is repressed and the sensor is in a primarily lycopene state. As zinc increases further, lycopene is consumed and cells enter a primarily β-carotene state. (b) Cell pellets from the experiment in panel a. (c) Fluorescent reporter output in decoy Zur operator test. Asterisks indicate significance at $p<0.05$. (d) Violacein extract levels from decoy Zur operator test and varying RBS strength on inducible Zur. A construct without a decoy array or inducible Zur is presented for comparison (blue). Double asterisks denote statistical significance ($p<0.05$) between red and blue. Single asterisks denote statistical significance between grey and blue ($p<0.05$). Error bars indicate standard deviation.

appreciable quantities in extractions. The result of this is three distinct color states between 0 and 20 µM Zn^{2+}.

Replicates two and three with no supplemented zinc displayed some inhomogeneity in pigment production and formed a striated pellet in which cells with low or no violacein production formed the base of the pellet, making violacein difficult to detect visually (Figure 9b). Similar behavior was not observed at 0.1 µM. This behavior was not apparent in the extracts, as no substantial difference in normalized violacein production was measured at the two lowest zinc conditions (Figure 9a).

3.2.3 Tuning P_{znuC} response with decoy operators

Unfortunately, the concentration range at which violacein production becomes visually undetectable in the construct depicted in Figure 9a,b (less than 1 µM) is far below medically relevant levels in human serum. To address this issue, we explored the use of additional "decoy" binding sites to sequester zinc-bound Zur and thus increase the zinc concentration necessary to yield sufficient zinc-bound Zur to repress express of the violacein operon. We introduced to the plasmid an array of eight decoy binding sites for Zur comprising a combination of P_{ZinT}[85] operators and completely palindromic P_{znuC} operators. On a fluorescent reporter construct for P_{zntA} and P_{znuC} with no additional regulator expression (only genomic expression), the decoy array had the effect of significantly increasing the levels of the fluorescent reporter under full zinc repression, but did not significantly alter (Figure 10) the zinc concentration at which expression first became unobservable.

In an attempt to rectify this, the number of decoy binding sites was increased to thirty two and *zur* was placed under the control of P_{zntA} with either a weak (33) or intermediate strength (31) ribosomal binding site (Figure 9c), forming an inverter for P_{zntA} Induction

from 0-20 µM produced higher P_{znuC} output in the reporter with the weaker RBS for Zur compared to the stronger RBS at all zinc concentrations, though these differences were only significant ($p<0.05$) at 0.1 and 5 µM Zn^{2+}. This is consistent with the hypothesis that driving expression of Zur from P_{zntA} yields insufficient Zur at low zinc concentrations to saturate the decoy array and P_{znuC}. As transcription from P_{zntA} increases with Zn^{2+} concentration, additional Zur is produced, further repressing P_{znuC} (though with the weaker RBS, there is still insufficient Zur to fully repress fluorescence). P_{zntA} output was also increased significantly at all concentrations except 0, 0.1, and 5 µM Zn^{2+} ($p<0.05$). The interpretation of this is less straightforward, but a possibility is that for any given concentration of zinc, there should be less Zur expressed from plasmids with the weaker RBS and thus fewer molecules to compete with constant ZntR levels for zinc binding. Though this strategy no longer relies directly on the natural dynamics of zinc binding to Zur to regulate P_{znuC}, these results demonstrate that the simple inverter and decoy array are effective at shifting the apparent concentration at which expression from P_{znuC} is repressed from about 0.3 µM (no decoys and Regulator Pair 1, data not shown), to between 1 and 5 µM (32 decoys with strong RBS on Zur), to greater than 20 µM (32 decoys and weak RBS on Zur). This suggests that the threshold between sensor color output for a given strain can be effectively tuned based on the final needs of the sensor using this approach.

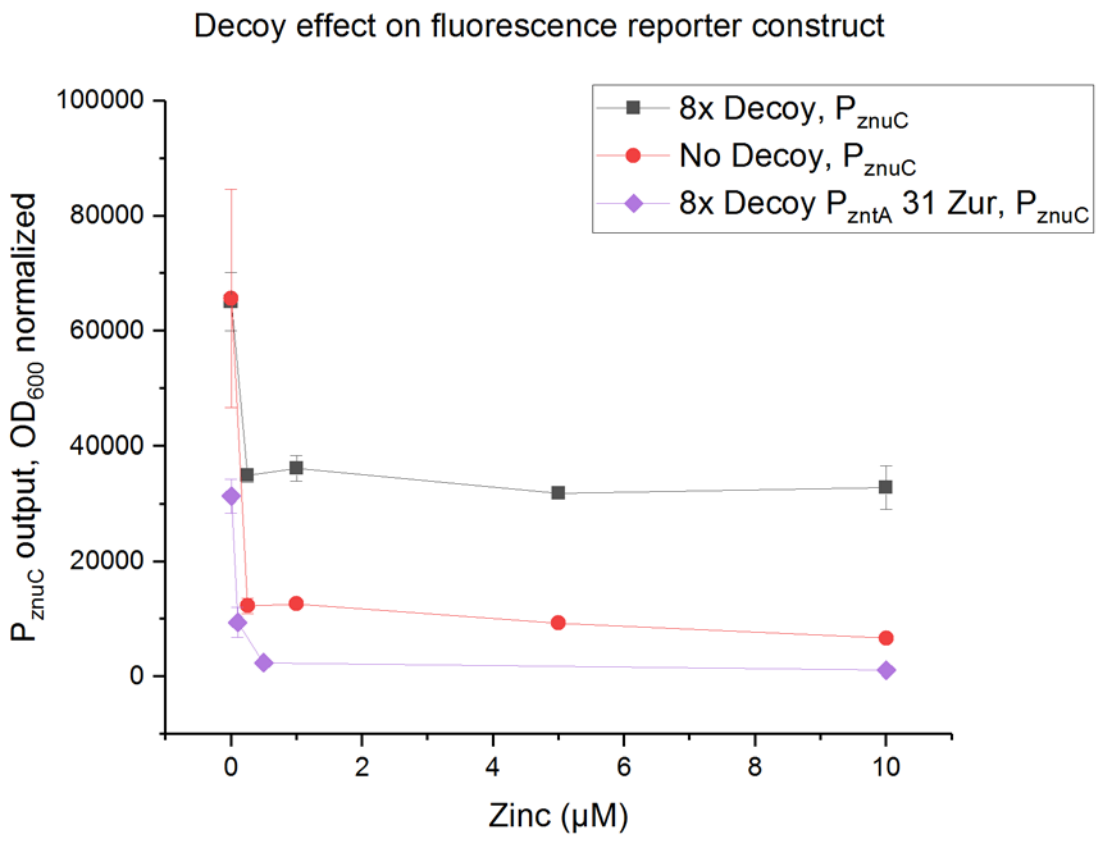

Figure 10: Effect of decoy Zur operators on the output of P_{znuC}. The unregulated reporter (red) has substantially lower expression in the repressed state than the construct with an 8x decoy array (grey). This is rectified upon zinc-dependent expression of Zur (purple). Error bars represent standard deviation.

The same changes were made to the pigment reporter construct. Violacein extractions (Figure 9d) and cell pellets (Figure 11) both show trends similar to those seen with the fluorescent reporter. The violacein content of strains with the stronger RBS on *zur* was significantly higher at all zinc concentrations above zero and the weaker RBS was significant at all conditions except 5 and 20 μM Zn^{2+} (while the trends were consistent, increased variability brought the differences below $p < 0.05$). Though the strain harboring

the weaker RBS had more violacein on average, the difference between the two decoy strains was not statistically significant at any concentration of zinc. These results demonstrate that behavior of the decoy array and inverter is replicated using pigments, meaning that the concentrations at which violacein becomes undetectable and thus the sensor color output changes can be effectively tuned using this approach.

A likely source of variance in the violacein measurements is instability in the decoy array. We observed significant loss of violacein pigmentation in biological replicates during some experiments and suspected that the decoy array might be altered in cultures exhibiting that behavior due to the number and proximity of repeated nucleotide sequences in the decoy array and the high cellular strain of enzyme expression. To assess this, plasmid DNA from a sample of the cultures was amplified using PCR, showing significant deviations from the expected band length (Figure 12) and frequently revealing an assortment of decoy array lengths. Though the presence of repeated sequences on a plasmid might be inherently unstable, we note that we only observed this phenomenon in plasmids using pigments as reporters. Since loss of decoy sites would significantly reduce expression of the *vio* operon, this observation suggests that violacein expression is a significant burden on cells and such deletions are probably selected for evolutionarily, putting practical limits on the number of decoy sites possible in arrays.

3.2.4 Growth and testing in serum

Ultimately, the application of a field-deployable biosensor will require the direct measurement of a common biofluid. For zinc, this necessitates biosensor growth and/or

response in human serum or plasma. One of the prevailing recommendations for evaluating zinc status is plasma zinc[86] ,but to facilitate development, we chose to use

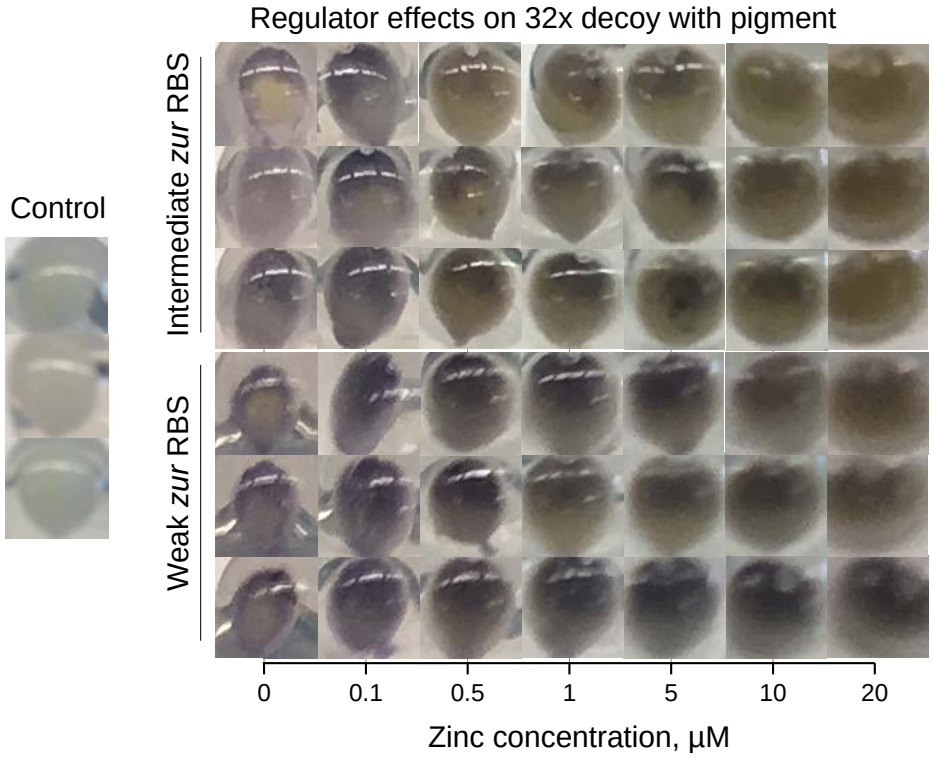

Figure 11: Cell pellets from the violacein extraction experiment described in Figure 9d. Note lower pigmentation at higher zinc with intermediate strength RBS.

pooled commercial off-the-clot serum to avoid any potential interference from coagulants or anticoagulants. While there is a potential discrepancy between serum and plasma zinc levels, this is solely due to how the fluids are commonly handled prior to analysis, and choosing serum zinc allowed us to evaluate the sensor in a similar matrix to what would be expected in the field[86]. To simulate zinc deficiency, the serum was treated with Chelex

100 resin to remove zinc, allowing retitration to measure the response of the sensor at various concentrations of zinc.

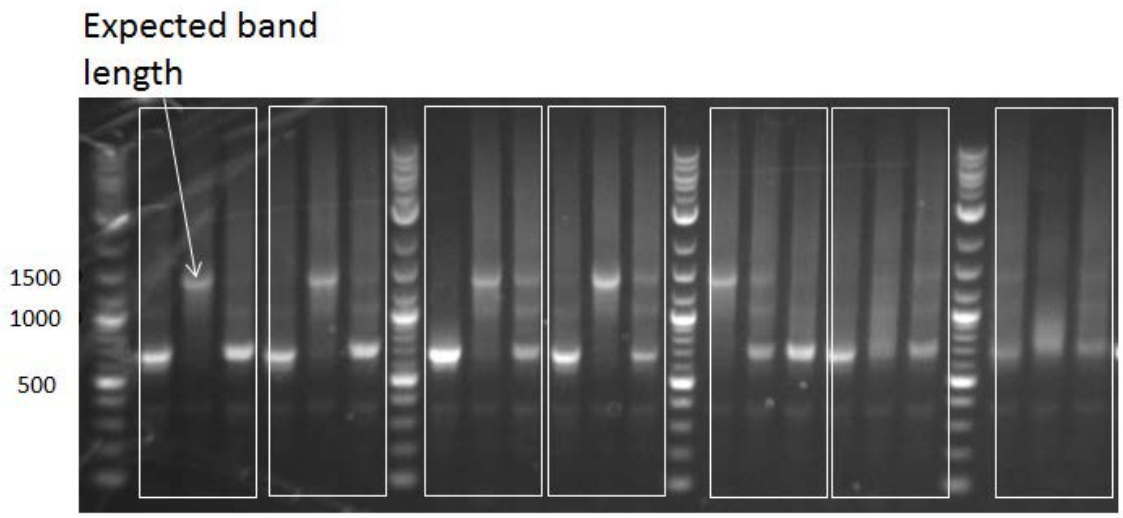

Figure 12: Characteristic banding pattern of CPCR of cells taken from a 32x decoy pigment induction experiment. The expected banding pattern for an intact decoy array is 1.4 kb. Other bands indicate an inhomogeneous population with varying band length. Each box indicates biological replicates run in triplicate.

In initial experiments, cultures were inoculated with small volumes of resuspended colonies from agar plates. We grew these in mixtures of serum and media with increasing percentages of serum, but were unable to grow cultures in even our lowest (10%) serumconcentration (data not shown). This interference with bacterial growth may have been due to the passive immune functionality present in human serum in the form of the complement system[87], a cascade of proteins with the ability to form pores in foreign cell membranes, ultimately causing lysis.

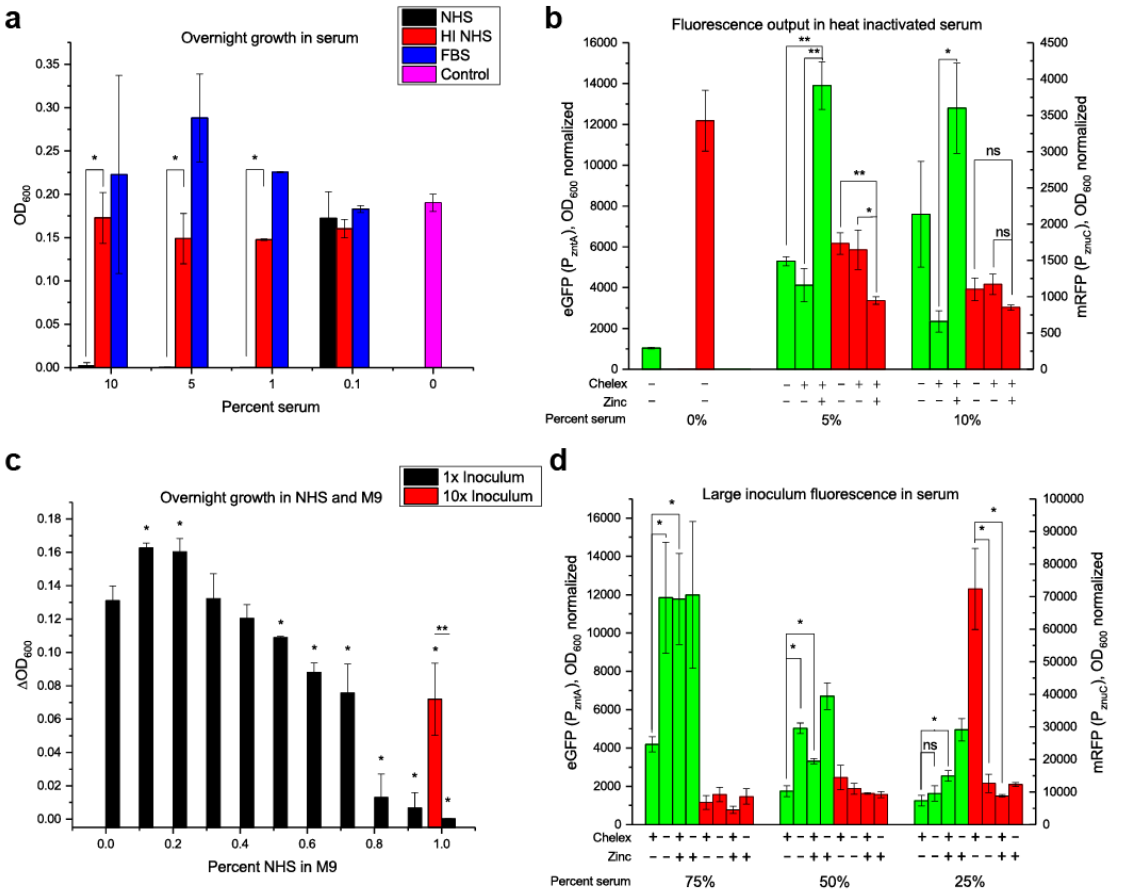

Figure 13: (a) Growth of DH10B in decreasing concentrations of normal human serum, heat-inactivated human serum, and fetal bovine serum. Normal human serum cultures failed to grow at all concentrations above 0.1%. Asterisks indicate differences at $p < 0.05$. (b) Fluorescent reporter demonstrating sensor response in heat-inactivated human serum treated with Chelex 100 resin. At 5% serum, differences were significant between cultures with and without zinc supplementation for both P_{znuC} and P_{zntA} ($p<0.01$, * $p<0.05$). Zinc supplemented as if serum had 10 µM zinc. (c) NHS titration in M9 (* $p<0.05$). (d) Large-inoculum test of fluorescent reporter in human serum (* $p<0.05$). Zinc supplemented as if serum had 5 µM zinc. Only selected important statistical comparisons are presented. Error bars indicate standard deviation.**

To test if complement system protein activity in serum was interfering with growth, we compared cultures with low percentages of normal human serum (NHS), heat-inactivated normal human serum (HI NHS), and fetal bovine serum (FBS) that had not been heat-

inactivated. Heat inactivation should render the complement system inactive and prevent lysis of the biosensor and, while FBS should have some form of a complement system, it should have lower levels of complement than adult serum[88] . DH10B grew robustly in all tested concentrations below 10% in both HI NHS and FBS but only at 0.1% NHS (Figure 13a), suggesting that the complement system interferes with cell growth. Achieving consistent and inexpensive heat inactivation in the field poses significant challenges, so we investigated alternative methods of achieving growth in NHS.

To test sensor response, we compared our fluorescent reporter in HI NHS, Chelex-treated HI NHS, and zinc-supplemented resin-treated HI NHS (Figure 13b). We achieved robust growth up to 10% serum in all conditions, but none at 50% serum. The difference in fluorescent reporter output was statistically significant ($p<.05$) between Chelex-treated and 10 μM supplemented Chelex-treated serum at 5% for P_{znuC} and at both 5% and 10% for P_{zntA}, indicating that both promoter/regulator pairs could detect changes in a physiologically relevant zinc concentration in low-percentage serum media. The lack of significant difference in P_{znuC} output observed with and without the addition of zinc could be due to an incomplete removal of zinc by the commercial resin. P_{znuC} and Zur respond below 0.5 μM in minimal media, and a small amount of zinc remaining in serum could cause the discrepancy between 5% and 10% serum media. While a standard protocol was used for heat inactivation, it is likely that the complement system was not completely inactivated in these experiments, as growth was observed in higher percentage serum in subsequent experiments.

Since growth was observed in initial serum experiments at 0.1%, we asked at what percentage serum does growth become significantly reduced and if that was dependent on

the initial inoculum. Titrating serum down in 0.1% increments from 1%, we saw significant growth below 0.7% NHS (Figure 13c) with significantly increased growth relative to no serum at 0.2% and 0.1%. Additionally, a 10-fold increase in inoculum achieved growth in 1% serum, suggesting that it may be possible to simply overwhelm the complement system with a sufficient bacterial inoculum.

To further investigate the potential for using high inoculation density to overcome growth limitations due to the complement system, overnight cultures were grown, pelleted, and concentrated in small volumes of media (OD_{600}: 68). Different volumes of the resuspension were inoculated in 96-well plates in 100% and 50% normal human serum in M9 media. After incubation for 24 hours, there was a clear cutoff between a starting OD_{600} of 0.227 (0.5 µL inoculum) and 0.0612 (0.135 µL inoculum) in 50% NHS (Figure 14). Only higher inoculum volumes were used in 100% NHS, and all conditions had positive changes in OD_{600}; however, optical density changes were significantly lower in 100% serum compared to 50%.

It is important to note that most optical density measurements reported here are actually changes in OD_{600} after culture. Viable cell counts were not measured in most experiments; however, to assess whether change in OD_{600} was a useful indicator of growth, CFU counts were assessed on a 50% by volume NHS culture with a high, positive change in optical density (+0.667) and a 100% serum culture with a low, negative change in optical density (-0.095). The 50% NHS culture was initially inoculated to 4.6×10^6 CFUs/mL. After overnight incubation, the 50% NHS culture was serially diluted and plated and found to have had 3.75×10^8 CFUs/mL, an increase of approximately two orders of magnitude. Conversely, the 100% NHS culture was

inoculated to $1.13x10^8$ CFUs/mL. After overnight incubation, the 100% serum culture was measured to contain $3.86x10^6$ CFUs/mL, a reduction of approximately two orders of magnitude. This suggests that positive increases in optical density in serum experiments are in fact due to expansion of bacterial cells. Additionally, decreases in optical density appear to be due to significant reductions in viable cells, but with a significantly lower absolute change in optical density relative to growth. This can be reasonably explained by lysis of cells resulting in roughly cell-shaped debris which still significantly increases turbidity, though less than a whole, live cell.

To determine appropriate serum conditions to test response of the biosensor, the fluorescent reporter was inoculated in 75%, 50%, and 25% NHS and Chelex-treated NHS with and without supplemented zinc (Figure 13d). The fluorescent readings of P_{zntA} could differentiate between NHS and Chelex-treated NHS with and without zinc at 75% and 50% serum by volume ($p<0.05$), but differences did not meet the cutoff for significance at 25% ($p=0.0557$ and $p=0.0544$, respectively). Since zinc is supplemented as if the serum contained 5 μM zinc, it is possible that the net 1.25 μM difference in culture concentration is below the resolution of this sensor/regulator pair. Results for P_{znuC} fluorescent output were inverted, with detectable differences between NHS and treated

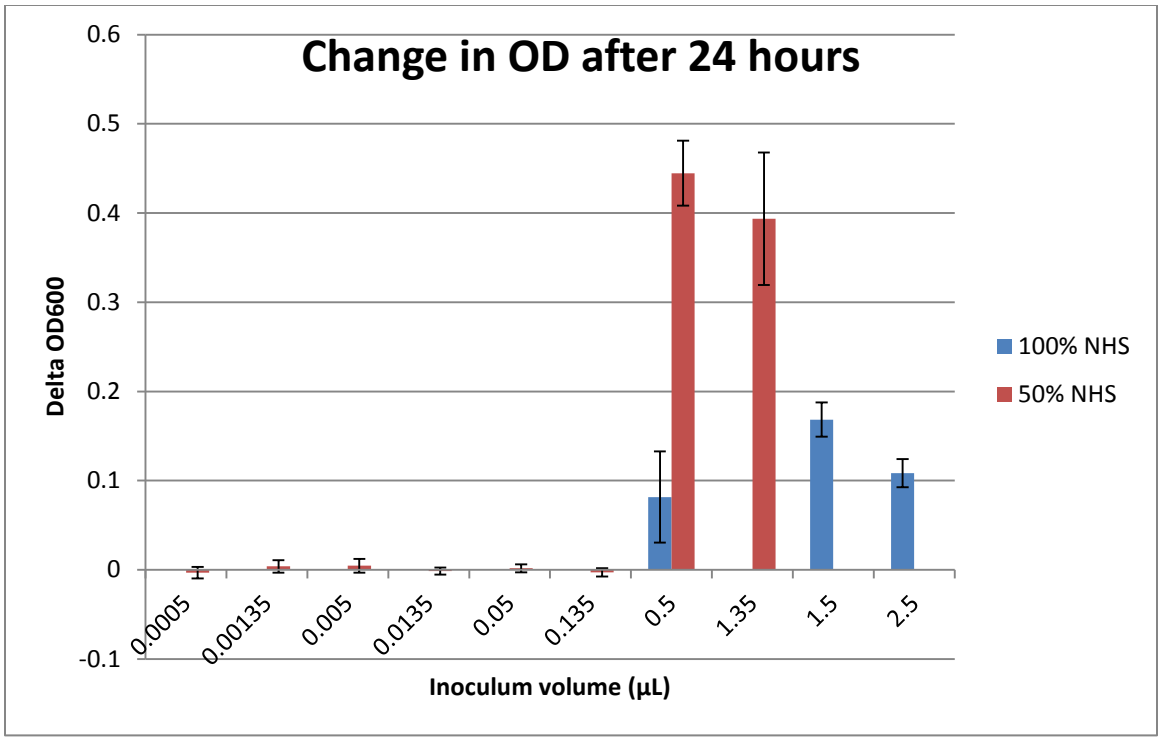

Figure 14: Overnight changes in OD in 100% and 50% serum in plates with volume of OD_{600}:68 feeder culture. Error bars represent standard deviation.

NHS and between treated with and without zinc supplementation at 25% only ($p<0.05$).

As the most significant challenge with the three color pigment system is sufficiently precise tuning of the highly zinc sensitive Zur/P_{znuC}, 25% serum was used to test the sensor response in human serum. A starter culture with pigment reporter plasmid harboring a 32x Zur operator decoy array and an intermediate strength RBS on *zur* was concentrated as above, inoculated at a starting OD_{600} of 0.325, and grown for 24 hours in 25% NHS and Chelex-treated serum with varying levels of zinc supplementation. Extracts (Figure 15A) and cell pellets (Figure 15b) demonstrate a high violacein and lycopene state at the lowest zinc concentration. All higher-zinc conditions have a mixture

between lycopene and β-carotene and decreasing expression of violacein, showing the sensor in transition between carotenoid states. Violacein production is substantial in all conditions except for untreated NHS. Since pooled commercial NHS should contain healthy zinc levels, these results clearly indicate that more tuning of the carotenoid transition point will be necessary (which we have previously demonstrated[54]); however, it is extremely promising that violacein production has dropped to a level such that it is not visible in cell pellets at healthy zinc levels (Figure 15B, left).

Notably, violacein production is significantly higher at low zinc conditions in 25% serum than in M9 alone (Figure 9d) and a large fraction of violacein is found in the supernatant of serum cultures. This could due to metabolic changes in *E. coli* induced by human serum. Another explanation is that since violacein preferentially partitions into the media when serum is present, intracellular levels of violacein are kept lower in serum cultures than in M9 alone. Removal of product from the cells could help pull on the metabolic pathway. Supernatants from M9 cultures show no visible violacein retention, though small differences in absorbance are detectable between butanol extractions of supernatant from cultures with cells harboring different amounts of violacein. Cell pellets from M9 cultures were observed to contain more violacein than those in 25% serum, even as total violacein production in serum cultures was significantly greater as assessed by measurement of violacein in the supernatant (Figure 16).

3.3 Conclusion

In summary, we have demonstrated a proof of concept whole-cell biosensor that produces outputs detectable and interpretable by the naked eye at physiologically relevant zinc

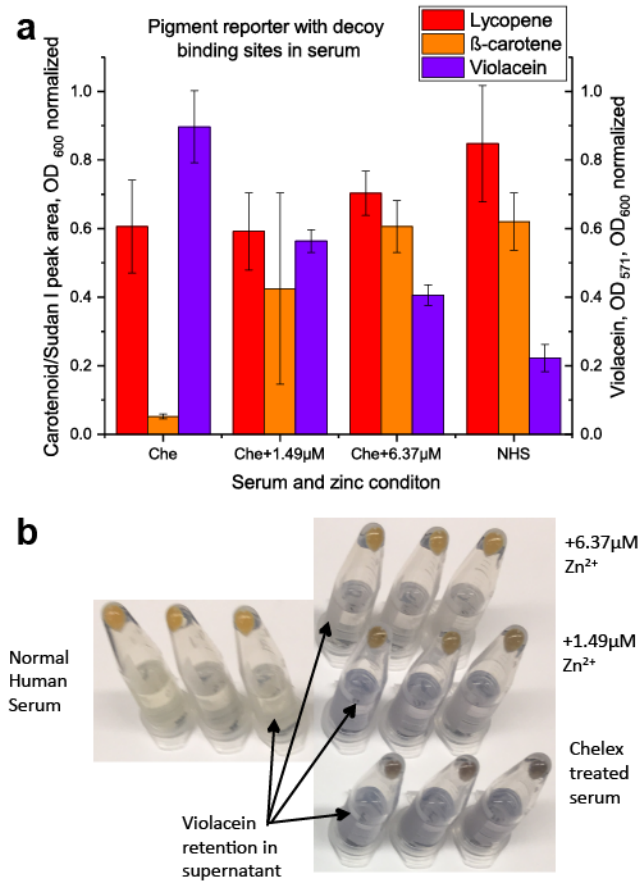

Figure 15: Three color output in serum. (a) Extract from biosensor culture in 25% NHS. Chelex serum exhibits the violacein dominated low zinc output. NHS is characteristic of output in a healthy individual. (b) Cell pellets from 1 mL of 24 hour culture of biosensor in 25% serum. Zinc supplementation levels were selected to mimic NHS. Here, NHS (left) shows characteristic pigment output of sensor in the presence of healthy zinc levels from commercial pooled serum. Chelex 100-treated serum (right) shows pigment output characteristic of low zinc to intermediate zinc states.

levels in 25% human serum. By optimizing expression levels of regulators for improved dynamic range of P_{zntA}/ZntR and P_{znuC}/Zur between 0-20 µM Zn^{2+}, we demonstrated the ability to tune the sensor output between the carotenoids lycopene and β-carotene to indicate borderline and healthy zinc levels. A strategy to adjust the response of P_{znuC}, initially occurring at non-physiologically low concentrations of zinc, was demonstrated

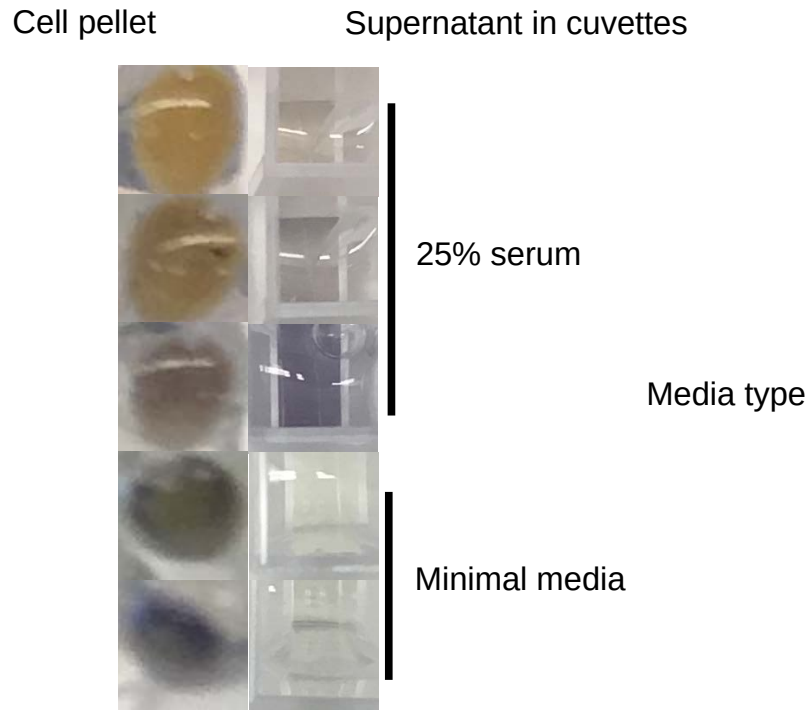

Figure 16: Comparison of images of cell pellets (left) and culture supernatants (right) from three color experiments in 25% serum versus M9 alone. Note the presence of substantial violacein in 25% serum supernatant, even as cell pellets from M9 alone demonstrate comparatively more violacein in cell pellets without visible presence in supernatant.

using arrays of decoy binding sites for Zur and using P_{zntA} output to control Zur, fully repressing it at zinc levels found in healthy serum and allowing violacein expression at levels expected to be physiologically relevant. Complement system interference with sensor cell growth in human serum was overcome via high-density inoculations, and a proof-of-concept test of a three color sensor was presented. The final transition thresholds between purple, red, and orange will ultimately need to be tuned based on the final form

factor and assay protocol (e.g., percentage serum) of a field-friendly packaged and preserved device (which is the subject of ongoing efforts); the proof-of-principle presented here for both the sensor and the ability to tune those transition thresholds suggests that those goals will be readily achievable using the tools and approaches demonstrated here.

3.4 Materials and methods

Plasmids and oligonucleotides

Plasmids and primers from this work appear in Supplementary Tables. Oligonucleotide synthesis and sequence verification of all constructed plasmids were performed by Operon.

Molecular biology

All enzymes were purchased from New England Biolabs. PCR amplification was performed with Q5 polymerase. Plasmids were constructed with standard restriction endonuclease cloning or Gibson assembly[69]. All experiments used the *E. coli* strain DH10B. For routine cloning, cultures were grown in LB supplemented as necessary with chloramphenicol, tetracycline HCl, and kanamycin sulfate at final concentrations of 33 µg/mL, 15 µg/mL and 50 µg/mL, respectively. Plasmid purification was performed with (Omega) kits. Purification of PCR products was performed with Qiagen kits.

Zur decoy array construction

To construct the array of decoy Zur operators, oligonucleotides were synthesized containing portions of a modified palindrome and the Zur operator site in P_{ZinT} and

appropriate restriction sites with sufficient overlapping sequneces. These oligonucleotides were mixed and extended with Q5 polymerase (New England Biolabs) to create double stranded DNA, which was purified with a Qiaquick PCR purification kit (Qiagen), digested, and cloned into vectors to convert them to standard BioBrick format. These were then serially cloned to produce the 8x and 32x decoy arrays.

Violacein extraction

1 mL of culture was centrifuged for five minutes at 17,900 rcf. The supernatant was decanted, 50 µL of deionized water was added, and the pellets were vortexed for five minutes in a VWR VX-2500 multi-tube vortexer on the maximum speed setting. 250 µL of water-saturated butanol was added and tubes were vortexed for an additional five minutes. Butanol suspensions were centrifuged for five minutes at 17,900 rcf and the organic phase was transferred to fresh tubes and centrifuged again. The supernatant was transferred into microcuvettes and measured in a Genesys 20 spectrophotometer for absorbance at 571 nm using water-saturated butanol as a blank. For serum cultures and select M9 cultures, an additional measurement of the supernatant was taken for absorbance at 571 nm.

Acetone extraction

Cultures were centrifuged and resuspended as above, then mixed with 800 µL of acetone at 50C to which 1 µg/mL Sudan I had been added as an internal standard. Tubes were agitated regularly for 10 minutes, and then centrifuged at 17,900 rcf for five minutes. 450 µL of the extract was transferred to autosampler vials for HPLC analysis. Vials were stored at -80°C until analysis for no more than 24 hours.

Carotenoid analysis

HPLC analysis was performed on a Shimadzu Prominence UFLC with a UV-Vis detector. Separation was done on an Agilent Zorbax Extend-C18 Analytical 4.6x50mm 5-micron column. Mobile phase composition was 50/30/20 methanol/acetonitrile/isopropanol at a flow rate of 1 mL/min. Peaks were identified by comparison with standards purchased from Sigma (Lycopene, ≥90%) and TCI America (ß carotene, 97%). Reported carotenoid levels were calculated from the ratios of carotenoid peak areas with Sudan I peak areas normalized by the OD_{600} of the source culture.

Chelex 100 treatment

When indicated, materials were treated with pH-corrected Chelex 100 resin (Bio-rad) using a batch protocol. All steps were carried out according to the manufacturer's protocols. Following treatment with Chelex resin, media were filter sterilized with 0.2 micron filters.

Modified M9 media

A modified minimal medium similar to M9 except with organic phosphate to allow zinc titration was used for all experiments in minimal medium. A 5x salt solution was made containing 10 g/L ß-glycerophosphate, 8.2 g/L KCl, 22.5 g/L NaCl, 5 g/L NH_4Cl, and 19.5 g/L MES which was adjusted to pH 7.4. The salt solution was combined with 1.92g SC-ura amino acid mixture (Sunrise Science), 2 mL 1M $MgSO_4$, 100 µL $CaCl_2$, 5 mL 80% glycerol, 10 mL 20% glucose, and 10 mL 1% Thiamine HCl, diluted to a final volume of 1L, and filter sterilized.

Cell culture

All cultures were inoculated from freshly transformed DH10B colonies. For minimal media and small-inoculum serum experiments, colonies were resuspended in 52 µL of M9. 5 mL cultures were inoculated with 3 µL of these resuspensions. For large-inoculum serum experiments, six 8 mL overnight feeder cultures were grown in M9 with 1 µM supplemented $ZnSO_4$ and resuspended in a volume of 400 µL of M9. The optical density of a serial dilution of the resuspension was used to determine inoculum volumes. Cultures were grown aerobically for 24 hours at 37°C. For fluorescence experiments, optical density measurements and fluorescence readings were taken on a Synergy H4 (Biotek) plate reader using 150 µL aliquots of cultures in 96-well plates.

Estimation of relative protein expression

The relative transcriptional strength of the constitutive reporters was taken from the registry of standard biological parts. The RBS efficiency was calculated with RBScalc[83]. These two numbers were multiplied to approximate expected relative protein expression (Table 2). The naming convention used lists promoter-ribosomal binding site for ZntR and then promoter-ribosomal binding site for Zur. For example, 7-4 7-1 denotes a construct with J23117 B0034 ZntR and J23117 B0031 Zur. ‘c’ denotes the results were from Chelex-treated media.

CHAPTER 4. INVESTIGATING GROWTH RESTRICTION IN THE CAROTENOID PATHWAY

4.1 Introduction

The carotenoid pathway has been the target of extensive metabolic engineering efforts, aimed both towards lycopene itself as a valuable product, and as a reporter to demonstrate increased flux through engineered mevalonate or DXP pathways which produce the precursors to the bacterial carotenoid pathway (isopentenyl pyrophosphate and dimethylallyl pyrophosphate). Typically, the genes used efforts in *E. coli* are from *Pantoea ananatis*[89] or *Pantoea agglomerans*[47,48,64]. Many efforts in metabolic engineering in *E. coli* have involved expression of genomic fragments containing the carotenoid genes, meaning the genes possessed wild-type RBSs and promoters. The genomic coding sequences for *crtIB* overlap in *P. agglomerans*, and even when genes were separated, this operon was often kept as a single, intact fragment. Additionally, some of these efforts noted that induction of the cloned fragments caused extreme disparities in cell growth[48], so many metabolic engineering efforts were carried out in the absence of inducers (with leaky expression from repressed promoters), or without explicit promoters at all[47,48,90]

One study in the literature compared different combinations of single-copy integration of two carotenoid genes from *P. ananatis* with a third expressed from a plasmid with lac-inducible expression[89]. Multi-copy expression of *crtB* led to a severe decrease in cellular growth and substantially lower levels of lycopene production. The author suggested that

CrtB was simply toxic to *E. coli* when overexpressed; however, induction of *crtB* was never performed in the absence of CrtE and CrtI. Data presented later in this chapter suggest that this explanation is not sufficient. An alternative hypothesis that we sought to investigate was that imbalanced enzyme expression led to overproduction of the intermediate phytoene which was causing the reduction in growth.

Ultimately, successful overproduction of lycopene has been carried out through various metabolic engineering efforts without too much thought to the observed phenomenon of growth restriction under gene overexpression. For the purposes of constructing our biosensor, however, we were interested in determining an optimal ratio of enzyme expression for lycopene production. In chapter two, our plasmid-encoded biosensor had extremely low expression of *crtEBI*, and attempts to clone the operon with medium- or high-strength constitutive or inducible promoters repeatedly failed. We thus investigated the cause of the apparent toxicity to help determine optimal or at least sufficient performance of these genes, which could decrease the time to response for our micronutrient biosensor.

4.2 Results

We first isolated the coding sequences for CrtE, CrtB, and CrtI, and assembled them with a variety of different efficiency ribosomal binding sites (RBSs). Constitutive expression of individual carotenoid enzymes with relatively strong combinations of promoter strength and RBS efficiency were isolated, as were combinations of CrtE and CrtI; however, we were unable to isolate plasmids constitutively expressing both CrtE and CrtB in the absence of CrtI. To further investigate these issues and the extreme growth

restriction upon induction of *crtEIB* in the literature, we constructed a test reporter with inducible expression of the lycopene biosynthesis pathway.

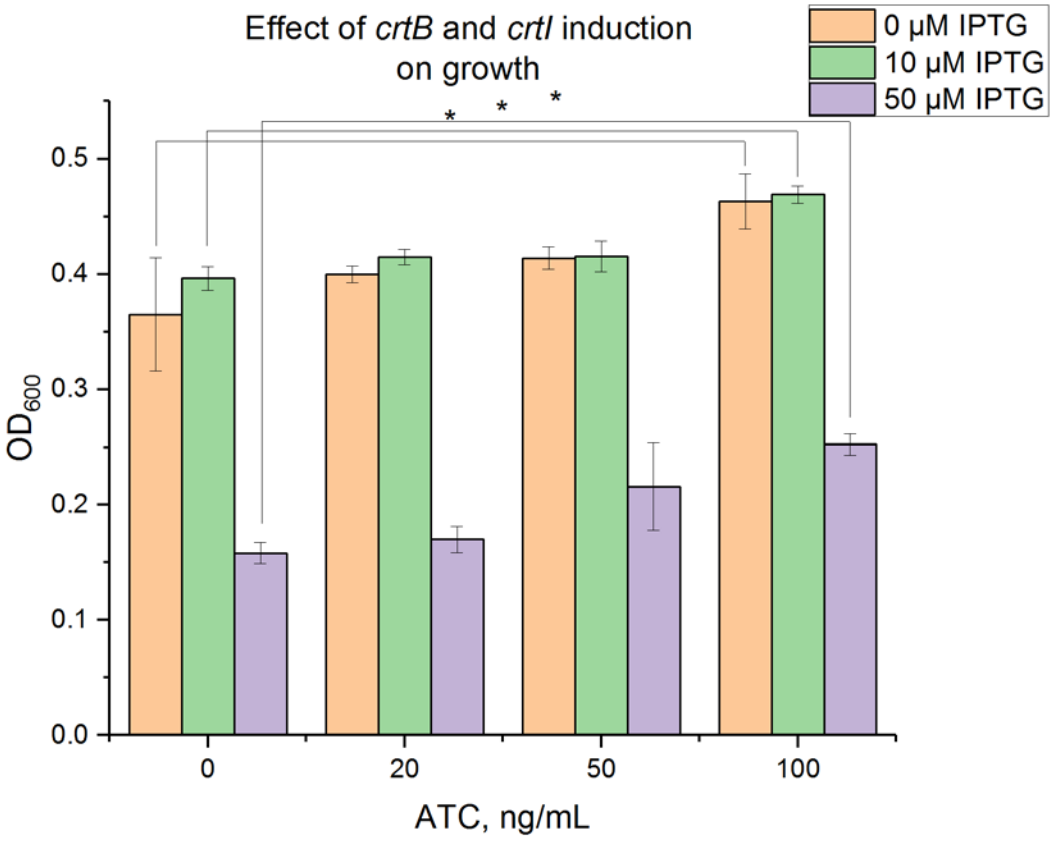

Figure 17: Initial carotenoid experiment demonstrating significant growth restriction on induction of *crtB* with IPTG and comparative growth advantage on induction of *crtI* with ATC in the presence of high, constitutive expression of *crtE*. Error bars indicate standard deviation.

4.2.1 Initial crtEIB induction

To test the relative effects of crtB and crtI expression, a plasmid was constructed with expression of crtE controlled by a strong, constitutive promoter with a high efficiency RBS. *crtB* and *crtI* were placed under control of a LacI-regulated promoter and a TetR-regulated promoter, respectively, with identical weak RBSs on each coding sequence. This plasmid was transformed into *E. coli* DH10B which was grown at varying concentrations of ATC and IPTG. We found a strong negative ($r=-0.957$, $p<1x10^{-8}$) correlation between IPTG concentration (*crtB* induction) and culture OD_{600}, consistent with the previous inability to isolate plasmids cloned with most combinations of crtE and crtB expression. Additionally, at all tested concentrations there was a significant decrease in optical density between 10 and 50 μM IPTG (Figure 17). Interestingly, for all but the highest concentration of IPTG (100 μM, data not shown), there was a trend of increasing OD with ATC, with a significant increase in OD at the highest concentration of ATC ($p<0.05$) for each concentration of IPTG. With the highest level of both inducers, these conditions should be the most burdensome in terms of heterologous protein expression, suggesting that simple transgene expression-dependent stress response was inadequate to explain the observed behavior.

4.2.2 Dual crtEIB and fluorescent reporter induction

To follow up on the initial apparent growth benefit of co-induction of *crtB* and *crtI* relative to *crtB* alone in the presence of CrtE, we constructed a fluorescent reporter plasmid using the same induction systems but without any carotenoid biosynthesis genes. This construct allowed us to use fluorescence as a simply measured proxy for protein expression in the inducible crtB/crtI construct made in the previous section and compare it with observed changes in growth. Strains harboring either the fluorescence reporter

plasmid or the inducible carotenoid plasmid were cultured under various concentrations of inducer, including higher levels of ATC to determine if a higher apparent growth rescue could be obtained by increasing *crtI* expression further.

We found both a statistically significant negative correlation between eGFP expression from IPTG induction (proxy for CrtB) and OD in the carotenoid construct and a significant positive correlation between mRFP induction (proxy for CrtI) and OD in the carotenoid construct (Table 4), suggesting that, in general, more CrtB resulted in a lower optical density, and more CrtI resulted in a higher optical density.

Table 4: Correlation between fluorescence reporters and carotenoid construct optical densities.

	Pearson correlation coefficient	p
eGFP (crtB) to carotenoid construct OD	-0.74417	0.000947075
mRFP (crtI) to carotenoid construct OD	0.557534	0.02483918

In the carotenoid construct, there was no significant difference in OD between 0 and 50 ng/mL ATC (CrtI) at all but100 µM IPTG, but at 0, 10, and 50 µM IPTG (CrtB), there was an increase in optical density at 100 and 150 ng/mL ATC. No positive effect of ATC was observed at 100 µM IPTG. This suggests that for lower expression levels of CrtB,

increasing levels of CrtI result in less growth restriction, though there is an apparent limit to this effect as it was not observed at the highest induction of CrtB (Figure 18b,d).

Comparing the carotenoid construct across IPTG concentrations, there is a significant reduction in optical density at the highest level of IPTG for all levels of ATC. This reduction was dose dependent in the absence of ATC (Figure 18e): intermediate induction levels had significantly different optical densities than both the lowest and highest induction levels. This suggests that increased levels of crtB are directly responsible for the growth restriction.

Looking at optical density in the fluorescent reporter (Figure 18a), maximal IPTG induction significantly decreased the optical density relative to zero-IPTG conditions, but only at 0 and 50 ng/mL ATC (Figure 18c). No differences in optical density as a function of either inducer appeared to be dose-dependent. In all cases, the differences in growth are most pronounced in the carotenoid construct (Figure 18b).

While it could be expected that inducing significant amounts of protein expression could have a detrimental effect on cell growth, even with well tolerated fluorescent reporters, it was not expected that there would be significant increases in optical density with increasing induction of fluorescent reporter expression as seen in Figure 18a, when at 100 μM IPTG, a statistically significant increase in OD is seen at 100 ng/mL ATC.

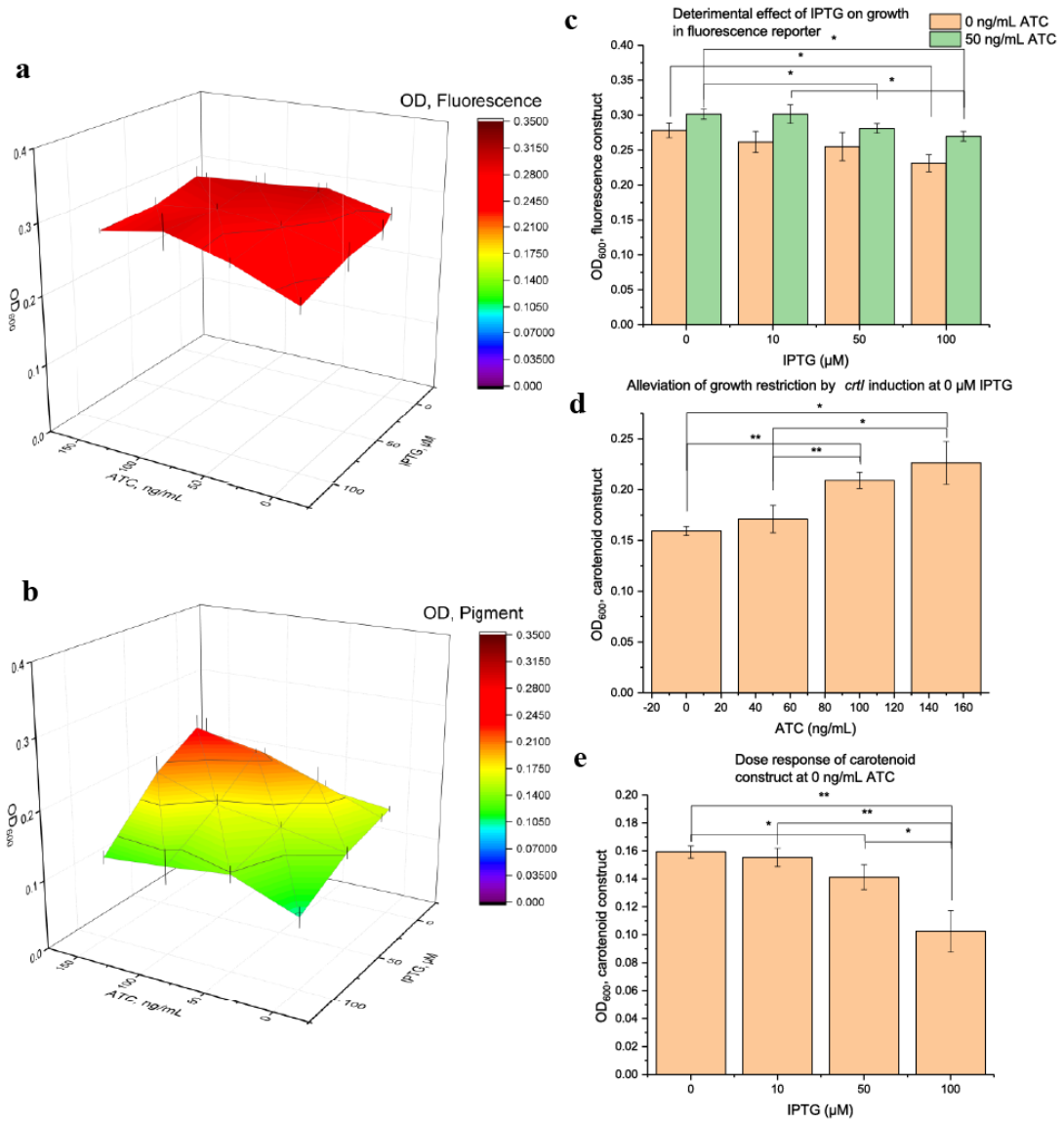

Figure 18: Optical density of (a) fluorescent reporter and (b) carotenoid construct showing induction dependent growth restriction by IPTG and partial rescue by ATC. (c) Growth restriction present at highest IPTG in the fluorescent reporter. (d) Carotenoid construct growth is enhanced by ATC. (e) Carotenoid construct growth shows dose-dependent reduction by IPTG. Error bars denote standard deviation. Bars indicate statistical significance (* p<0.05, ** p<0.005). ATC induces *crtI*. IPTG induces *crtB*.

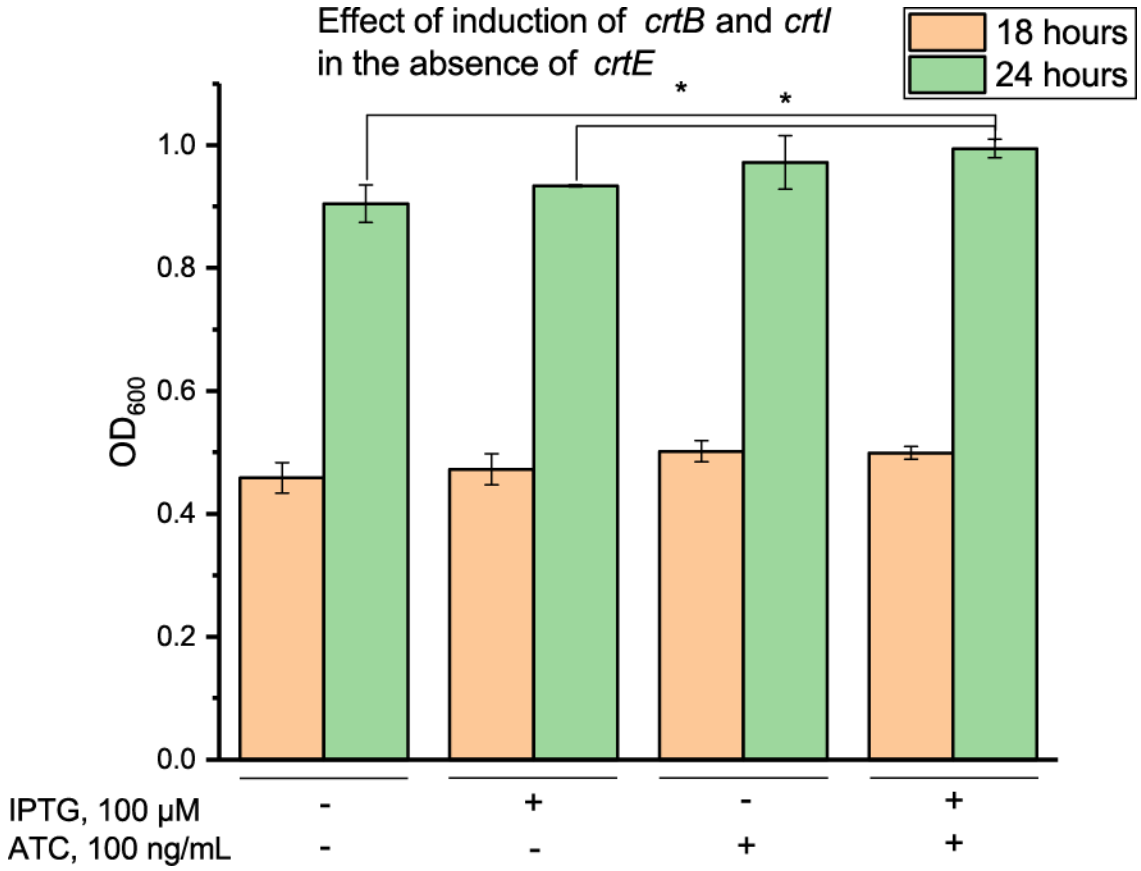

Figure 19: Induction of pigment test construct in the absence of CrtE. No growth restriction was observed upon induction of any combination of *crtB* and *crtI*. Significant ($p<0.05$) differences were detected at 24 hours, but ODs were strictly higher under induction. Error bars indicate standard deviation. ATC induces *crtI*. IPTG induces *crtB*.

4.2.3 Inducible crtIB, weak crtE inducible crtB

To investigate whether the cause of the observed growth restriction and partial rescue due to induction of *crtI* and *crtB* was due to some other effect of proteins alone, a plasmid identical to EIB, but lacking constitutive expression of *crtE* was developed and tested at 18 and 24 hours (Figure 19). At 18 hours, there was no observable significant difference in average OD_{600} between any induction conditions. At 24 hours, there was a small but

significant difference between uninduced and dual-induced and between induction with IPTG alone and with both IPTG and ATC; however, all observed induced ODs were *higher* than uninduced, though the difference was not significant for crtB induction alone. In no cases was any combination of inducers causing growth restriction. This is an interesting result as the metabolic precursor to crtB is not present in these experiments. Any enzymatic activity would be nonspecific activity on endogenous *E. coli* metabolites. Whatever the cause of an increase in terminal OD with expression of crtBI, these results suggest that the presence of CrtB or CrtI themselves is not causing the observed growth restriction in other experiments. The lack of an observable effect of CrtB expression on OD does not support suggestions from the literature that CrtB itself is toxic to *E. coli*.

It is worth noting that Figure 18 and Figure 19 show different behaviors for terminal OD in non-lycopene-producing strains as a function of increasing IPTG induction. A possible explanation for the discrepancy in growth disadvantage upon IPTG induction between the two constructs is disparities in overall transgene expression burden, as the fluorescent reporter has a high-efficiency RBS on *eGFP* and the carotenoid construct has an RBS with approximately 100-fold lower efficiency on *crtI*. This is not, however, easily reconcilable with the disappearance of this effect at dual-induction with IPTG and ATC which should be strictly more burdensome.

To follow up on these findings, constructs with different promoter and RBS strengths on crtE were assembled with either weak or strong ribosomal binding sites on IPTG-inducible crtB. With low expression of crtE, the induction of crtB with a strong RBS shows a small, but increasingly significant decrease in OD as a function of IPTG (Figure 20). The same construct with a 100-fold weaker RBS on *crtE* shows no change at any

IPTG concentrations, suggesting the growth restriction is directly dependent on the presence of CrtE. Constitutive expression of *crtE* with a much stronger promoter alone was not an issue. This strongly suggests that the combined presence of CrtE and CrtB is responsible for the observed growth restriction in the carotenoid pathway.

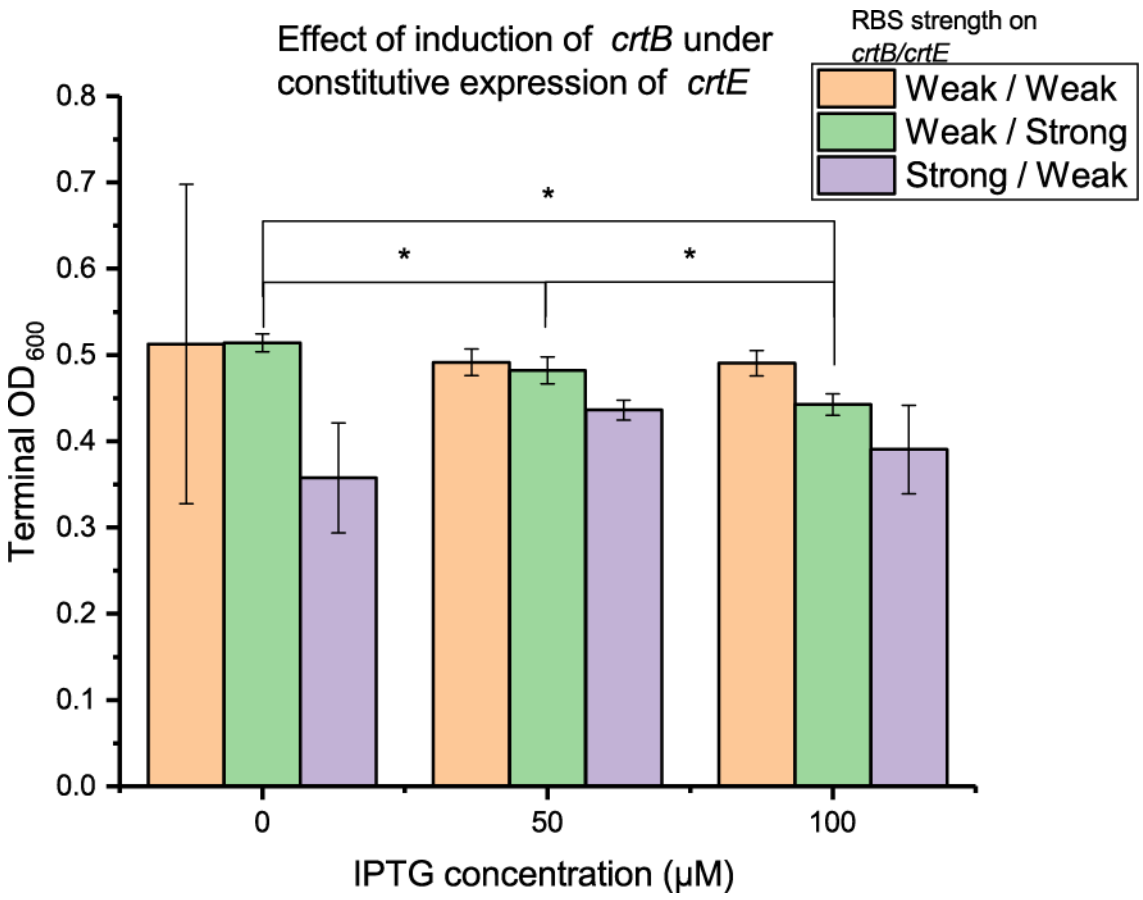

Figure 20: Induction of *crtB* with varying constitutive expression of *crtE* showing dependence of growth restriction on presence of high *crtE*. Error bars indicate standard deviation. IPTG induces *crtB*

4.2.4 Vector and strain controls

To ensure that the observed growth restriction was not solely due to the inducers or the induction systems alone, we grew DH10B and an empty inducible vector control at the same concentrations as above (Figure 21). We observed no significant difference in OD_{600} between inducer concentrations at 18 hours in the DH10B control and no difference in the empty vector control except at 360 µM IPTG, which resulted in a slight reduction in OD (Figure 21c). At 360 µM IPTG, ATC concentration has no significant effect on OD at any IPTG concentration. It is important to note that the growth reduction observed at 360 µM IPTG is at a significantly higher IPTG concentration than was used in the previous experiments with *crtEBI* in which induction-dependent growth restriction was observed. These controls suggest that the observed reduction in OD in the crtEIB experiments is not caused by either a natural response of DH10B to the inducers or by binding of inducers to their regulated proteins and alleviation of repression on an empty plasmid.

4.2.5 HPLC investigation of phytoene

Based on previously published work reporting high carotenoid intermediate yields in BL21(DE3)[91] (which was inconsistent with our initial hypothesis that phytoene accumulation was the source of the growth restriction), we asked whether similar experiments in BL21(DE3) might show lower growth restriction, perhaps due to inherent differences in intermediate toxicity between strains. To test this, both BL21(DE3) and DH10B were transformed with the carotenoid construct and grown overnight in LB supplemented with different concentrations of inducers. Acetone extractions were performed on combined replicates of samples to ensure a sufficient amount of carotenoids for detection on HPLC.

Both strains showed growth restriction upon induction with the most profound growth restriction observed in DH10B. We detected peaks at 274 nm with a retention

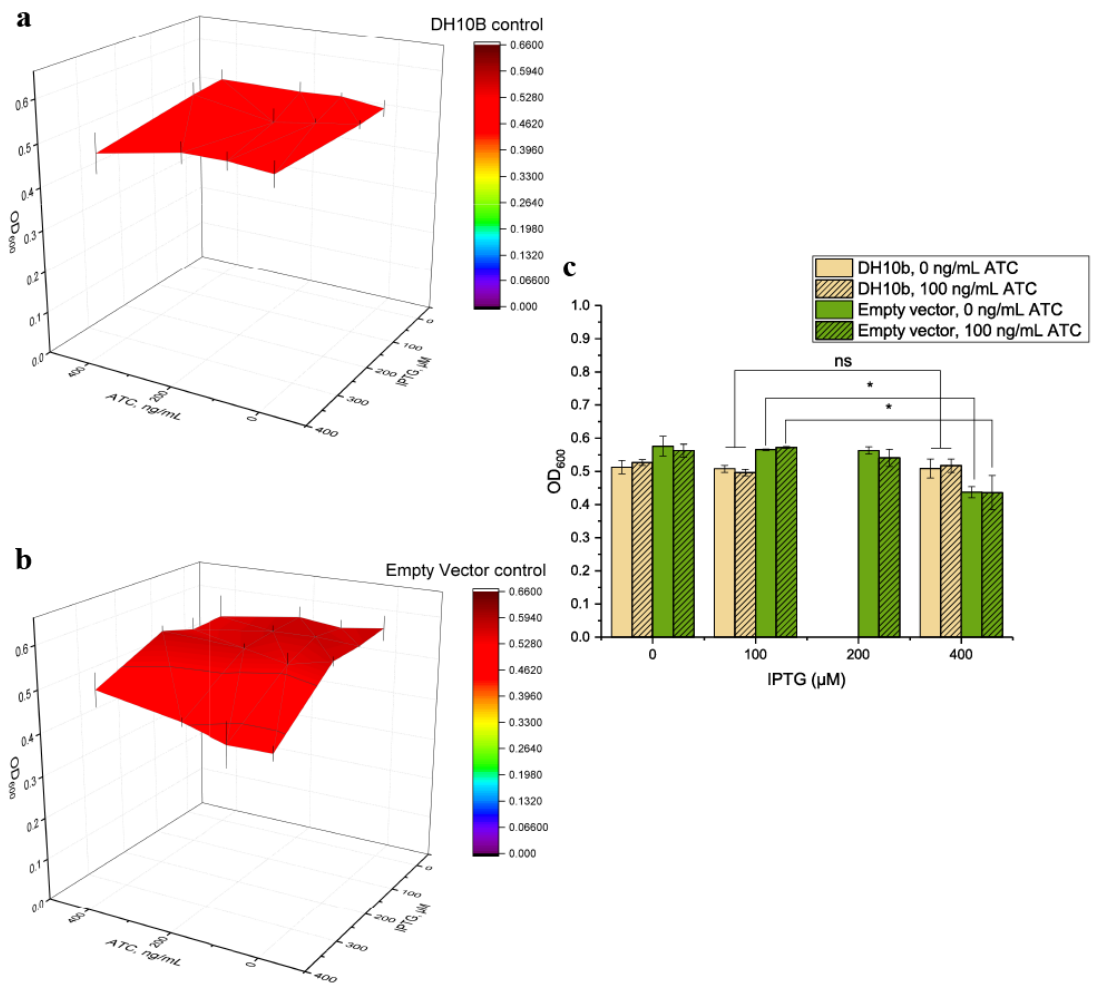

Figure 21: Parent strain and empty vector growth controls. (a) DH10b shows no effect of inducers. (b) Empty vector control shows decrease in growth at 360 µM IPTG. (c) Empty vector and DH10b at 0, 100 ng/mL ATC. Optical density differences only present at 360 µM IPTG in empty vector control. (* p<0.05) Error bars indicate standard deviation. ATC induces *crtI*. IPTG induces *crtB*.

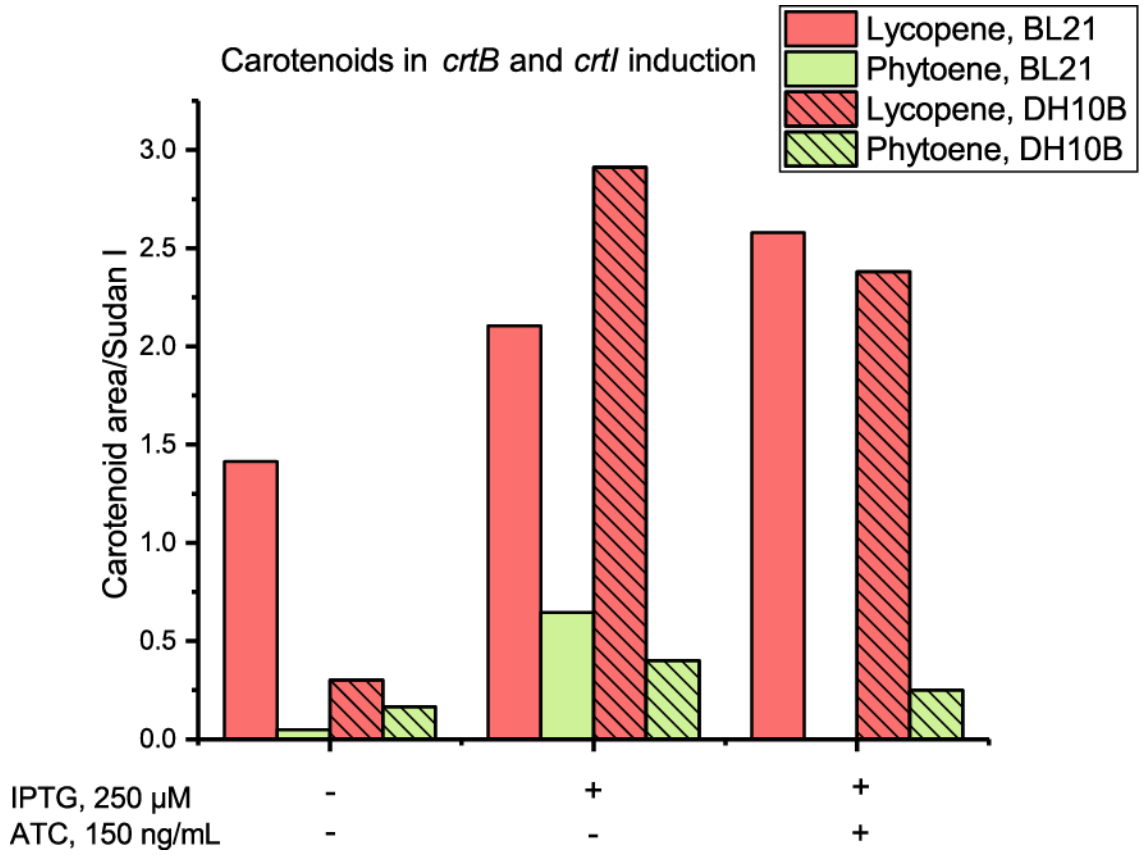

Figure 22: Carotenoid production in BL21 versus DH10B from combined extractions. Quantity run on instrument was proportional to culture optical density. ATC induces *crtI*. IPTG induces *crtB*.

time of 8.9 minutes and a spectrum consistent with phytoene which were highest at IPTG only conditions in both strains. Phytoene was undetectable under dual induction in BL21 and 1.8-fold reduced in DH10B (Figure 22). This is consistent with increased CrtI reducing the amount of accumulated phytoene; however, lycopene production apparently drops with induction in DH10B, though it increases in BL21(DE3). These results suggest that a difference in strain response to phytoene is not the explanation for growth defects,

since growth restriction was observed in both BL21(DE3) and DH10B and BL21(DE3) has been used to overproduce phytoene in the literature.

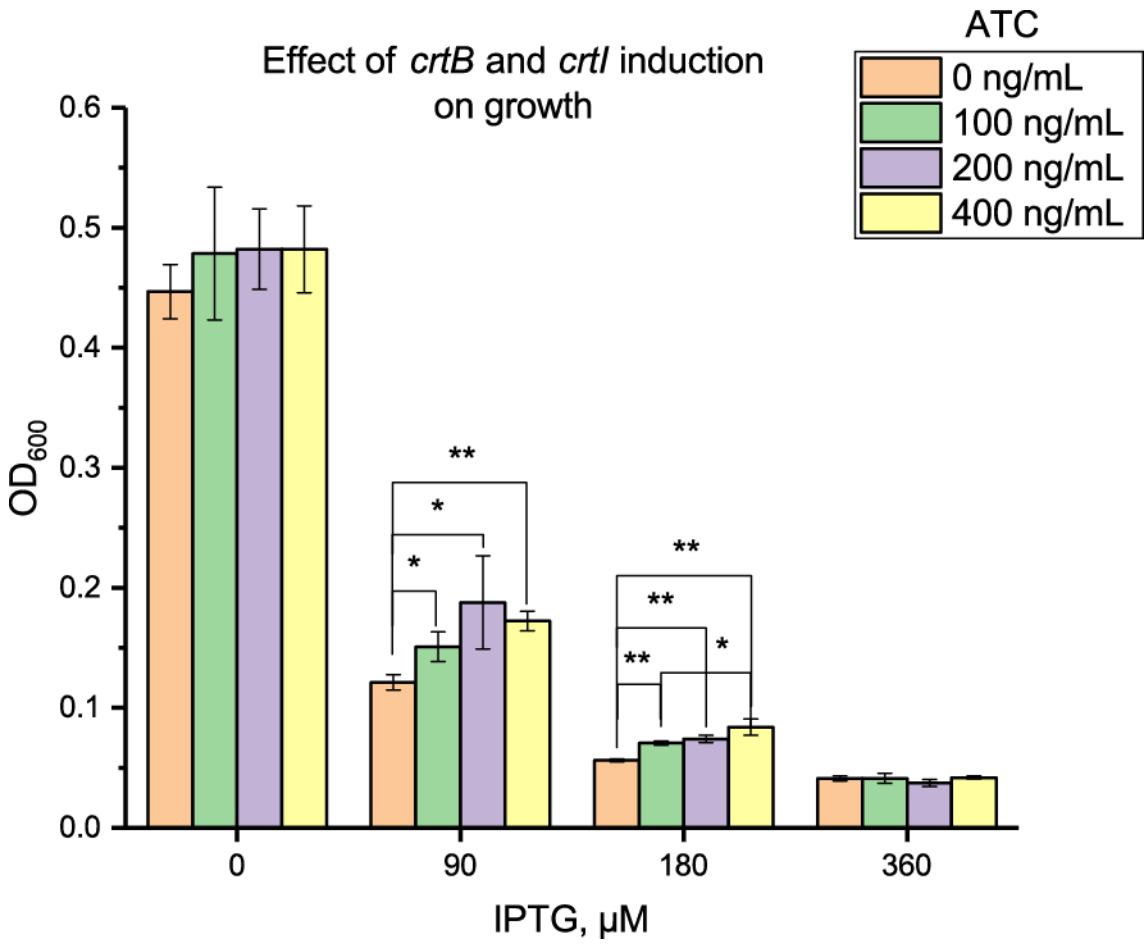

Figure 23: DH10B growth in carotenoid extraction experiment. Growth restriction and rescue similar to previous experiments. Error bars indicate standard deviation. ATC induces *crtI*. IPTG induces *crtB*.

To expand upon this, a higher-resolution induction was performed in DH10B at increasing concentrations of ATC (0, 100 ng/µL, 200 ng/µL, 400 ng/µL) and IPTG (0 µM, 90 µM IPTG, 180 µM IPTG, 360 µM IPTG). Again, cell densities decreased universally with increasing IPTG (Figure 23). At these higher induction levels, we

expected to see an enhanced alleviation of growth restriction upon *crtI* expression, but this effect was not observed.

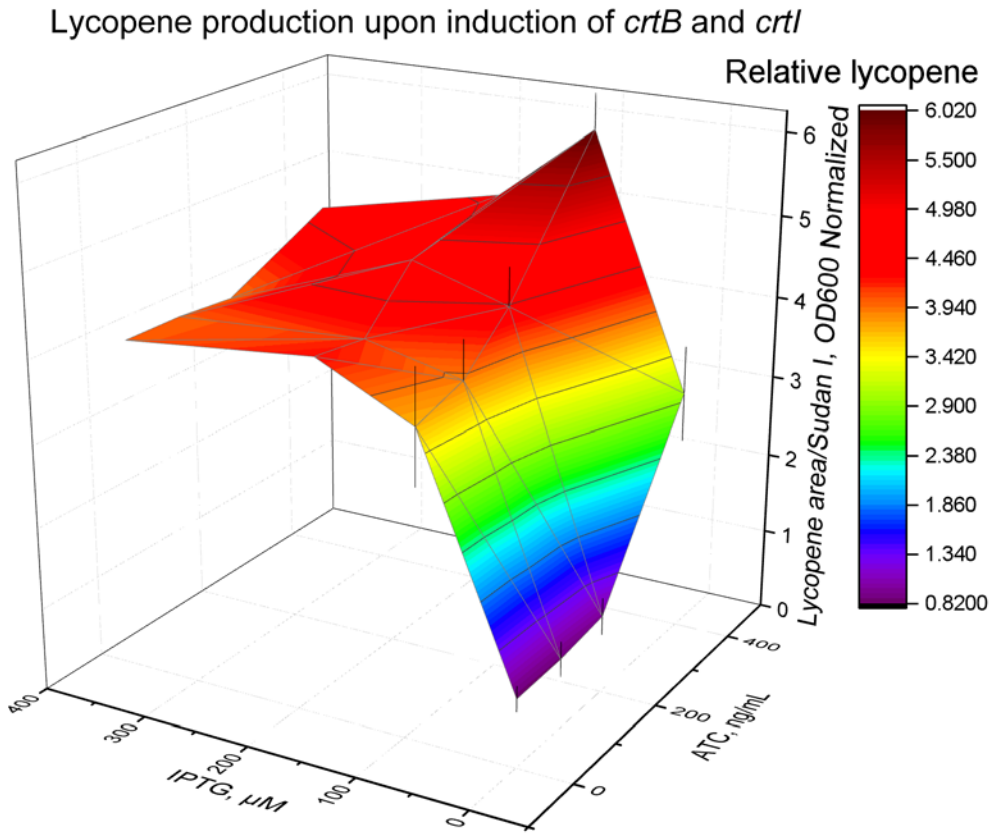

Figure 24: Lycopene production upon induction of *crtB*, *crtI* in the presence of constitutive *crtE*. Note the local maximum apparent at 90 µM IPTG at 400 ng/mL ATC. Error bars indicate standard deviation. ATC induces *crtI*. IPTG induces *crtB*.

At similar IPTG concentrations to previous experiments (90,180 µM IPTG), there were statistically significant differences in optical density between cultures with and without ATC (growth "rescue"). Indeed, at 180 µM IPTG there was an apparent dose response,

with significant differences between the highest and the two lowest ATC concentrations. This effect was not observed in the absence of IPTG or at the highest concentration of IPTG. In previous experiments, induction of *crtI* by addition of ATC produced an increase in culture density at 0 µM IPTG; however, we failed to observe this effect here.

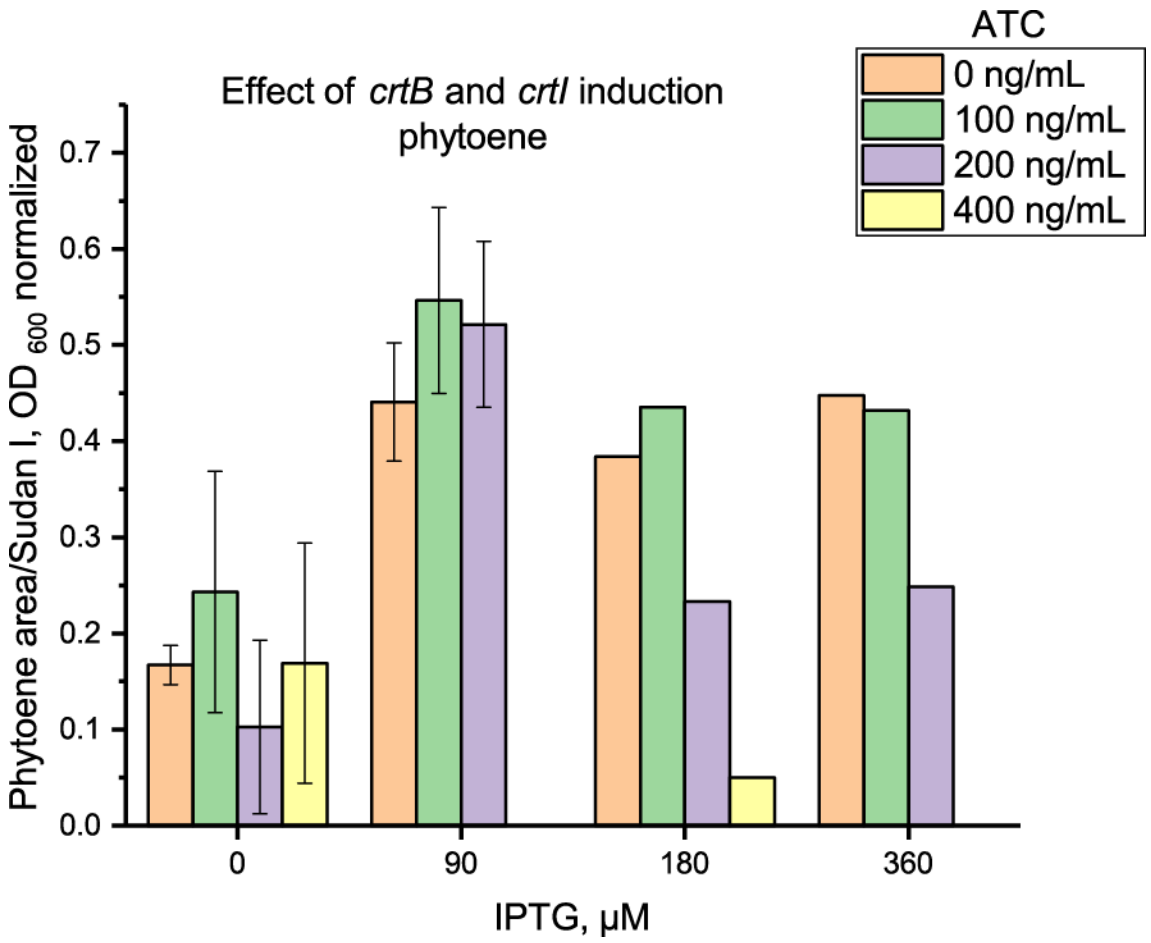

Figure 25: Relative phytoene production as a function of induction of independent *crtB* and *crtI*. In general, phytoene decreases with increasing CrtI. Error bars indicate standard deviation. Replicates from cultures at 180 µM and 360 µM IPTG were combined due to low optical density to ensure enough phytoene for detection. ATC induces *crtI*. IPTG induces *crtB*.

While the absence of this effect at 360 µM is also unexpected, it is not inconsistent with previous experiments, as 360 µM IPTG is a substantially higher concentration than was used in previous experiments. It is interesting to note that based on inductions in the fluorescent reporter construct, 360 µM is outside the linear response range of lacI, so *crtB* expression would be expected to be only marginally higher than in the previous experiment at 150 µM.

Acetone extractions were analyzed to determine the effects of enzyme expression on lycopene and phytoene accumulation. In order to get enough analyte to measure, replicates of samples with the lowest optical densities were combined and extracted. As such, no statistics were performed on 180 or 360 µM IPTG carotenoid data, though single measurements normalized by the combined optical density are presented.

Lycopene was strictly higher at the highest ATC concentrations for all concentrations of IPTG and, in general, increased with increasing IPTG (Figure 24). The most notable exception to that behavior is at 90 µM IPTG and 400 ng/mL ATC, at which there is an apparent local maximum for lycopene production per culture optical density. Lycopene at these concentrations was significantly higher ($p<0.05$) than any of the nearest comparable measurements for ATC or IPTG concentration.

Phytoene was either undetectable or lower at the highest ATC concentration in all cases except for the absence of IPTG (Figure 25). This is consistent with the expectation that higher levels of CrtI would result in a decrease in the precursor phytoene. Phytoene was significantly higher at 90 µM IPTG than in the absence of IPTG for all but the highest concentration of ATC. Again, this is consistent with increased CrtB production

converting more GGPP to phytoene. The absence of this difference at the highest concentration of ATC could be attributed to ample CrtI being present to completely convert any phytoene produced to lycopene. In support of this, those induction conditions resulted in the highest amount of lycopene produced; however, that same relative imbalance between CrtB and CrtI levels could reasonably be expected in the absence of IPTG as well, and while relatively higher lycopene levels were observed, nonzero levels of phytoene were measured in that case as well.

4.3 Conclusion

The phytoene measurements in this chapter are also inconsistent with the initial hypothesis that the intermediate phytoene was primarily responsible for the observed growth restriction. As phytoene levels are nearly universally lower at maximal *crtI* induction, we would expect these conditions to have the most significant rescue of growth, yet this is not observed. Indeed, we found no significant correlation between measured phytoene levels and optical density.

We have investigated growth restriction upon differential expression of the carotenoid pathway genes *crtEIB.* Early experiments led us to propose that the intermediate phytoene was primarily responsible for this phenomenon, although further analysis suggested that the real underlying mechanism is not that simple. Lycopene production is well-documented in *E. coli*, and the accumulation of carotenoids in these experiments is far lower than other experiments in the literature, suggesting that simple toxicity of the product of this pathway is not the cause. A cofactor imbalance could also cause significant stress; however, we showed that the effect primarily depends on the induction

of *crtB* in the presence of CrtE. If a cofactor imbalance were the primary cause, we would still expect to observe a correlation between phytoene accumulation and optical density, because relative levels of lycopene and phytoene indicate the extent of each intermediate reaction and thus presumably cofactor usage.

Another possibility that we have not investigated is the formation of a relatively insoluble protein complex, CrtEB. It is difficult to reconcile the positive effect on optical density upon induction of crtI with this model, but it is not completely unreasonable that a third protein could stabilize an EB complex; however, we would again expect that increasing CrtI should be able to more effectively ameliorate the negative effects of CrtEB if that were indeed the explanation, but the capacity for "rescue" of growth restriction seems to be limited.

A final takeaway from these experiments is the local maximum observed in lycopene production. In our work on a biosensor, we have constitutively expressed these carotenoid genes from operon that was previously available and not deliberately balanced. This work suggests that there is an optimal ratio of enzyme expression that could improve lycopene production from a constitutive reporter with relatively little effort.

CHAPTER 5. FUTURE DIRECTIONS

Here I have presented the development of a whole-cell zinc biosensor based on *E. coli* for the evaluation of zinc status in human serum; however, there remain significant steps to translate the work here into a functional, field-deployable device. In this chapter, I will discuss immediate next steps to move forward the advances and findings presented in this thesis, as well as critical next steps that to move the work from this thesis closer to deployment in the field, including possible alternative strategies that may allow accelerated implementation. To conclude, I will summarize my contributions and discuss them in the context of continued efforts to produce a field-deployable assay.

5.1 Extension of thesis results

An important next step is to evaluate the actual zinc concentrations in serum and media combinations used in our in experiments to date using currently accepted quantitative techniques, such as ICP-MS. In this work, we used a chelating resin to remove zinc from serum of indeterminate zinc content. Prior to final tuning, it was sufficient to demonstrate differences between treated and untreated serum and serum with or without zinc supplementation. This showed that matrix effects of serum would not in principle prevent *E. coli* from differentially responding to zinc in its environment. The quantitative zinc levels will be important for final tuning of the response thresholds to zinc levels.

We have demonstrated here that the sensor response can be manipulated in serum using synthetic biology approaches, but the different concentration ranges at which the sensor produces different pigments is not yet properly tuned for physiologically relevant

concentrations in serum. With information on the actual zinc content of the serum samples we are using, the expression of *crtY* can be fine-tuned to control the switch point between lycopene and ß-carotene. To identify improved constructs, the performance of plasmids tested in this work can be used in concert with computational tools like the Ribosomal Binding Site Calculator to hone in on an acceptable RBS efficiency. The efficiency of current constructs can be evaluated *in silico* and the results used as bounds for *de novo* design of new intermediate efficiency candidates with the same computational tool.

Additionally, similar techniques will be needed to tune P_{zntA}-controlled expression of *zur* in concert with decoy binding sites to adjust the zinc concentrations at which violacein production is sufficient to produce a purple sensor output. Based on array loss observed in experiments with decoy arrays and pigment reporters, a 32 decoy site array is probably too unstable for application in a final device. Experiments titrating down the number of decoys in concert with adjustment of the RBS efficiency on *zur* will be necessary to sustain violacein production out to an acceptably high zinc concentration.

To extend on the work presented here on carotenoid gene toxicity and optimal expression for lycopene production, a higher-resolution investigation of a local maximum in lycopene could result in improved sensor performance by reducing transgene expression required by cells, though it is unclear whether that is strictly necessary. Current efforts into improving time-to-response in our lab involve adjusting lycopene production, and this approach could be useful in those efforts as well. As it is impractical to use chemical inducers for any final device implementation, constitutive expression of carotenoid enzymes in the range determined by our induction experiments in Chapter 4 would need

to be implemented for integration into the biosensor. Further investigation of CrtB-dependent toxicity, while scientifically interesting, is likely not necessary for improving performance of the sensor. Efforts towards elucidating the mechanism of the growth restriction would involve significant work assessing actual protein levels under different conditions rather than the convenient fluorescence proxies we used in this work and possibly metabolomics work to investigate the impact of enzyme expression and activity on native *E. coli* metabolism.

5.2 Towards a field-deployable sensor

Creating a useful device out of the whole-cell sensor I have described requires a few crucial steps that fell beyond the scope of this thesis work. For instance, a suitable preservation method for the biosensor must be investigated. One of the critical challenges that is directly addressed by minimal equipment, on-site assays is elimination of the logistical challenges involved in properly transporting blood or other biological samples appropriately though areas with poorly developed or maintained infrastructure. Thus, a successful device cannot come with its own cold chain requirements or other onerous requirements for storage or use. Since cells are typically stored in some sort of refrigerated format for later use, a long-term preservation strategy for the biosensor cells must be developed and tested. Lyophilization is a well-established method of preserving cells. As the strategy I presented here for growing biosensor cells in serum appears to involve exhausting the human complement system present in the serum with sufficient bacterial load, lyophilization techniques that require high starting cell densities and have fairly low percentage cell viability may actually achieve the same end. Cells compromised by the lyophilization procedure may still serve as adequate decoys to “soak

up" complement proteins and allow the remaining viable cells to grow and respond appropriately to zinc in the serum.

Another alternative to help address long-term storage and transportation requirements is to implement the circuitry and sensing elements developed and tuned here for *E. coli* in an alternative bacterial chassis that can sporulate, such as *Bacillus subtilis*. The bacterial endospore is an evolutionarily developed long-term preservation mechanism that is naturally robust to changes in many environmental variables, especially desiccation and temperature changes[92]. Proper packaging of bacterial spores could result in a device without stringent requirements for storage and transportation. Some examples of whole cell biosensors from bacterial endospores exist, including for zinc detection[62] (however, the intended applications and design of the sensor were substantially different). While there are clear advantages to using spore forming bacteria, a number of potential challenges would have to be investigated and mitigated. The genetic circuits developed here are highly unlikely to work in a plug-and-play manner in a different bacterial host. Suitable vectors compatible with the new chassis must also be used, or the circuits must be chromosomally integrated. Neither of these issues is particularly challenging, but they would almost invariably require re-tuning of the circuitry due to copy number variation. Additionally, all of the promoters here are unlikely to function similarly, or perhaps at all, in a different host. Other constitutive promoters to control regulator expression and the lycopene biosynthesis pathway must be implemented. The promoters P_{zntA} and P_{znuC} would have to be engineered to function with the new chassis' RNAP holoenzyme. Finally, while ZntR and Zur are more likely to function, the natural intracellular zinc concentration in different bacterial hosts or response of intracellular zinc to changes in

the environment may vary, altering the extracellular concentrations that cause differential regulation by ZntR and Zur. These challenges could be addressed, but the work would be substantial. For this reason, the limits of preservation of *E. coli* should be exhaustively investigated before a decision to switch to a new host is made.

A third strategy would be to abandon the idea of a "whole-cell" biosensor completely and to use cell-free extracts (CFE) produced from *E. coli*. Briefly, this involves removing the cell membrane and genetic material of *E. coli*, effectively creating a large volume of cytoplasm with intact transcriptional and translational machinery. With proper reagent supplementation, CFE can be used to express proteins or execute the programs encoded in arbitrary genetic circuits. Lyophilization has already been demonstrated as a suitable storage strategy for cell-free approaches, and because the cellular machinery of *E. coli* is retained, all of the genetic components in the zinc biosensor should retain their native functions. Nevertheless, the circuitry would still likely need to be retuned to respond appropriately at the desired zinc levels, and this strategy would introduce new variables that would also need to be tuned or explored, including the appropriate amount of DNA added per volume of CFE and methods to mitigate batch to batch variation in functionality of the CFE—both of which could decrease the robustness of any ultimate device. Additionally, the strategy I employed in designing the whole-cell sensor relies on sensing mechanisms that respond to extracellular zinc downstream of a complex cascade of biological interactions that affect the mapping of extracellular zinc to intracellular zinc. Indeed, both transcription factors used here have been reported to respond to femtomolar levels of zinc *in vitro*, making it uncertain whether they could be useful in a CFE-based zinc assay with serum added directly to the cell-free extract. One approach to

circumventing this issue may be to express a subset of additional zinc-binding proteins naturally present within the cell to mimic the protein-bound zinc pool in which the proteins evolved to function.

A logical expansion to the work here would be the introduction of sensing components for different micronutrients. During my time in graduate school, I had the opportunity to participate in the NSF-sponsored I-Corps program during which I met with leaders in the field of global micronutrient health and organizations involved in monitoring population micronutrient status. Conversations with program directors at the Demographic and Health Surveys program funded by USAID suggested that a device similar to the one envisioned here that incorporated an assay for even one additional micronutrient would be very likely to be included in DHS surveys. Prospective adoption of an assay would go a long way towards getting a device actually manufactured and commercialized. Obvious candidates for other assays to pursue would be for the remaining micronutrients in the NIH's BOND program: iron, vitamin A, folate, and vitamin B_{12}.

5.3 Closing remarks

In this thesis, I have described my efforts to implement a whole-cell bacterial biosensor to be used as an assay for zinc levels in human serum. The work I have done demonstrates the feasibility of using these sensing components and *E. coli* as the basis for a useful device.

I demonstrated that P_{zntA}/ZntR could be coupled with the carotenoid pathway to produce orange and red sensor output by controlling the transition from lycopene to ß-carotene, and that this transition could be tuned to occur over zinc ranges that were physiologically

relevant. I demonstrated that violacein production could be controlled over a physiologically-relevant zinc concentration range by the use of P_{znuC} and Zur and arrays of decoy Zur operators. Furthermore, I combined these systems and demonstrated growth and sensor response in human serum. Though the concentration at which each color state is induced in serum is not yet optimal for an assay for human zinc status, the ultimate form factor of such an assay and preservation method selected for the biosensor will almost certainly necessitate additional tuning of the sensor anyway, and the methods I employed here can be used to perform that tuning. Additionally, the quantitative characterization of the two zinc-responsive promoters with fluorescence coupled with data on which zinc concentrations trigger changes in pigmentation in the carotenoid pathway allow others to more easily use these pathways as reporting mechanisms with different sensors. As long as the ultimate output of the sensing mechanism is transcriptional, performance of an arbitrary sensor can be investigated in fluorescence space and compared against the data presented here, facilitating selection of post-transcriptional regulatory features to enable color switching from lycopene to ß-carotene over a novel concentration range of interest. This allows the reporting machinery used in these experiments to be easily ported to other synthetic biology applications for which differential pigment production would be useful. Finally, I investigated expression of carotenoid pathway genes and found that models to explain widely reported growth restriction were inadequate; I also identified the existence of a local maximum in lycopene production at specific induction levels of CrtB and CrtI, which can be used to further improve the biosensor or carotenoid synthesis in other applications.

Through both my scientific work in the lab and practical, nonscientific engagement with policy makers and prospective end users, it became apparent over the course of my project that a successful device would require more effort than was feasible for a single graduate student. Fortunately, my lab is continuing to develop these ideas and it is my hope that my efforts will help lead to a practical, field deployed device to help scientists and policymakers addressing pressing global health issues.

APPENDIX A. SUPPLEMENTARY FIGURES

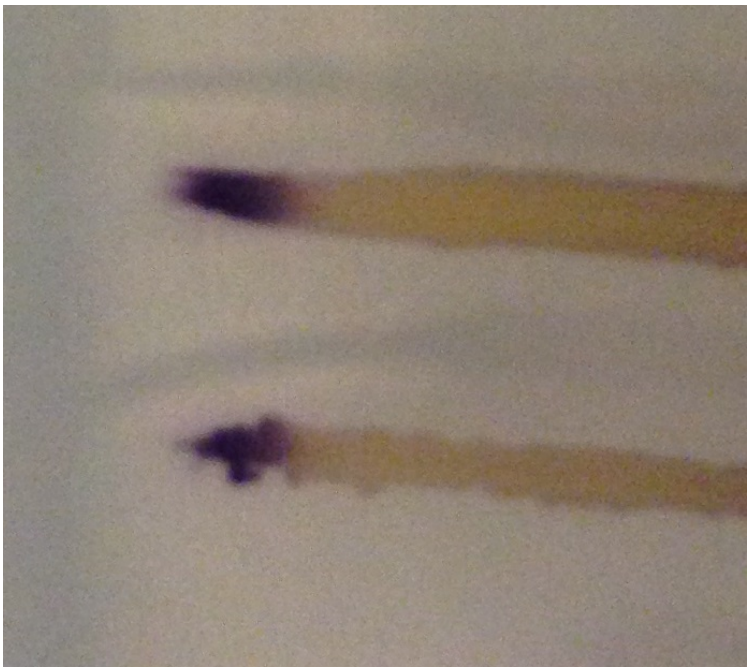

Figure 26: Streak from a zinc gradient plate demonstrating direct transition from purple to orange without an intervening lycopene-dominated, red state. This is the original image from Figure 2C before any contrast adjustment.

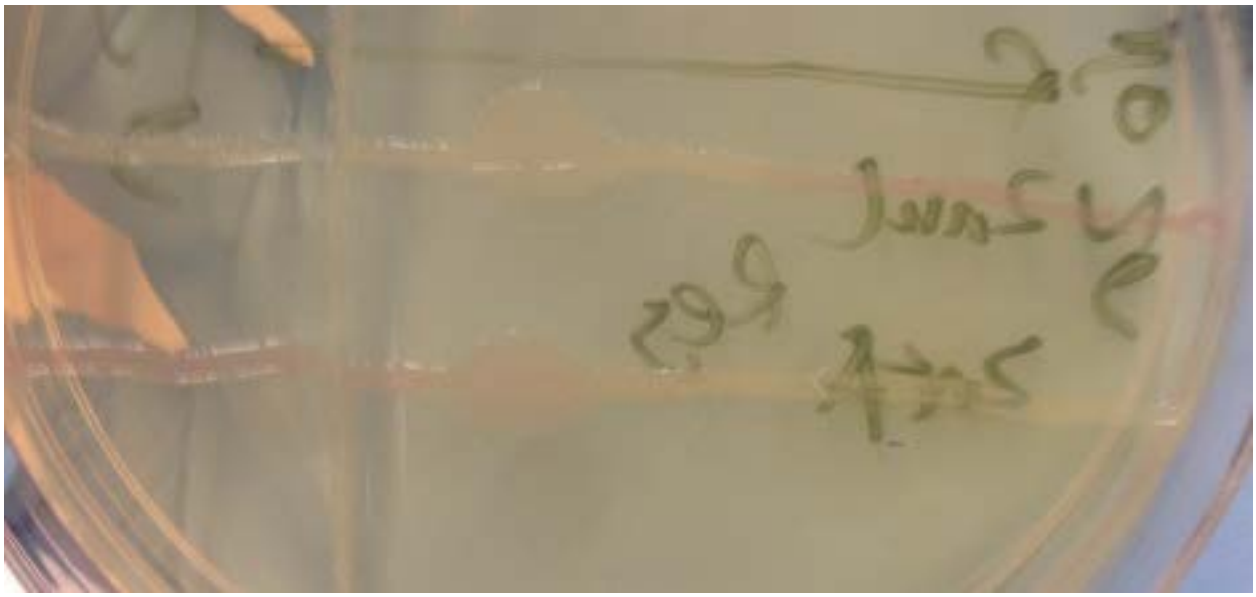

Figure 27: The visible induction regimes of P_{zntA} and P_{znuC} do not overlap. The plate is a zinc gradient plate, with [Zn^{2+}] increasing to the left. The top strain has P_{znuC} driving expression of mRFP, while the bottom strain has P_{zntA} driving expression of mRFP. Based on expression visible to the naked eye, there is a regime where each promoter has low expression. This suggested the possibility that the expression of pigment-producing enzymes from either of these promoters would yield non-overlapping regimes each dominated by one pigment.

REFERENCES

1 Mabey, D., Peeling, R. W., Ustianowski, A. & Perkins, M. D. Tropical infectious diseases: Diagnostics for the developing world. *Nat Rev Micro* **2**, 231-240 (2004).

2 Wessells, K. R. & Brown, K. H. Estimating the Global Prevalence of Zinc Deficiency: Results Based on Zinc Availability in National Food Supplies and the Prevalence of Stunting. *PLoS ONE* **7**, e50568, doi:10.1371/journal.pone.0050568 (2012).

3 Black, R. E. Maternal and child undernutrition: global and regional exposures and health consequences. *The Lancet* **371**, doi:10.1016/S0140-6736(07)61690-0 (2008).

4 King, J. C. Determinants of maternal zinc status during pregnancy. *American Journal of Clinical Nutrition* (2000).

5 UNICEF/WHO. Diarrhoea: Why children are still dying and what can be done. (2009).

6 Black, R. E. *et al.* Maternal and child undernutrition and overweight in low-income and middle-income countries. *The Lancet*, doi:10.1016/s0140-6736(13)60937-x (2013).

7 Wapnir, R. A. Zinc deficiency, malnutrition and the gastrointestinal tract. *The Journal of nutrition* **130**, 1388S-1392S (2000).

8 Hess, S. Y., Peerson, J. M., King, J. C. & Brown, K. H. Use of serum zinc concentration as an indicator of population zinc status. *Food Nutr Bull* **28**, S403-429, doi:10.1177/15648265070283s303 (2007).

9 Ye, X. A.-B., S. Kloti,A. Zhang, J. Lucca, P. Beyer, P. Potrykus, I. Engineering the Provitamin A (B-Carotene) Biosynthetic Pathway into (Carotenoid-Free) Rice Endosperm. *Science* **287** (2000).

10 Beyer, P. A.-B., S. Ye, X. Lucca, P. Schuabl, P. Welsch, R. Potrykus, Ingo. Golden Rice: Introducing the B-Carotene Biosynthesis Pathway into Rice Endosperm by Genetic Engineering to Defeat Vitamin A Deficiency. *American Society for Nutritional Sciences* (2002).

11 Ruel, M. T. & Alderman, H. Nutrition-sensitive interventions and programmes: how can they help to accelerate progress in improving maternal and child nutrition? *The Lancet*, doi:10.1016/s0140-6736(13)60843-0 (2013).

12 Brown, K. H., Peerson, J M, Baker, S K, Hess, S Y. Preventive zinc supllementation among infants, preschoolers, and older prepubertal childern. *Food and Nutrition Bulletin* **30**, 29 (2009).

13 Yakoob, M. Y. *et al.* Preventive zinc supplementation in developing countries: impact on mortality and morbidity due to diarrhea, pneumonia and malaria. *BMC public health* **11 Suppl 3**, S23, doi:10.1186/1471-2458-11-S3-S23 (2011).

14 Soofi, S. *et al.* Effect of provision of daily zinc and iron with several micronutrients on growth and morbidity among young children in Pakistan: a cluster-randomised trial. *The Lancet* **382**, 29-40, doi:10.1016/s0140-6736(13)60437-7 (2013).

15 Imdad, A. & Bhutta, Z. A. Effect of preventive zinc supplementation on linear growth in children under 5 years of age in developing countries: a meta-analysis of studies for input to the lives saved tool. *BMC public health* **11 Suppl 3**, S22, doi:10.1186/1471-2458-11-S3-S22 (2011).

16 Mission, J. a. K. N. R. H. Operational Guidelines for State Programme Implementation Plan. (2012).

17 Bhutta, Z. A. *et al.* Evidence-based interventions for improvement of maternal and child nutrition: what can be done and at what cost? *The Lancet*, doi:10.1016/s0140-6736(13)60996-4 (2013).

18 Keasling, J. D. Synthetic Biology for Synthetic Chemistry. *ACS Chemical Biology* **3**, 64-76, doi:10.1021/cb7002434 (2008).

19 Gardner, T. S., Cantor, C. R. & Collins, J. J. Construction of a genetic toggle switch in Escherichia coli. *Nature* **403**, 339-342, doi:10.1038/35002131 (2000).

20 Tamsir, A., Tabor, J. J. & Voigt, C. A. Robust multicellular computing using genetically encoded NOR gates and chemical /`wires/'. *Nature* **469**, 212-215, doi:http://www.nature.com/nature/journal/v469/n7329/abs/nature09565.html#supplementary-information (2011).

21 Leth, S. *et al.* Engineered Bacteria Based Biosensors for Monitoring Bioavailable Heavy Metals. *Electroanalysis* **14**, 35-42, doi:10.1002/1521-4109(200201)14:1<35::AID-ELAN35>3.0.CO;2-W (2002).

22 Charrier, T. *et al.* A multi-channel bioluminescent bacterial biosensor for the on-line detection of metals and toxicity. Part I: design and optimization of bioluminescent bacterial strains. *Analytical and bioanalytical chemistry* **400**, 1051-1060, doi:10.1007/s00216-010-4353-9 (2011).

23 Daunert, S. *et al.* Genetically engineered whole-cell sensing systems: coupling biological recognition with reporter genes. *Chemical reviews* **100**, 2705-2738 (2000).

24 Olaniran, A. O., Hiralal, L. & Pillay, B. Whole-cell bacterial biosensors for rapid and effective monitoring of heavy metals and inorganic pollutants in wastewater. *Journal of environmental monitoring : JEM* **13**, 2914-2920, doi:10.1039/c1em10032g (2011).

25 Jouanneau, S., Durand, M. J. & Thouand, G. Online detection of metals in environmental samples: comparing two concepts of bioluminescent bacterial biosensors. *Environmental science & technology* **46**, 11979-11987, doi:10.1021/es3024918 (2012).

26 Gierach, I., Li, J., Wu, W. Y., Grover, G. J. & Wood, D. W. Bacterial biosensors for screening isoform-selective ligands for human thyroid receptors alpha-1 and beta-1. *FEBS open bio* **2**, 247-253, doi:10.1016/j.fob.2012.08.002 (2012).

27 Weber, W. & Fussenegger, M. The impact of synthetic biology on drug discovery. *Drug discovery today* **14**, 956-963, doi:10.1016/j.drudis.2009.06.010 (2009).

28 Looger, L. L., Dwyer, M. A., Smith, J. J. & Hellinga, H. W. Computational design of receptor and sensor proteins with novel functions. *Nature* **423**, 185-190, doi:10.1038/nature01556 (2003).

29 Beggah, S., Vogne, C., Zenaro, E. & Van Der Meer, J. R. Mutant HbpR transcription activator isolation for 2-chlorobiphenyl via green fluorescent protein-based flow cytometry and cell sorting. *Microbial biotechnology* **1**, 68-78, doi:10.1111/j.1751-7915.2007.00008.x (2008).

30 Alper, H., Fischer, C., Nevoigt, E. & Stephanopoulos, G. Tuning genetic control through promoter engineering. *Proceedings of the National Academy of Sciences of the United States of America* **102**, 12678-12683, doi:10.1073/pnas.0504604102 (2005).

31 Brocklehurst, K. R. *et al.* ZntR is a Zn(II)-responsive MerR-like transcriptional regulator of zntA in Escherichia coli. *Molecular microbiology* **31**, 893-902 (1999).

32 Busenlehner, L. S., Pennella, M. A. & Giedroc, D. P. The SmtB/ArsR family of metalloregulatory transcriptional repressors: structural insights into prokaryotic metal resistance. *FEMS Microbiology Reviews* **27**, 131-143, doi:10.1016/s0168-6445(03)00054-8 (2003).

33 Yong, Y.-C. & Zhong, J.-J. A genetically engineered whole-cell pigment-based bacterial biosensing system for quantification of N-butyryl homoserine lactone quorum sensing signal. *Biosensors and Bioelectronics* **25**, 41-47, doi:http://dx.doi.org/10.1016/j.bios.2009.06.010 (2009).

34 Yoshida, K. *et al.* Novel carotenoid-based biosensor for simple visual detection of arsenite: characterization and preliminary evaluation for environmental

application. *Applied and environmental microbiology* **74**, 6730-6738, doi:10.1128/aem.00498-08 (2008).

35 Lee, L. J., Barrett, J. A. & Poole, R. K. Genome-wide transcriptional response of chemostat-cultured Escherichia coli to zinc. *Journal of bacteriology* **187**, 1124-1134, doi:10.1128/JB.187.3.1124-1134.2005 (2005).

36 Wang, D., Hosteen, O. & Fierke, C. A. ZntR-mediated transcription of zntA responds to nanomolar intracellular free zinc. *Journal of inorganic biochemistry* **111**, 173-181, doi:10.1016/j.jinorgbio.2012.02.008 (2012).

37 Graham, A. I. *et al.* Severe zinc depletion of Escherichia coli: roles for high affinity zinc binding by ZinT, zinc transport and zinc-independent proteins. *The Journal of biological chemistry* **284**, 18377-18389, doi:10.1074/jbc.M109.001503 (2009).

38 Yamamoto, K. & Ishihama, A. Transcriptional response of Escherichia coli to external zinc. *Journal of bacteriology* **187**, 6333-6340, doi:10.1128/JB.187.18.6333-6340.2005 (2005).

39 Easton, J. A., Thompson, P. & Crowder, M. W. Time-dependent translational response of E. coli to excess Zn(II). *Journal of biomolecular techniques : JBT* **17**, 303-307 (2006).

40 Sigdel, T. K. *et al.* Probing the adaptive response of Escherichia coli to extracellular Zn(II). *Biometals : an international journal on the role of metal ions in biology, biochemistry, and medicine* **19**, 461-471, doi:10.1007/s10534-005-4962-5 (2006).

41 Gireesh-Babu, P. & Chaudhari, A. Development of a broad-spectrum fluorescent heavy metal bacterial biosensor. *Molecular biology reports* **39**, 11225-11229, doi:10.1007/s11033-012-2033-x (2012).

42 Michelini, E. *et al.* Field-deployable whole-cell bioluminescent biosensors: so near and yet so far. *Analytical and bioanalytical chemistry* **405**, 6155-6163, doi:10.1007/s00216-013-7043-6 (2013).

43 Pemberton, J., Vincent, K. & Penfold, R. Cloning and heterologous expression of the violacein biosynthesis gene cluster fromChromobacterium violaceum. *Current Microbiology* **22**, 355-358, doi:10.1007/BF02092154 (1991).

44 Duran, N. *et al.* Violacein: properties and biological activities. *Biotechnology and applied biochemistry* **48**, 127-133, doi:10.1042/BA20070115 (2007).

45 Hoshino, T. Violacein and related tryptophan metabolites produced by Chromobacterium violaceum: biosynthetic mechanism and pathway for construction of violacein core. *Applied microbiology and biotechnology* **91**, 1463-1475, doi:10.1007/s00253-011-3468-z (2011).

46 Ahmetagic, A. & Pemberton, J. M. Stable high level expression of the violacein indolocarbazole anti-tumour gene cluster and the Streptomyces lividans amyA gene in E. coli K12. *Plasmid* **63**, 79-85, doi:10.1016/j.plasmid.2009.11.004 (2010).

47 Alper, H., Jin, Y. S., Moxley, J. F. & Stephanopoulos, G. Identifying gene targets for the metabolic engineering of lycopene biosynthesis in Escherichia coli. *Metabolic engineering* **7**, 155-164, doi:10.1016/j.ymben.2004.12.003 (2005).

48 Jin, Y. S. & Stephanopoulos, G. Multi-dimensional gene target search for improving lycopene biosynthesis in Escherichia coli. *Metabolic engineering* **9**, 337-347, doi:10.1016/j.ymben.2007.03.003 (2007).

49 Pitera, D. J., Paddon, C. J., Newman, J. D. & Keasling, J. D. Balancing a heterologous mevalonate pathway for improved isoprenoid production in Escherichia coli. *Metabolic engineering* **9**, 193-207, doi:10.1016/j.ymben.2006.11.002 (2007).

50 Ajikumar, P. K. *et al.* Isoprenoid pathway optimization for Taxol precursor overproduction in Escherichia coli. *Science* **330**, 70-74, doi:10.1126/science.1191652 (2010).

51 Wong, A. P., Gupta, M., Shevkoplyas, S. S. & Whitesides, G. M. Egg beater as centrifuge: isolating human blood plasma from whole blood in resource-poor settings. *Lab on a Chip* **8**, 2032-2037, doi:10.1039/B809830C (2008).

52 Bhamla, M. S. *et al.* Hand-powered ultralow-cost paper centrifuge. **1**, 0009, doi:10.1038/s41551-016-0009 (2017).

53 Yang, X., Forouzan, O., Brown, T. P. & Shevkoplyas, S. S. Integrated separation of blood plasma from whole blood for microfluidic paper-based analytical devices. *Lab on a Chip* **12**, 274-280, doi:10.1039/C1LC20803A (2012).

54 Watstein, D. M., McNerney, M. P. & Styczynski, M. P. Precise metabolic engineering of carotenoid biosynthesis in Escherichia coli towards a low-cost biosensor. *Metabolic engineering* **31**, 171-180, doi:10.1016/j.ymben.2015.06.007 (2015).

55 Atsumi, S. *et al.* Metabolic engineering of Escherichia coli for 1-butanol production. *Metabolic engineering* **10**, 305-311, doi:http://dx.doi.org/10.1016/j.ymben.2007.08.003 (2008).

56 Atsumi, S., Hanai, T. & Liao, J. C. Non-fermentative pathways for synthesis of branched-chain higher alcohols as biofuels. *Nature* **451**, 86-89, doi:10.1038/nature06450 (2008).

57 Jin, Y. S., Alper, H., Yang, Y. T. & Stephanopoulos, G. Improvement of xylose uptake and ethanol production in recombinant Saccharomyces cerevisiae through

an inverse metabolic engineering approach. *Applied and environmental microbiology* **71**, 8249-8256, doi:10.1128/aem.71.12.8249-8256.2005 (2005).

58 Alonso-Gutierrez, J. *et al.* Metabolic engineering of Escherichia coli for limonene and perillyl alcohol production. *Metabolic engineering* **19**, 33-41, doi:10.1016/j.ymben.2013.05.004 (2013).

59 Ro, D. K. *et al.* Production of the antimalarial drug precursor artemisinic acid in engineered yeast. *Nature* **440**, 940-943, doi:10.1038/nature04640 (2006).

60 Chemler, J. A., Fowler, Z. L., McHugh, K. P. & Koffas, M. A. Improving NADPH availability for natural product biosynthesis in Escherichia coli by metabolic engineering. *Metabolic engineering* **12**, 96-104, doi:10.1016/j.ymben.2009.07.003 (2010).

61 Raab, A. M., Gebhardt, G., Bolotina, N., Weuster-Botz, D. & Lang, C. Metabolic engineering of Saccharomyces cerevisiae for the biotechnological production of succinic acid. *Metabolic engineering* **12**, 518-525, doi:10.1016/j.ymben.2010.08.005 (2010).

62 Date, A., Pasini, P. & Daunert, S. Integration of spore-based genetically engineered whole-cell sensing systems into portable centrifugal microfluidic platforms. *Analytical and bioanalytical chemistry* **398**, 349-356, doi:10.1007/s00216-010-3930-2 (2010).

63 Farmer, W. R. & Liao, J. C. Precursor balancing for metabolic engineering of lycopene production in Escherichia coli. *Biotechnol Prog* **17**, 57-61, doi:10.1021/bp000137t (2001).

64 Yoon, S. H. *et al.* Enhanced lycopene production in Escherichia coli engineered to synthesize isopentenyl diphosphate and dimethylallyl diphosphate from mevalonate. *Biotechnology and bioengineering* **94**, 1025-1032, doi:10.1002/bit.20912 (2006).

65 Alper, H., Miyaoku, K. & Stephanopoulos, G. Construction of lycopene-overproducing E. coli strains by combining systematic and combinatorial gene knockout targets. *Nature biotechnology* **23**, 612-616, doi:10.1038/nbt1083 (2005).

66 Rodrigues, A. L. *et al.* Systems metabolic engineering of Escherichia coli for production of the antitumor drugs violacein and deoxyviolacein. *Metabolic engineering* **20**, 29-41, doi:10.1016/j.ymben.2013.08.004 (2013).

67 Lee, M. E., Aswani, A., Han, A. S., Tomlin, C. J. & Dueber, J. E. Expression-level optimization of a multi-enzyme pathway in the absence of a high-throughput assay. *Nucleic acids research* **41**, 10668-10678, doi:10.1093/nar/gkt809 (2013).

68 Fang, M. Y. *et al.* High crude violacein production from glucose by Escherichia coli engineered with interactive control of tryptophan pathway and violacein

biosynthetic pathway. *Microbial cell factories* **14**, 8, doi:10.1186/s12934-015-0192-x (2015).

69 Gibson, D. G. *et al.* Enzymatic assembly of DNA molecules up to several hundred kilobases. *Nat Meth* **6**, 343-345, doi:http://www.nature.com/nmeth/journal/v6/n5/suppinfo/nmeth.1318_S1.html (2009).

70 Wong, A. P., Gupta, M., Shevkoplyas, S. S. & Whitesides, G. M. Egg beater as centrifuge: isolating human blood plasma from whole blood in resource-poor settings. *Lab on a chip* **8**, 2032-2037, doi:10.1039/b809830c (2008).

71 McGinness, K. E., Baker, T. A. & Sauer, R. T. Engineering Controllable Protein Degradation. *Molecular Cell* **22**, 701-707, doi:http://dx.doi.org/10.1016/j.molcel.2006.04.027 (2006).

72 Khan, S., Brocklehurst, K. R., Jones, G. W. & Morby, A. P. The functional analysis of directed amino-acid alterations in ZntR from Escherichia coli. *Biochemical and biophysical research communications* **299**, 438-445 (2002).

73 Solomon, K. V., Sanders, T. M. & Prather, K. L. A dynamic metabolite valve for the control of central carbon metabolism. *Metabolic engineering* **14**, 661-671, doi:10.1016/j.ymben.2012.08.006 (2012).

74 Soma, Y., Tsuruno, K., Wada, M., Yokota, A. & Hanai, T. Metabolic flux redirection from a central metabolic pathway toward a synthetic pathway using a metabolic toggle switch. *Metabolic engineering* **23**, 175-184, doi:10.1016/j.ymben.2014.02.008 (2014).

75 Torella, J. P. *et al.* Tailored fatty acid synthesis via dynamic control of fatty acid elongation. *Proceedings of the National Academy of Sciences of the United States of America* **110**, 11290-11295, doi:10.1073/pnas.1307129110 (2013).

76 Zalatan, J. G. *et al.* Engineering complex synthetic transcriptional programs with CRISPR RNA scaffolds. *Cell* **160**, 339-350, doi:10.1016/j.cell.2014.11.052 (2015).

77 Anesiadis, N., Cluett, W. R. & Mahadevan, R. Dynamic metabolic engineering for increasing bioprocess productivity. *Metabolic engineering* **10**, 255-266, doi:10.1016/j.ymben.2008.06.004 (2008).

78 Callura, J. M., Cantor, C. R. & Collins, J. J. Genetic switchboard for synthetic biology applications. *Proceedings of the National Academy of Sciences of the United States of America* **109**, 5850-5855, doi:10.1073/pnas.1203808109 (2012).

79 Kobayashi, H. *et al.* Programmable cells: interfacing natural and engineered gene networks. *Proceedings of the National Academy of Sciences of the United States of America* **101**, 8414-8419, doi:10.1073/pnas.0402940101 (2004).

80 Tsao, C. Y., Hooshangi, S., Wu, H. C., Valdes, J. J. & Bentley, W. E. Autonomous induction of recombinant proteins by minimally rewiring native quorum sensing regulon of E. coli. *Metabolic engineering* **12**, 291-297, doi:10.1016/j.ymben.2010.01.002 (2010).

81 Williams, T. C. *et al.* Quorum-sensing linked RNA interference for dynamic metabolic pathway control in Saccharomyces cerevisiae. *Metabolic engineering* **29**, 124-134, doi:10.1016/j.ymben.2015.03.008 (2015).

82 McNerney, M. P., Watstein, D. M. & Styczynski, M. P. Precision metabolic engineering: The design of responsive, selective, and controllable metabolic systems. *Metabolic engineering* **31**, 123-131, doi:10.1016/j.ymben.2015.06.011 (2015).

83 Espah Borujeni, A., Channarasappa, A. S. & Salis, H. M. Translation rate is controlled by coupled trade-offs between site accessibility, selective RNA unfolding and sliding at upstream standby sites. *Nucleic Acids Research* **42**, 2646-2659, doi:10.1093/nar/gkt1139 (2014).

84 Outten, C. E. & O'Halloran, T. V. Femtomolar sensitivity of metalloregulatory proteins controlling zinc homeostasis. *Science* **292**, 2488-2492, doi:10.1126/science.1060331 (2001).

85 Gilston, B. A. *et al.* Structural and Mechanistic Basis of Zinc Regulation Across the E. coli Zur Regulon. *PLoS Biology* **12**, e1001987, doi:10.1371/journal.pbio.1001987 (2014).

86 King, J. C. *et al.* Biomarkers of Nutrition for Development (BOND)-Zinc Review. *The Journal of nutrition*, doi:10.3945/jn.115.220079 (2016).

87 Dunkelberger, J. R. & Song, W. C. Complement and its role in innate and adaptive immune responses. *Cell research* **20**, 34-50, doi:10.1038/cr.2009.139 (2010).

88 Linscott, W. D. & Triglia, R. P. The bovine complement system. *Advances in experimental medicine and biology* **137**, 413-430 (1981).

89 Albermann, C. High versus low level expression of the lycopene biosynthesis genes from Pantoea ananatis in Escherichia coli. *Biotechnology letters* **33**, 313-319, doi:10.1007/s10529-010-0422-6 (2011).

90 Cunningham, F. X., Jr., Sun, Z., Chamovitz, D., Hirschberg, J. & Gantt, E. Molecular structure and enzymatic function of lycopene cyclase from the cyanobacterium Synechococcus sp strain PCC7942. *The Plant cell* **6**, 1107-1121, doi:10.1105/tpc.6.8.1107 (1994).

91 Lu, C.-H., Choi, J.-H., Moran, N. E., Jin, Y.-S. & Erdman, J. W. Laboratory-Scale Production of (13)C-Labeled Lycopene and Phytoene by Bioengineered

Escherichia coli. *Journal of agricultural and food chemistry* **59**, 9996-10005, doi:10.1021/jf202599z (2011).

92 Nicholson, W. L., Munakata, N., Horneck, G., Melosh, H. J. & Setlow, P. Resistance of Bacillus endospores to extreme terrestrial and extraterrestrial environments. *Microbiology and molecular biology reviews : MMBR* **64**, 548-572 (2000).